Title
Characterization and High Throughput Analysis of Metal Hydrides for Hydrogen Storage

Author
Barcelo, Steven James

Publication Date
2009

Peer reviewed|Thesis/dissertation

Characterization and High Throughput Analysis of Metal Hydrides for Hydrogen Storage

by

Steven James Barcelo

A dissertation submitted in partial satisfaction of the

requirements for the degree of

Doctor of Philosophy

in

Engineering-Mechanical Engineering

in the

Graduate Division

of the

University of California, Berkeley

Committee in charge:

Professor Samuel Mao, Co-chair
Professor Ralph Greif, Co-chair
Professor Costas P. Grigoropoulos
Professor Nathan Cheung

Fall 2009

Abstract

Characterization and High Throughput Analysis of Metal Hydrides for Hydrogen Storage

by

Steven James Barcelo

Doctor of Philosophy in Engineering-Mechanical Engineering

University of California, Berkeley

Professor Samuel Mao, Co-chair
Professor Ralph Greif, Co-chair

Efficient hydrogen storage is required for fuel cell vehicles to be competitive with those driven by internal combustion engines. Current methods of storage such as compressed gas and liquid hydrogen cannot meet this standard, so novel hydrogen storage materials such as metal hydrides are required. No simple metal hydride meets the required specifications. Research is required to find new materials or improve existing materials.

This thesis describes the research practices necessary to achieve legitimate and repeatable results in laboratories across the world. Examples of experiments using these techniques are presented, such as a high throughput technique to optimize materials systems with up to three components such as calcium borohydride with titanium catalyst and magnesium hydride with nickel and aluminum as destabilizing elements and catalysts. Thin films composed of gradients of each material were deposited by sputtering, creating a single thin film sample covering all potential material combinations. Optical properties of the samples under hydrogen pressure were monitored to identify the regions with largest and fastest hydrogen uptake. In the Ca-B-Ti system, titanium did not sufficiently catalyze the borohydride formation reaction at low temperature. Substantial hydrogen uptake was shown in the Mg-Ni region of the Mg-Ni-Al films. Al did not participate in the reaction at low temperature.

Further investigation of the role of catalysts and destabilizing elements in improving hydrogen storage performance through X-ray Absorption and Emission Spectroscopy measurements of the Mg-Ni system during hydrogenation is presented. Typical X-ray spectroscopy measurements use a synchrotron radiation source and require ultra high vacuum conditions. For these experiments we designed a chamber which can be inserted into a vacuum chamber allowing in situ measurements of a sample under hydrogen pressure, providing information on the role of Ni in hydrogen absorption of Mg-Ni mixtures.

Finally, another technique for improving hydrogen storage performance is presented which focuses on promising materials studied using the high throughput technique. TiO_2 powder was ball milled together with $NaBH_4$, and gravimetric analysis shows a 50% improvement in the kinetics of the hydrogen desorption reaction and a reduction in desorption temperature of 60 ^{o}C.

Dedication

To my parents, Jack and Lucy Barcelo

Table of Contents

List of Tables

List of Figures

Acknowledgements

I would like to thank my advisor Professor Sam Mao for his support and guidance throughout this process. I would also like to thank my dissertation committee, Professors Ralph Greif, Costas Grigoropoulos and Nathan Cheung as well as Professors David Attwood and Stephen Morris from my qualifying exam committee, for helping me pull everything together and making this a reality. Their teaching in the classroom was equally important, helping me understand a variety of subjects from microfabrication and synchrotron radiation to heat transfer and fluid mechanics. Dr. Jinghua Guo's help with my work at the ALS was also invaluable and educational. Dr. Karl Gross was a great mentor in my work on the Best Practices document for hydrogen storage research. Without all of them, I could not have completed this work.

I would also like to thank all of my fellow graduate students and lab mates that have helped me by bouncing ideas back and forth, or simply passing some time at the office or on campus and restoring my energy to dive back into some research. People deserving specific mention for their contribution to my personal and scientific development include, in no particular order, Matt Rogers, Russell Carrington, Teresa Zhang, Tim Suen, Xiaojun Zhang, Zhong Jun, Tyler Tong, Mike Fina, Travis Owens, Coleman Kronawitter, Tony Ho, Matt Beres, Memo Garcia, and Matt Lucas.

Finally, I would like to thank my family for all of their love and support. My parents have guided me through my most difficult choices, and their advice is always some of the best I receive, even when I ignore it. My sisters are my greatest allies, and always helpful when I'm looking to ignore some well meant advice. Most importantly, my wife, Kari, has been a wonderful part of every minute of my life since I met her just before starting this program. It is impossible to describe how important she is in everything I do.

Chapter 1: Introduction to Hydrogen Storage

1.1 Introduction

Rising concerns over the use of fossil fuels as our primary energy resource due to its contribution to pollution and global warming, as well as its limited availability, have led to a search for new energy sources. The transportation industry consumed 20% of delivered energy in 2005 globally, and over 27% in the US[1], so finding a new fuel to drive the transportation industry is of crucial. Hydrogen is compelling choice, since it has the highest energy density per unit mass of any fuel.

Electricity is another compelling source of energy for vehicles, although current battery technology significantly limits the range of electric vehicles. Hydrogen fuel cell vehicles share many advantages with electric vehicles, such as zero emissions and high efficiency, but also some of the disadvantages such as limited range. The amount of hydrogen that can be efficiently stored on board a vehicle is therefore a critical parameter. It is essential to find a lightweight, low volume, energy efficient hydrogen storage system if fuel cell vehicles are to answer the needs of the transportation industry.

A second problem that must be resolved for both electric and fuel cell vehicles is the source of the "fuel". If all cars run on electricity, but fossil fuels are still used to generate that electricity in large power plants, we have simply relocated the problem. Cities may be free from smog, but we will still face the problems of limited resources and pollution from power plants. Similarly, the hydrogen used in fuel cell vehicles must come from somewhere. Currently, 95% of the hydrogen produced in the United States comes from reforming methane. If all of the hydrogen supplying fuel cell vehicles came from reforming methane or other fuels such as propane and ethanol, greenhouse gas emissions would be reduced by only 60%.[2] Electrolysis, the splitting of water into hydrogen and oxygen using electricity, is a more appealing source of hydrogen from an environmental perspective, but again requires a clean source of electricity. Research on hydrogen production using sunlight to directly split water into hydrogen and oxygen through photoelectrochemical processes shows promise as a clean source.[3] Alternatively, excess electricity generated by solar and wind power plants operating beyond the demand of the grid can be used as a clean input for hydrolosis.

Storage Parameter	Units	2010	2015	Ultimate
Gravimetric Storage Capacity	kg H_2/kg system	0.045	0.055	0.075
Volumetric Storage Capacity	kg H_2/L system	0.028	0.040	0.070
Min/max delivery temperature	^oC	-40/85	-40/85	-40/85
Cycle life	Cycles	1000	1500	1500
System fill time (for 5 kg H_2)	Minutes	4.2	3.3	2.5

Table 1. Standards for a hydrogen storage system as defined by the Department of Energy.

Assuming that the need for a clean source of hydrogen can be met, this still leaves the need for a storage system that can provide a suitable range to a fuel cell vehicle. The Department of Energy (DOE) has set out a range of basic parameters shown in Table 1 that a hydrogen storage system must meet to be a viable option for use in the transportation industry on a large scale. On the most general level, the three options for meeting these standards are storing hydrogen as a solid, liquid or gas. The focus of the research presented here is on solid state hydrogen storage in metal hydride materials, but it is important to understand the competing alternatives.

1.2 Compressed gas storage

Technology is already well-developed for compressing gas and storing it in high pressure cylinders. However, compressing hydrogen to pressures greater than 10,000 psi takes a large amount of energy, lowering the overall efficiency of the fuel cell vehicle. In addition, safely storing hydrogen under such high pressures requires heavy, bulky storage containers usually made from stainless steel. This further reduces the efficiency of the car, while also taking up potential cargo space.

One of the biggest advantages of the compressed gas storage method is that it has been demonstrated and can be implemented today. Many public transportation buses currently run on hydrogen fuel cells with compressed gas storage, and Honda has developed a car with a 240 mile range with a 5,000 psi tank. The downside is that the technology does not currently meet all of the DOE standards presented in Table 1 and is not likely to improve significantly. Current developments are focused on lightweight carbon fiber tanks, but these are expensive and only address one aspect of the concerns above. Still, compressed gas storage represents the established standard that all competing technologies must surpass.

1.3 Liquid storage

Significant research has also gone into storing hydrogen in liquid form, which requires temperatures below 50 K. Liquid hydrogen (LH_2) already meets the ultimate volumetric storage capacity goal of 0.07 kg H_2/L shown in Table 1, while compressed gas at 10,000 psi has a volumetric storage capacity of only 0.03 kg H_2/L.[2] However, Table 1 lists the parameters required at a system level, and clearly any addition of a cooling system and insulation will reduce the final system volumetric capacity to below the required value. Additionally, the required energy for cooling and maintaining cryogenic temperatures limits the energy efficiency of the fuel cycle. Cooling hydrogen even further to solid state leads to no advantage.[4]

While still in the research and development phase, liquid storage systems have been demonstrated to work on the system level. Current research efforts are focused on optimizing the insulation layers of storage tanks to reduce both the required volume and cooling energy load.

1.4 Solid state hydrogen storage

Solid state hydrogen storage comes in many forms and has much promise for fulfilling the requirements of a hydrogen economy, but is still in the research and development stage. It is the only method of storage which has the potential to meet the volumetric storage criteria listed in Table 1. For example, metal hydrides such as Mg_2FeH_6 can reach a volumetric density of greater than 0.15 kg H_2/L, and could require less supporting structure than liquid systems, making it easier to reach the system level targets.[5] However, the inclusion of transition metals such as Fe with large atomic mass in many metal hydrides leads to materials with a low gravimetric density. Hydrogen makes up less than 5% of the total mass of Mg_2FeH_6. Other metal hydrides offer lower gravimetric densities, but suffer from poor kinetic and thermodynamic properties. No material has yet been identified that can meet all of the requirements in Table 1, but a material can be found that outperforms liquid or compressed gas storage in almost any given category.

Hydrogen is stored in a solid either through absorption in a chemical form or adsorption onto a high surface area material. These two modes of storage are sometimes referred to as chemisorption and physisorption, respectively. Some advanced materials attempt to combine these two effects by distributing hydride forming materials in a high surface area structure, such as Metal-Organic Frameworks (MOF).

1.4.1 Physisorption materials

Physisorption storage materials capitalize on the weak intermolecular forces, also known as van der Waals forces, leading to an increased density of hydrogen in a small region near the surface. Good candidates for storage materials, such as carbon nanotubes and silica aerogels, therefore have high surface area to volume ratios so that a large portion of the sample volume contains hydrogen at increased density. The quantity of hydrogen present beyond what would normally exist at the ambient hydrogen pressure is termed the Gibbs excess capacity, and is the standard measure for the effectiveness of a physisorption storage process.

Since the intermolecular attractive forces are on the order of thermal excitations at room temperature, significant hydrogen storage in physisorption materials often requires cryogenic temperatures. For simplicity, most experiments use liquid nitrogen to test samples at around 77 K. Pressures of up to 20 MPa can also be necessary to achieve hydrogen density near that of liquid hydrogen at 50 K. However, by taking advantage of weak intermolecular forces, it is possible to achieve equivalent storage at higher temperature and lower pressure than either compressed gas or liquid hydrogen storage alone.

1.4.2 Chemisorption storage materials

Chemisorption materials bond hydrogen to the material through valence forces, often leading to a recognized chemical compound. There is no hard line between chemical bonds and physical forces, but this distinction is often not important in hydrogen storage applications. Since valence forces and chemical bonds are often much stronger than van der Waals forces, chemical compounds are more stable and can require a significant input of energy to release the stored hydrogen. It is clearly inefficient to use energy to release a fuel source, so the dependence of the kinetics of a reaction on temperature is a crucial relationship for all chemisorption materials. Fortunately the fuel cell itself generally operates above room temperature, around 80-100 ^{o}C for PEM fuel cells. The DOE standard for the maximum temperature range in Table 1 is derived from this fact.

The ideal material would have fast kinetics at low temperature to allow fueling at a hydrogen station in an amount of time comparable to current gasoline filling times (< 5 minutes), while also releasing hydrogen fast enough to supply a fuel cell reaction. No material exists that meets all of these requirements, so current research is focused on developing catalysts and alloys to improve the kinetic properties of existing materials.

Since the ideal material may never be found, it is important to consider possible compromises to the standards set out in Table 1. For example, it seems impossible to compromise on the kinetics of hydrogen reabsorption, since no consumer would be willing to wait one hour at a fueling station. However, it is possible to consider a system where removable fuel tanks are exchanged at a fueling station and recharged onsite, reducing the kinetics limitations on the rehydrogenation process. This is termed off-board storage, while a tank that can be filled without removal from the car is termed on-board storage. The off-board storage approach would require a large standardization effort across all fuel cell car designers, and is therefore not ideal. Another possible compromise is that consumers may be willing to sacrifice on the range of their car, and therefore be required to stop more frequently to refuel, in exchange for an energy efficient, pollution free vehicle with a fast refueling time.

1.4.2.1 Metal hydrides

Metal hydrides represent a broad category of potential hydrogen storage materials, and will be the primary focus of this work. Figure 1 shows a tree chart of the categories of metal hydrides. The most basic metal hydride is a pure elemental material bonded with hydrogen. One of the most researched elemental hydrides is magnesium hydride, MgH_2, due to its high

theoretical storage capacity of 7.7 wt%. However, many elemental hydrides are highly exothermic and require high temperatures to store and release hydrogen.

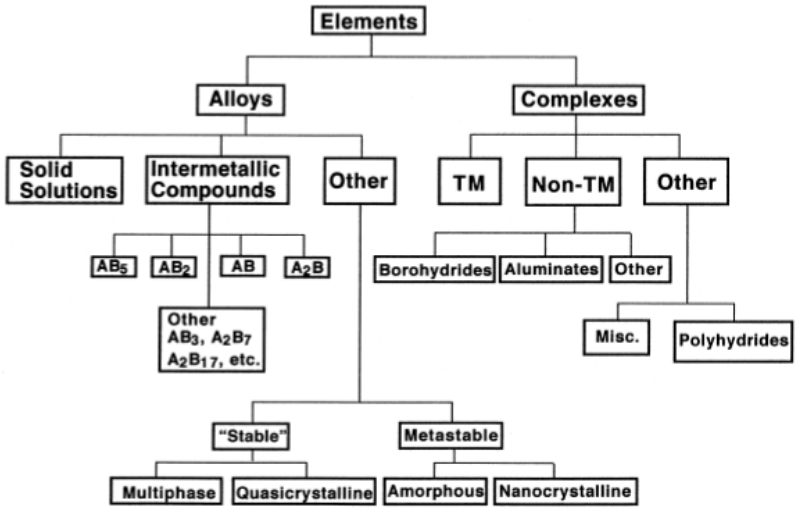

Figure 1. Categorization of various metal hydride types. Intermetallic compounds and borohydrides are of specific interest for this work.

One common technique is to alloy an element which forms a stable hydride with an element forming a less stable hydride. This can be in the form of solid solutions with disordered substitutions and varying composition or intermetallic compounds with a specific crystal and chemical structure. Standard terminology has been developed for intermetallic compounds where A represents a strong hydriding material and B represents a weak hydriding material, which usually each have an integer relation in the stoichiometric composition. Materials with the same ratio of A to B tend to exhibit similar hydrogen absorption behavior, so that $LaNi_5$ can be used as a representative of the AB_5 group and Mg_2Ni is a good representative of the A_2B group for many purposes.

Complex metal hydrides are an interesting subset, characterized by a series of decomposition and recombination reactions which often have a high theoretical storage capacity. Two prime examples of this category are alanates and borohydrides. For example, sodium alanate has a two step decomposition process given by:

$$NaAlH_4 \rightarrow \frac{1}{3}Na_3AlH_6 + \frac{2}{3}Al + H_2 \rightarrow NaH + Al + \frac{3}{2}H_2$$

While sodium alanate has a theoretical storage capacity of 7.4 %, only 3.7% is released in the first step, occurring between 185 and 230 ^oC in the absence of catalysts. An additional 1.9% is released in the second step of the reaction, which occurs at temperatures above 260 ^oC. The remaining hydrogen, 1.8% of the original sample weight, is stored as sodium hydride, which does not decompose below 425 ^oC.[6] Doping with Ti compounds has been shown to significantly reduce these temperatures of desorption.[7,8]

Borohydrides are another category of complex hydrides that are of particular interest. They consist of one or two borohydride ions, BH_4^-, combined with an ion from the first two columns of the periodic table, usually Li, Mg, Ca, or Na. They are attractive candidates due to their high theoretical storage capacities, usually greater than 10%. However, they are also largely exothermic and generally exhibit poor kinetics. Current research is involved in finding methods to destabilize borohydrides or a catalyst similar to Ti compounds for alanates.

The formation reaction of most borohydrides is difficult to achieve. Currently there is no process to regenerate spent borohydrides without a chemical reprocessing step that would be difficult or impossible to achieve without removing the fuel tank from the vehicle. In the long run, a gas phase formation reaction may be necessary for successful implementation of a borohydride hydrogen storage system.

1.4.2.2 Chemical Hydrides

The other main category of materials with potentially favorable properties for hydrogen storage is chemical hydrides. Chemical hydrides are compounds where a heteroatom such as C, B or N forms covalent bonds with hydrogen atoms. Typical examples include hydrocarbons and ammonia. Metal borohydrides are also sometimes considered chemical hydrides as well as metal hydrides. Chemical hydrides are typically largely exothermic and therefore tend to require regeneration outside of the fuel tank of a vehicle. The energy required in the regeneration process is an important component of the fuel cycle which can reduce its overall energy efficiency significantly.

Chapter 2: Fundamentals of Hydrogen Storage

2.1 Introduction

The recent spike in interest in hydrogen storage materials has led to a need for standardized definitions of the properties and measurement methods. The DOE has taken on the project of leading this organization in the form of a document outlining the recommended best practices in hydrogen storage research. The document is a compilation of inputs from various researchers which are then edited by the leading experts in the field. The research presented in this thesis on metal hydrides as regenerable on board storage materials was used to develop significant portions of this document. The following is a brief summary of some of the most relevant sections.

2.2 Thermodynamics of Hydrogen Storage

The thermodynamic properties of a material are the most fundamental, in that they are independent of reaction conditions such as temperature and pressure. It is not always simple to distinguish between thermodynamic properties and kinetic effects, but it is important to understand the difference since different techniques are required to enhance the performance of a material based on whether it is thermodynamically of kinetically limited. The following sections outline a few of the most important thermodynamic properties and concepts for evaluating the performance of hydrogen storage materials.

2.2.1 Equilibrium

There are many definitions of equilibrium corresponding to various properties and applications. For example, chemical equilibrium is defined as the state when the forward rate of a reaction is equal to the rate of the reverse reaction, so that there is no change in the overall chemical nature of the system over time. Similarly, thermal equilibrium is achieved between two objects which exchange no heat and whose temperatures do not change when they are brought into contact.

The definition of thermodynamic equilibrium is broader, encompassing thermal, mechanical, phase and chemical equilibrium, to name a few. The simplest method to determine if a system is in equilibrium is to isolate it from its surroundings. When there are no longer any changes in its observable or measureable properties, then the system is in equilibrium.

Equilibrium can also be described as a minimum in a thermodynamic potential. The Helmholtz free energy is used to describe systems with constant temperature and volume and is defined by Equation 1, where U is the internal energy, T is the temperature and S is the entropy of the system.

Equation 1 $$A = U - TS$$

The Gibbs free energy describes systems at constant temperature and pressure and is defined by Equation 2, where H is the enthalpy of the system.

Equation 2 $$G = H - TS$$

It is clear from this definition that there can be no temperature gradients in a system in equilibrium. Since the assumption of equilibrium is essential to thermodynamics calculations, the concept of local thermal equilibrium (LTE) is used to analyze systems in which temperature gradients are present. LTE can be applied to systems where the variation in properties across space and time is small enough that the molecules surrounding a given point can be assumed to be in equilibrium. This assumption breaks down in systems with large variations in properties or low densities, so that molecules are unlikely to have enough collisions to establish equilibrium even locally.

2.2.2 Reversibility

A process is thermodynamically reversible if the system and its surroundings can be returned to its original state. An equivalent statement is that a process is reversible if each step in the process can be achieved through infinitesimal changes to properties of the system without loss or dissipation of energy so that the system is in equilibrium throughout the entire process. In practice this is impossible, since all real processes lead to a net increase in entropy of a system and its surroundings. Additionally, it would take infinitely long for a system to adjust to infinitesimal changes. However, it is possible for a process to be approximately reversible if the system responds rapidly to small changes. Another approximation is an internally reversible process, where all irreversibilities are assumed to occur in the surroundings so that the system itself could return to its original state.

2.2.3 Enthalpy of Formation

The most important thermodynamic property for hydrogen storage materials is the standard enthalpy of formation, ΔH_f^o. It is defined as the change in enthalpy during the formation of 1 mole of a material in its standard state from its constituent elements in their standard states. The standard state of an element or material is defined as its most stable form at 1 bar and 298.15 K. A material with a negative ΔH_f^o is termed exothermic, since it releases heat during its formation. A material with a positive ΔH_f^o is endothermic and requires an input of heat to form.

The enthalpy of formation is important because it determines the stability of a compound. A material with a largely negative enthalpy of formation will be very stable, since by definition the reverse reaction is endothermic and would require a large input of energy.

The enthalpy of reaction is a more general term. It refers to the change in enthalpy of a specific reaction that does not necessarily include any of the elements in their most stable form. Positive and negative enthalpies of reaction are used to define reactions as endothermic or exothermic, respectively.

It should be noted that an exothermic reaction does not necessarily occur spontaneously, nor does an endothermic reaction occur if an amount of heat equal to its enthalpy of formation is supplied. This is due to the activation energy, which is the amount of energy required to drive a reaction as shown in Figure 2.

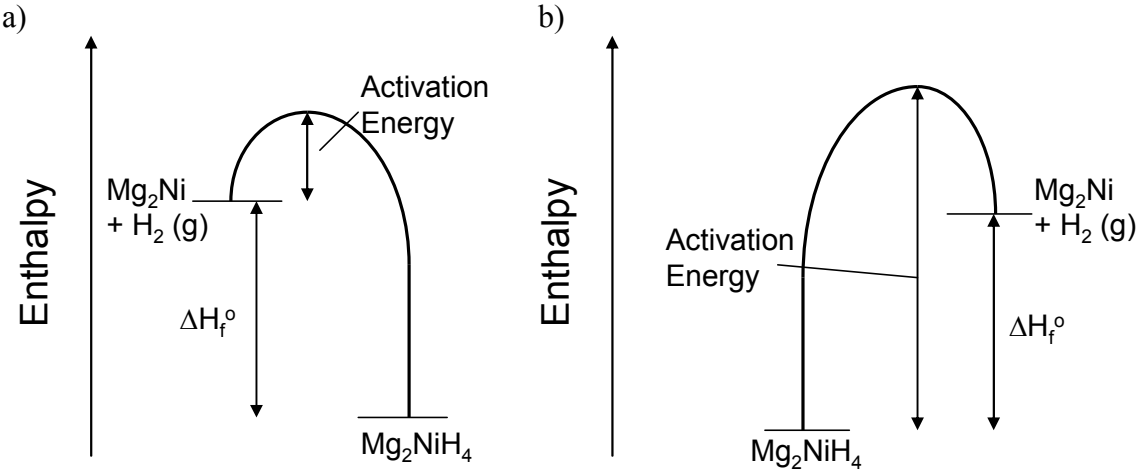

Figure 2. Diagrams depicting the activation energy and enthalpy of formation for a) an exothermic process and b) an endothermic process.

Since this dissertation is focused on improving the performance of hydrogen storage materials, it is important to note here the difference between catalysts and destabilizing elements. A catalyst reduces the activation energy of the reaction, effectively lowering the peak of the curve in Figure 2, but does not change the chemical state of the reactants. Therefore the thermodynamic properties of the material, such as the enthalpy of formation, remain unchanged. A destabilizing element actually raises the enthalpy of the bottom state of a metal hydride formation reaction, making it less exothermic. Since the chemical structure of the reactants is changed, it is also possible for the activation energy to change due to the incorporation of destabilizing elements.

2.2.4 Entropy of Formation

Another important thermodynamic property is the entropy of formation, ΔS_f^o. Similar to the enthalpy of formation, ΔS_f^o is the difference in entropy between its standard state and the final state of interest. In general, the change in entropy in the formation of a metal hydride can be attributed mostly to the change from H_2 gas to H in solid solution in the metal, yielding a standard value of -130 kJ/K•mol H_2.

The entropy and enthalpy of formation can be used to determine the equilibrium pressure of a reaction using the Van 't Hoff Equation:

Equation 3

$$\ln\left(\frac{P_{eq}}{P_o}\right) = \frac{\Delta H_f^o}{RT} - \frac{\Delta S_f^o}{R}$$

where R is the universal gas constant, T is the absolute temperature, P_0 is the standard pressure (1 atm) and P_{eq} is the equilibrium pressure. With knowledge of ΔS_f^o and ΔH_f^o, it is possible to determine the relationship between temperature and equilibrium pressure. Gremaud et. al determined the ideal value of ΔH_f^o for Mg_2Ni system to be -39.2 kJ/mol H_2 for a dissociation pressure of 1 atm at 27 ^oC.[9,10] A better standard might be the DOE targets, which require a dissociation pressure of 3 bar at 85 ^oC. This yields a slightly easier target of ΔH_f^o = -43.3 kJ/molH_2. This target will be valid for any procedure to reduce ΔH_f^o that does not significantly change ΔS_f^o.

2.3 Kinetics of Hydrogen Storage Reactions

While the thermodynamic properties of a material system determine whether or not a reaction occurs at a given temperature and pressure, they say nothing about the rate at which the reaction will proceed. Chemical kinetics is the study of reaction rates, which are determined from a number of factors such as concentration, catalysts, and chemical state in addition to the thermodynamic state variables such as temperature and pressure.

Another significant difference is that while thermodynamic properties require equilibrium for accurate measurements, chemical kinetics are a measure of the time required to reach equilibrium. These dynamic measurements can be difficult to quantify, especially since they depend on measurements which must be taken under an assumption of local thermodynamic equilibrium. This can be a particularly poor assumption for hydrogen storage materials, which are often largely exothermic. For example, the release of heat during the dehydrogenation reaction can lead to a local spike in temperature and large thermal gradients. Since a thermocouple cannot directly contact a sample without interfering with weight measurements, it is often necessary to measure the temperature a small distance away and use knowledge of the sample's environment to predict its actual temperature. For internal comparison, it is possible to use the same setup repeatedly to compare results across samples, but for comparison with outside research performed on different equipment, extreme care is essential.

2.4 Hydrogen Storage Capacity

In defining a standard terminology for hydrogen storage research it is important to consider both the experimental limitations and the end applications. If care is not used in defining measurements, different experimental techniques can lead to vastly different storage capacities reported for the same material system. Due to the variety of possible materials and even physical mechanisms for storage, it is both necessary and involved to create definitions that will be a legitimate metric for comparison.

2.4.1 Capacity and Concentration

Before describing the variety of capacity definitions, it is important to differentiate between capacity, a material property, and the concentration variable in hydrogen storage measurements. Concentration and capacity both provide information about the hydrogen content

of a sample. Concentration is the temporal measure of hydrogen content in a sample and is the most fundamental variable in hydrogen storage; it is also the one important variable that cannot be measured directly. In all cases, calculated relationships are used to determine hydrogen concentration from measurable (independent) variables. Concentration is needed for determining capacity and many other storage properties, including kinetics, thermodynamics and cycle life. Factors that affect concentration measurements will invariably affect the determination of other vital properties of a hydrogen storage material.

Capacity is a material property, not a variable, and therefore does not change with time as long as the sample composition and structure remains constant. In general, it is a measure of the maximum potential concentration of a given storage material. There are many distinctions which can be used to create more informative definitions of capacity which will be presented later in this chapter.

A simple example illustrates the difference between concentration and capacity. Figure 3 shows an idealized PCT isotherm of $LaNi_5$, a well-known hydrogen absorbing material, at two different stages of hydriding. At a specific temperature with a corresponding plateau pressure of 1 bar, the theoretical material capacity of $LaNi_5$ is 1.38 wt.% H_2 corresponding to $LaNi_5H_6$. Neglecting hydrogen in solid solution in the alloy or the hydride, this is the maximum steady-state hydrogen concentration achievable at this temperature and is therefore equal to the capacity. The sample's hydrogen concentration is a measure of hydrogen content which depends on pressure, temperature, time (kinetics and thermodynamics), and the quantity of hydrogen to which the sample is exposed. For example, a sample that has only been exposed to enough hydrogen in one dose to convert half of the sample to the $LaNi_5H_6$ hydride will have a hydrogen that increases in time from 0 to 0.69 wt.% H_2. When equilibrium is achieved, the sample's final concentration will be 0.69 wt.% H_2. Regardless, the sample's capacity under these conditions is still 1.38 wt.% H_2.

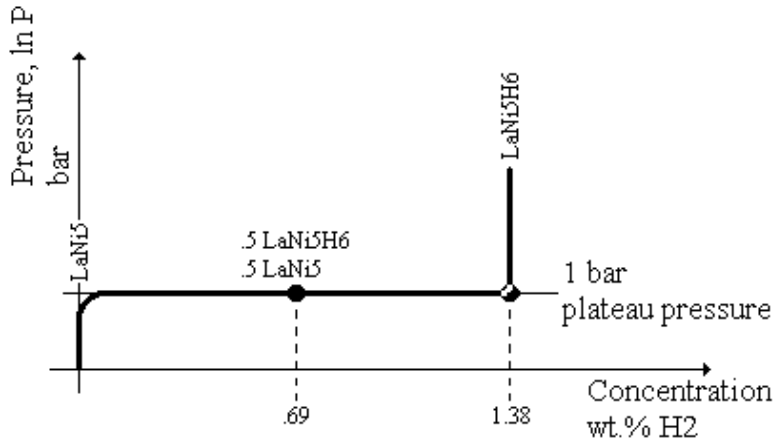

Figure 3. Illustration of classic flat plateau hydride material and relationship between concentration and capacity.

In this regard, concentration is treated as a variable and not a property of a material. Thus, concentration is used to describe the *state* of the material in the same way temperature is used. Capacity, on the other hand, is a specific material property that is dependent temperature and pressure.

Capacity measurements are central to developing materials and systems that meet the criteria established by the US Department of Energy (DOE) for on-board hydrogen storage. However, hydrogen capacity can be defined in a number of different ways which depend not only on the binding mechanisms of hydrogen in a material but also on the issues being addressed with respect to capacity.

2.4.2 Capacity Definitions

In creating the various definitions of hydrogen storage capacity, the first distinction that must be drawn is whether the capacity is determined on a volumetric or a gravimetric basis. In both cases, the mass of stored hydrogen is measured and the value is reported as wt% H_2. The volumetric material capacity is compared to the total material volume (Equation 4), while the gravimetric material capacity is compared to the total material mass (Equation 5). It is also important to distinguish between the capacity and a simple ratio of masses, as demonstrated in Equation 6.

Equation 4 **Volumetric material capacity (wt%) =** $\frac{M_{H_2}}{V_{H_2} + V_o} \times 100 \ \frac{kgH_2}{L}$

Equation 5 **Gravimetric material capacity (wt%) =** $\frac{M_{H_2}}{M_{H_2} + M_o} \times 100 \ \frac{kgH_2}{kg}$

Equation 6 **Ratio of masses =** $\frac{M_{H_2}}{M_o}$

V_o and M_o are the volume and mass of the unhydrided material, respectively. V_{H2} and M_{H2} are the volume and mass of the stored hydrogen, respectively.

A second fundamental distinction is between material capacity and total capacity. Material storage capacity compares the mass of the stored hydrogen to the mass or volume of the absorbing material only. This is the simplest measurement to make in the laboratory, but is not necessarily a great measure of the material's performance on the system level. The system storage capacity compares the mass of the stored hydrogen to the total mass of volume of the storage material and all of the additional components required for system level implementation such as the fuel tank, insulation and any required cooling or heating mechanisms.

Another distinction that is particularly important for the comparison of materials is between the theoretical and usable capacity. The theoretical capacity is the maximum amount of hydrogen that can be stored in a material. While this could be difficult to define for porous media, for bulk metal hydrides this is calculated directly from the molecular formula. The theoretical capacity is most useful in determining whether it is even possible for a material to meet the requirements described by the DOE.

The usable capacity is the amount of hydrogen that can be recovered from a storage material under reasonable temperature and pressure conditions. Taking the DOE standard, this would be all hydrogen desorbed from a material at temperatures up to 85 ^{o}C with a background pressure from 3 to 100 atm.

Name	Definition
Theoretical material capacity	The amount of hydrogen that could theoretically be absorbed in the bulk and adsorbed to the surface of a material and as a gas within the pores and cracks of individual particles of a material. Usually calculated using the molecular formula for metal hydrides and other chemical compounds.
Reversible capacity	The amount of hydrogen that can actually be taken up and subsequently released by a material. This is a thermodynamic definition.
Usable capacity	The amount of hydrogen that can be released by a material within the operating range of temperatures and pressures found in a mobile storage application.
Total material capacity	The amount of hydrogen absorbed in the bulk, adsorbed to the surface of a material, and present as a gas within the pores and cracks of individual particles of a material.
Total system capacity	The amount of hydrogen actually absorbed in the bulk, adsorbed to the surface of a material, and stored as a gas within the pores and cracks in a material and in the free volume of the storage container as a fraction of the total system mass or volume.
Gravimetric material capacity	The fraction of stored hydrogen with respect to the mass of the storage material. This may be energy/mass material, mass H_2/mass material, wt.%, etc.
Gravimetric system capacity	The fraction of stored hydrogen with respect to the mass of the storage system including the vessel and ancillary equipment. This may be energy/mass material, mass H_2/mass material, wt.%, etc.
Volumetric material capacity	The fraction of stored hydrogen with respect to the apparent volume of the storage material. This may be energy/volume material, mass H_2/volume material, wt.% w.r.t. material volume, etc.
Volumetric system capacity:	The fraction of stored hydrogen with respect to the total volume of the storage system including the vessel and ancillary equipment. This may be energy/volume material, mass H_2/volume material, wt.% w.r.t. material volume, etc.
Excess adsorption capacity	Extra hydrogen present due to physisorption (adsorption) to the surface of a material beyond that which would be present in the gas phase absent physisorption.
Maximum excess adsorption capacity	The peak excess hydrogen adsorption capacity at a specific temperature for a range of pressures.
Absolute adsorption capacity	The amount of hydrogen adsorbed to the material's surface of a material.

Table 2. Definitions of hydrogen storage capacity.

Finally, it is useful to describe the advantage gained by adding a high surface area material with little chemical reactivity to a tank of a given volume. This is determined by the excess capacity, which is the amount of hydrogen stored by physisorption exceeding the amount of hydrogen which would be present anyway under the pressure and temperature conditions of the fuel tank. The absolute capacity is a measure of the total amount of hydrogen within the higher density boundary layer near the sample surface due to physisorption. The various definitions of hydrogen storage capacity are summarized in Table 2.

Capacity measurements can be related to the various capacity definitions, as well as the kinetic and thermodynamic properties of the material, based on the conditions of the experiment. Figure 4 represents a typical example of a physisorption measurement where the concentration, measured as the wt% of hydrogen, is plotted vs. pressure. In this plot, the total capacity is slightly over 5.5 wt% H_2, but the usable capacity, considering the usable pressure range to be 3-100 atm, is only about 2.3 wt% H_2.

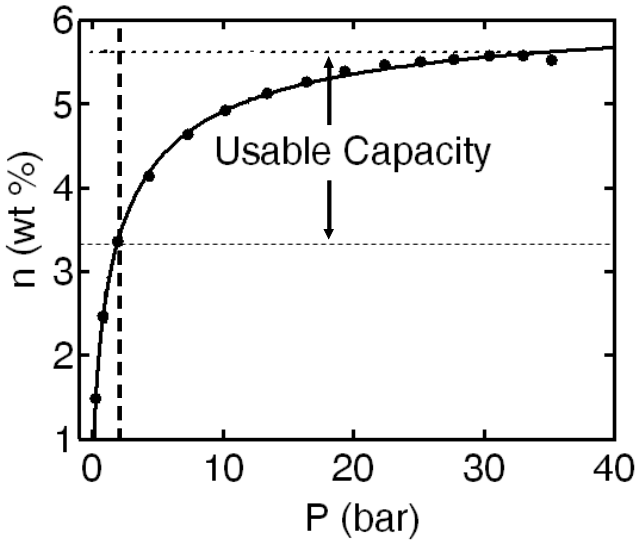

Figure 4. Demonstration of how usable capacity can be much less than the total capacity of a material.

2.5 Hydrogen Storage Measurement Techniques

Many different methods have been developed to measure the properties of hydrogen storage materials, each with their own strengths and drawbacks. It can be difficult to compare results from tests done on different machines with different experimental setups, but the difficulty compounds when a different measurement technique is used. A thorough understanding of all methods is necessary to evaluate and compare the potential materials.

Most measurements are taken using the gravimetric or volumetric method, since they provide the most information. Other common methods include Temperature-Programmed Desorption (TPD) and Differential Scanning Calorimetry (DSC). Each of these methods is used to determine a measurable variable which can then be used to calculate the hydrogen concentration. The rate of change of the concentration can be used to determine the kinetic

properties of the material, the temperature and pressure can be used to determine thermodynamic properties, or the total change in concentration can be used to determine the storage capacity.

It is also important to understand the most fundamental properties of hydrogen storage materials. The core, valence and conduction band electrons can be studied directly using synchrotron radiation techniques. Soft x-rays from synchrotron sources have been developed into an effective tool for studying a range of fundamental properties of specific elements in a material such as charge transfer. Its applications and a few examples will be presented in the next chapter.

2.5.1 Volumetric Method

The basic concept of the volumetric method is that if the temperature and volume of a system before and after exposure to hydrogen are held constant, then the change in pressure can be used to determine the amount of hydrogen absorbed by the sample. This is achieved by using a system of known volumes and maintaining constant temperature using an external temperature controller. Figure 5 shows a typical setup that can be used to make either static or dynamic measurements.

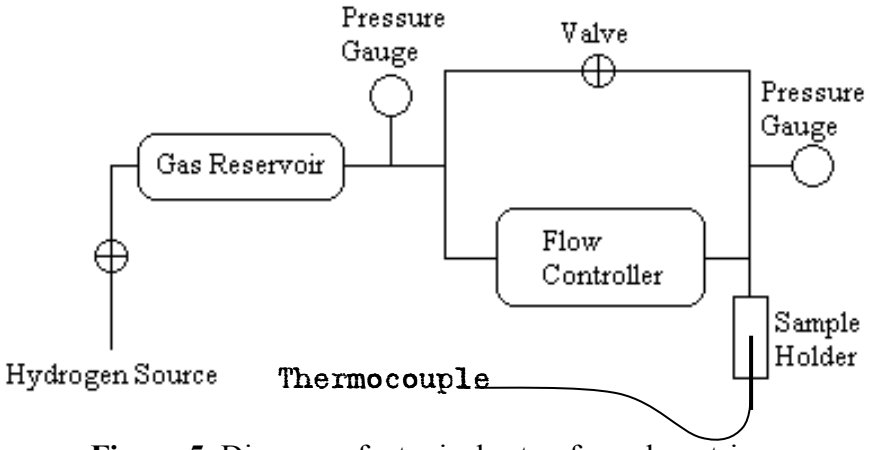

Figure 5. Diagram of a typical setup for volumetric measurements.

In a static measurement the temperature and pressure of the gas reservoir and the sample holder are measured. The valve is then opened and the temperature and pressure are measured again after the system has reached equilibrium. In a dynamic measurement, a flow controller is used to supply a constant, slow flow of hydrogen to the sample. Dynamic measurements must be taken with care, since it is difficult to maintain a constant temperature and conditions close to equilibrium, particularly during measurements of largely exothermic metal hydrides. Of course, it is also important to understand a material's non-equilibrium performance, for which dynamic measurements are ideal.

The largest errors in volumetric measurements come from determining the volume of the sample and measuring the temperature of a material undergoing a largely exothermic reaction. Temperature measurements are the most accurate for small samples attached to a highly conductive substrate so that equilibrium is reached quickly. There is no simple method for reducing errors in the volume calculation, particularly for porous media.

The volume of the sample is most commonly determined through helium pycnometry, which essentially consists of a volumetric measurement using helium instead of hydrogen. Under the assumption that helium does not adsorb to the sample, the volume can be calculated from the change in pressure when a known amount of helium is added to the system. However, this assumption breaks down for large surface area materials, where even a small amount of physisorption can lead to a large error in the volume calculation. At cryogenic temperatures, the ideal gas assumption also breaks down, and it is necessary to use an appropriate equation of state for both helium and hydrogen. Useful functions include the Benedict-Webb Rubin EOS,[11] the Bender EOS,[12] and an unnamed EOS developed at NIST specifically for low temperature hydrogen applications.[13]

2.5.2 Gravimetric Method

The gravimetric method measures the change in weight of a sample as it absorbs or releases hydrogen. Novel hydrogen storage materials can be difficult or expensive to produce in mass quantities, so sample sizes can often be on the order of a few milligrams. Measuring such small samples requires an extremely sensitive balance, sometimes called a microbalance. It can be difficult to mitigate error due to the high pressure and temperature gradients inherently present in the system, but the development of magnetic suspension balances has led to greatly improved accuracy. In a magnetic suspension balance, the harsh environment around the sample is separated from the sensitive microbalance. A magnetic coupling device is used to communicate the weight of the sample between the chambers, as shown in Figure 6.

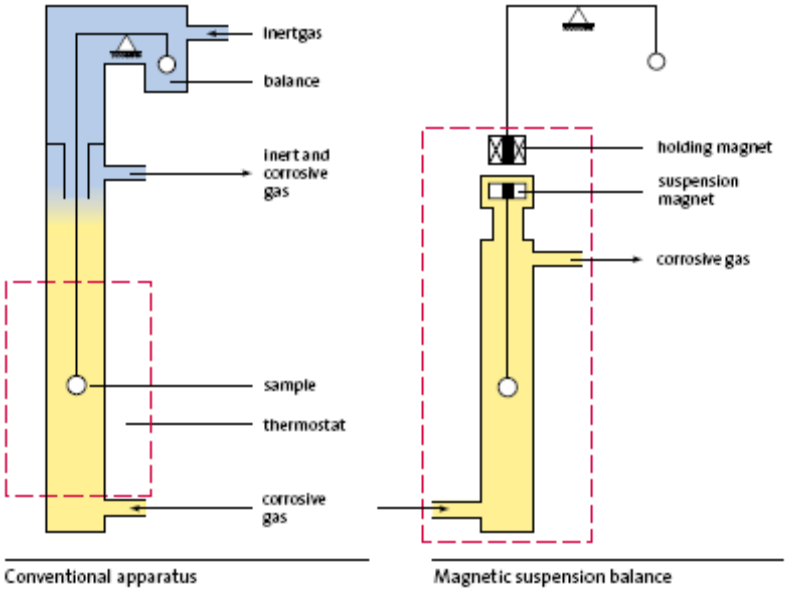

Figure 6. Depiction of the simple experimental setup for gravimetric measurements using a) the standard approach and b) a magnetic suspension balance.[14]

The force measured by the microbalance is the sum of the weight of the sample and the buoyancy force on the sample, given by Equation 7:

Equation 7 $$F = \rho_s g V - \rho_f g V$$

Where ρ_s is the density of the sample and ρ_f is the density of the fluid. At room temperature and pressure, the density of hydrogen is so small that this term can be neglected. However, hydrogen storage experiments are often done at high pressure and either cryogenic or high temperature. Under these conditions buoyancy force becomes significant and a correction factor based on the sample volume and the gas density must be used.

As in volumetric measurements, the sample volume is often measured using helium pycnometry and the density of the fluid, in this case hydrogen or helium, is determined from an appropriate equation of state. If the sample is small, it is important to also determine the density and volume of the sample holder, as this can have a larger contribution to the buoyancy force. If the sample is large, changes in volume due to hydrogen absorption may need to be included in the correction.

The error can be mitigated somewhat by using an inert tare of similar density and volume to the sample and sample holder. If the mass and volume of the tare material are assumed to remain unchanged, then the change in mass of the sample due to buoyancy is given by:

Equation 8

$$\Delta m = \rho_{gas}\left(\frac{m_s}{\rho_s} + \frac{m_{sh}}{\rho_{sh}} - \frac{m_t}{\rho_t}\right)$$

Where the subscript s refers to the sample, the subscript sh refers to the sample holder and the subscript t refers to the tare. It is clear from Equation 8 that if the mass and density of the tare are chosen appropriately, the buoyancy effect is essentially eliminated. Most gravimetric systems are equipped with a tare as shown in Figure 7.

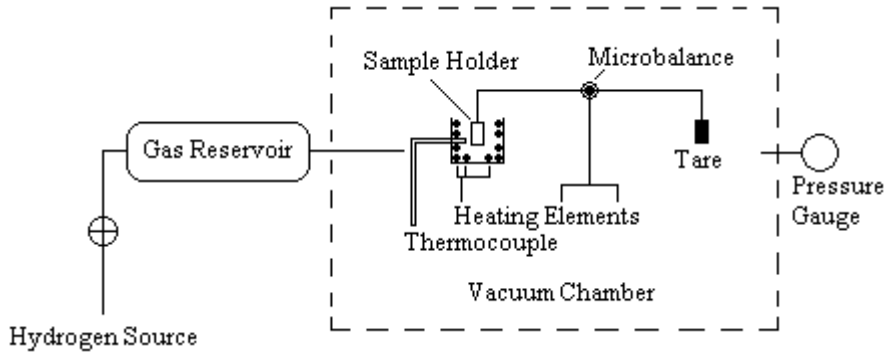

Figure 7. Depiction of a standard gravimetric system setup with a tare**.**

For materials with a significant portion of physisorption, it is important to note that when the buoyancy correction is used, the reported storage is not the total adsorption capacity. The amount of hydrogen that would be present at ambient pressure is subtracted as part of the buoyancy correction, and therefore the reported value is the excess capacity (see Table 2). To determine the absolute adsorption capacity it is necessary to make an assumption about the physisorption boundary layer thickness of the region of increased density. The simplest method is to assume constant density across a conservatively thin estimate of the boundary layer.

In general, most experiments that report using the gravimetric method will measure isothermal properties under varying hydrogen pressure. When the pressure is held constant and the temperature varied, the method is called Thermal Gravimetric Analysis (TGA). This is often used as a technique to determine the desorption temperature of hydrogen storage materials, but the reported numbers must be considered carefully. Most TGA experiments are conducted in an

inert atmosphere, while in a real application the material will be exposed to at least 1 bar H_2 pressure, which could have a significant effect on the desorption temperature.

2.5.3 Temperature Programmed Desorption

Temperature-Programmed Desorption (TPD) refers to a wide range of experimental methods that rely on temperature variation and generally include mass spectroscopy to investigate and quantify desorption reactions. The technique can be used for both reversible and irreversible processes, with the latter referred to as Temperature-Programmed Reaction Spectroscopy (TPRS).

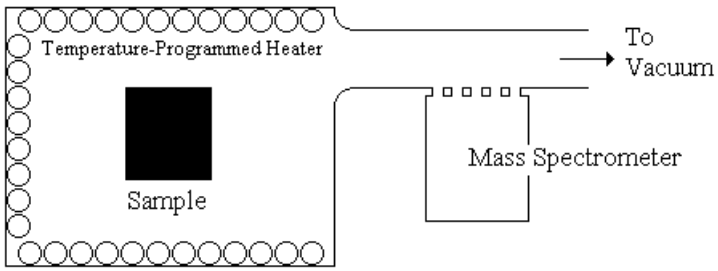

Figure 8. Schematic of typical Temperature-Programmed Desorption experimental set-up.

TPD measurements may be as simple as measuring pressure rise in a volumetric instrument or weight loss in a gravimetric instrument while ramping the sample temperature. However, TPD most often refers to desorption measurements coupled to a mass spectrometer. The basic set-up for TPD techniques is illustrated in Figure 8. The sample is loaded into a temperature-programmed heater contained in a vacuum chamber and charged with hydrogen until fully loaded. Hydrogen loading may also be performed in a separate apparatus prior to putting the sample in the TPD instrument. After the remaining gas has been drawn off, the computer-controlled heater slowly raises the temperature of the sample. This releases hydrogen that is immediately evacuated, maintaining a dynamic vacuum. A mass spectrometer connected to the evacuation line analyzes the composition of the desorbed gas and quantifies the amount of hydrogen desorbed by the sample. As with other methods that employ simultaneous mass spectrometry analysis, TPD systems have an advantage, in that they can distinguish between hydrogen and other constituents in the evacuated stream.

Concentration, temperature and time data is obtained during TPD measurements and can be used to determine capacity, kinetic and thermodynamic properties of a material. A common data representation format for TPD experiments is shown in Figure 9.

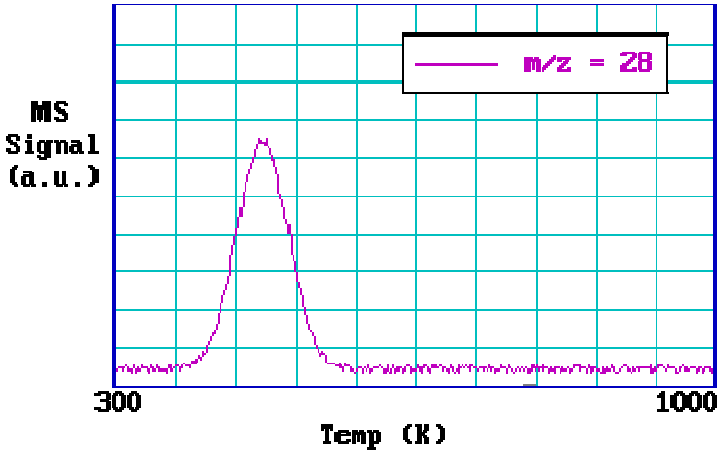

Figure 9. Typical data representation of single-component TPD experiment with CO.[15]

The area under the peak at ~475 K in Figure 9 is proportional to the amount originally absorbed by the sample. In the case of full charging, it represents the capacity of the material. Kinetic information is obtained from the contour of the spectroscopic peak and knowledge of the relationship between temperature and time based on the computer program. Lastly, the temperature associated with the peak is related to the reaction enthalpy of hydrogen-substrate desorption. Unfortunately, TPD measurements can only be done in vacuum due to limitations in analytical equipment, limiting the amount of thermodynamic information that can be collected. Quantitative analysis requires accurate calibration of the mass spectrometer against known flow rates. It is also important to understand that TPD or any other type of dynamic measurement gives results that depend on a combination of both the thermodynamic and kinetic properties of the hydrogen storage material. This may lead to misinterpretation of the results. For example a decrease in desorption temperature of a material that is modified through the addition of a dopant could mean that the thermodynamics of the host material has been altered. However, it is also possible that the dopant acts as a catalyst, increases the thermal conductivity, or modifies the morphology such that the kinetics is improved. For the development of new materials it is important to have information on both the dynamic and equilibrium hydrogen sorption behavior of the storage material.

2.5.4 Differential Scanning Calorimetry

Differential Scanning Calorimetry (DSC) is a thermal analysis technique used to investigate the thermodynamic properties of a material by measuring the energy necessary to maintain a sample material and an inert reference material at the same temperature over a range of conditions. The relative heat flow to the sample material as a function of temperature can be used to determine thermodynamic properties of the material such as the specific heat and enthalpy of reaction.

Temperature variation in DSC is controlled by a computer and is typically linear in order to simplify calculation, although nonlinear temperature variation can be used as well. The specific heat at constant pressure, C_p, of a sample material as a function of temperature on a per mass unit basis is determined by Equation 9:

Equation 9

$$c_p(T) = \left(\frac{\partial h}{\partial T}\right)_p = \frac{q(T)}{\frac{dT}{dt}(T)}$$

T is the temperature, h is the enthalpy, q is the heat flow and t is the time. The heat flow can be taken from the data and the temporal temperature variation is based on the computer program controlling the experiment. In this way, the specific heat as a function of temperature can be determined. Furthermore, the enthalpies of reactions can be determined from the measurement. For example, the enthalpy of crystallization is calculated by integrating the specific heat capacity determined from Equation 9 between the temperatures at which the heat flow varies ($T_{c,1}$ and $T_{c,2}$).

Equation 10

$$\Delta H_{crys} = \int_{T_{c,1}}^{T_{c,2}} c_p(T)dT$$

The two most commonly used methods for conducting DSC measurements are power-compensation DSC and heat-flux DSC. In the power-compensation method, the sample and reference material are placed in independent, identical furnaces. The furnaces are maintained at the same temperature over a variety of temperatures by varying the power input. The power input and temperature data are used to construct the DSC diagram. The indirect and direct variables in power-compensation DSC are flipped in heat-flux DSC. The sample and the reference material are placed in one furnace and exposed to the same heat flux. The variation in temperature between the sample and reference is used to determine the relationship between heat flux and temperature.[16]

In the context of hydrogen storage, DSC is primarily used for desorption testing because DSC equipment is not typically designed to handle the high pressures required for sorption. The advantage of DSC over other methods is that other thermal events such as melting or crystal structure changes may be observed. A significant limitation for testing hydrogen storage is that there is no way to determine the amount of hydrogen desorbed by a sample, only the total enthalpy change of a given reaction. For instance, DSC alone would be unable to distinguish between a material that desorbs 0.1 mol H_2 with an enthalpy of reaction of 30 kJ/mol H_2 and one that desorbs 1 mol H_2 with an enthalpy of reaction of 3 kJ/mol H_2. This can be remedied by coupling DSC with a mass spectrometer.

2.6 Types of Measurements

The techniques presented in the previous section can be used to measure a variety of properties related to the kinetics, thermodynamics and capacity of hydrogen storage materials. Similar techniques can often be applied to determine many material properties simultaneously if experiments are well planned. This section will focus on the details of a few of the most important types of experiments and the care that is required to obtain accurate results.

2.6.1 Kinetics

Kinetics measurements track the rate of change of hydrogen concentration in a sample after the sample has been perturbed from equilibrium. Perturbation from equilibrium is accomplished by changing the thermodynamic state of the sample's environment, causing the sample to absorb or desorb hydrogen to restore equilibrium. Kinetics measurements using the gravimetric and volumetric methods are generally conducted under isothermal conditions, with changes in pressure used to perturb equilibrium. This is done partly for compatibility with the Pressure-Composition Temperature measurements present in the next section and partly because of the profound effect of temperature on the kinetic character of almost all materials.

It is instructive to introduce a few fundamental features common to almost all kinetics measurements. The degree of perturbation from equilibrium is the driving force behind absorption/desorption in hydrogen storage materials. Large perturbations cause relatively large rates of change in concentration while smaller perturbations cause relatively small rates of change. The rate of change of hydrogen concentration in a sample is largest at the beginning of a kinetics measurement, when the sample is furthest from equilibrium with its environment. The distance from equilibrium diminishes as hydrogen is sorbed by the sample, slowing the sorption rate as the sample reaches a time independent equilibrium concentration.

2.6.2 Pressure-Composition Isotherms

The most common application of the gravimetric and volumetric measurement techniques is in compiling Pressure-Composition-Temperature (PCT) plots. In this context, composition refers to the concentration of hydrogen in the sample. A PCT measurement is a collection of data points that represents the pressure, concentration and temperature of a sample in equilibrium and relates the influence of the thermodynamic variables on concentration. PCTs are also commonly referred to as Pressure-Composition Isotherms (PCI) because they are taken at isothermal conditions. This minimizes the number of free variables and allows the relationship between concentration and pressure to be presented in two-dimensional graphs. The effect of temperature on hydrogen storage properties can be determined by comparing PCT isotherms at various temperatures. Because PCTs represent a sample in equilibrium, they can also be used to determine the thermodynamic properties of a hydrogen storage material. Unfortunately, the absolute interpretation of PCT data must be kept in perspective because it is difficult to make true equilibrium measurements. This is because as the pressure approaches the true equilibrium pressure, the driving force becomes diminishingly small and kinetics becomes increasingly slower. In other words, it would take an infinitely long time to reach equilibrium.

It is instructive to conceptualize the relationship between PCT measurements and kinetics measurements in the volumetric method as follows: a sample is perturbed from equilibrium by a change in the pressure of the system and is allowed to reach equilibrium through the dynamic process represented by a kinetics measurement. The last data point of each kinetics measurement, which most closely represents equilibrium, provides a single point of hydrogen concentration, pressure and temperature at equilibrium. In the volumetric method, this dosing process is performed repeatedly at one temperature until enough equilibrium data points are collected to construct a full PCT diagram. In this sense the PCT measurement can be thought of as a cumulative series of kinetics measurements.

2.6.3 Van 't Hoff Plots

Van't Hoff plots are typically generated from a series of PCT measurements at various temperatures. The equilibrium desorption plateau pressure from each isotherm is plotted on a log scale vs. the inverse of temperature. When the assumptions used in determining the van 't Hoff equation, Equation 3, are valid, the slope of a van 't Hoff plot will be linear and, for exothermic materials such as most metal hydrides, negative. The van't Hoff equation, can then be used to relate the slope to the enthalpy of reaction and the y-intercept to the entropy of reaction.

Van 't Hoff plots are also a useful mechanism for comparing the operating temperature and pressure of various materials. However, it is important to keep in mind that while a material look favorable on a van't Hoff plot, no information is given of the storage capacity of the materials. For example, $LaNi_5H_6$ has favorable thermodynamic properties, maintaining an equilibrium hydrogen pressure of about 1 atm at room temperature, but a theoretical storage capacity of only 1.38 wt%.

A van 't Hoff plot contains a lot of valuable information, but only if constructed properly. First, it is important that all of the points used in the van 't Hoff plot are taken from a point on the pressure plateau corresponding to the same hydrogen concentration. A common choice is the center of the pressure plateau. This consistency is particularly important for materials which tend to exhibit a sloping plateau. While many reversible chemical hydrides show a flat pressure plateau, metal hydrides can have a large slope even under equilibrium conditions. The slope of the plateau is due to lattice defects or atomic disorder. In general, a higher degree of disorder will lead to a large slope.[17]

Additionally, it should be noted that the van 't Hoff equation is an approximation, so not all measured profiles will fit a linear profile. One of the most important assumptions is that the enthalpy of formation is independent of temperature. If nonlinear effects appear to be important, the nonlinear integrated from of the van't Hoff equation can be used.[18]

Another important aspect of constructing van't Hoff plots from PCT curves is whether the pressure plateau points are taken from absorption or desorption measurements. These values will typically differ due to hysteresis, even if perfect equilibrium is achieved, which generally causes a lower pressure plateau during desorption measurements. The specific application will determine whether absorption or desorption points are preferred, but desorption points are more commonly reported. This is because the desorption temperature is one of the most important variable affected by the thermodynamics, so most measurements are attempting to reduce the enthalpy of reaction in order to lower the desorption temperature.

2.7 Experimental Considerations

The wide range of materials and equipment involved in the study of hydrogen storage materials can lead to practical difficulties in obtaining consistent results that can readily be compared to those of the international research community. The following sections describe some specific concerns which require consideration when planning hydrogen storage experiments.

2.7.1 Desorption vs. Sorption Testing

Storage capacity can be tested by either charging an uncharged sample or discharging a charged sample. The desorption approach is preferred because of the lower pressures and larger reservoir volumes associated with desorption, in contrast with the higher pressures required to drive the sorption reaction. Lower pressures and larger reservoir volumes significantly reduce the errors associated with measurements and capacity calculations.

To illustrate the advantage of desorption-based capacity testing, consider a 1 g sample of storage material with an excess material capacity of 10 wt% hydrogen (0.05 mol H_2) that is tested with both methods at room temperature. During sorption, the amount of gas in the reservoir must be much greater than that in the sample and the equilibrium pressure in the system must be much greater than the pressure of maximum sorption to drive the reaction to completion in a reasonable period of time. A gas reservoir of 200 mL and 20 bar contains .16 mol H_2. If the pressure transducer used is rated to 200 bar and is accurate to +/- 1%, then the corresponding error is .016 mol H_2, over 30 % of the excess material capacity of the sample (10 wt.% +/- 3 wt.%). In comparison, if a larger reservoir (1 L) and vacuum are used for desorption and the low-pressure transducer is rated to 10 bar with the same +/- 1% accuracy, the corresponding error measurement is .004 mol H_2. This represents an error of only 8 % of the sample (10 wt.% +/- .8 wt.%). With this simple calculation it is apparent that desorption testing, with its associated lower pressures and higher volumes, delivers more accurate results than the sorption-based alternative in many cases.

2.7.2 Gas Composition

Both gravimetric and volumetric methods rely on the assumption that weight change and equilibrium pressure change during sorption is due to hydrogen gas alone. Unfortunately, this assumption is not always valid. Many materials evolve gases other than hydrogen during decomposition or simply release adsorbed contaminants. These evolved gases can contribute to weight change and equilibrium pressure change measured with gravimetric and volumetric methods, respectively, and can create significant error in experimental data. One way to account for non-hydrogen gases is to use a residual gas analyzer (RGA) to determine the composition of the desorbed gas. The RGA is connected to the outlet line of the sample holder and tests a representative sample of the evolved gas, outputting the relative composition via the partial pressures of the individual species. An RGA does not perform chemical analysis, but rather reports only the molecular weight of components of the gas mixture. For example, hydrogen would show up as a peak at mass 2. However, both deuterium and helium would cause a peak at mass 4, so it is impossible to distinguish between them using just an RGA.

A good example comes from RGA analysis of the gas evolved from a titanium-doped alanate-amide mixture ($LiH + Al + 2LiNH_2 + Mg + TiF_3$) during desorption. Peaks in with mass of 16-18 and 26-31 indicate that the evolved gas was not entirely hydrogen, as shown in Figure 10. Inspection of the reactants indicates that the first peak is likely a combination of ammonia and water, while the second peak is probably composed of residual hydrocarbons in the test chamber which are a common background signal.

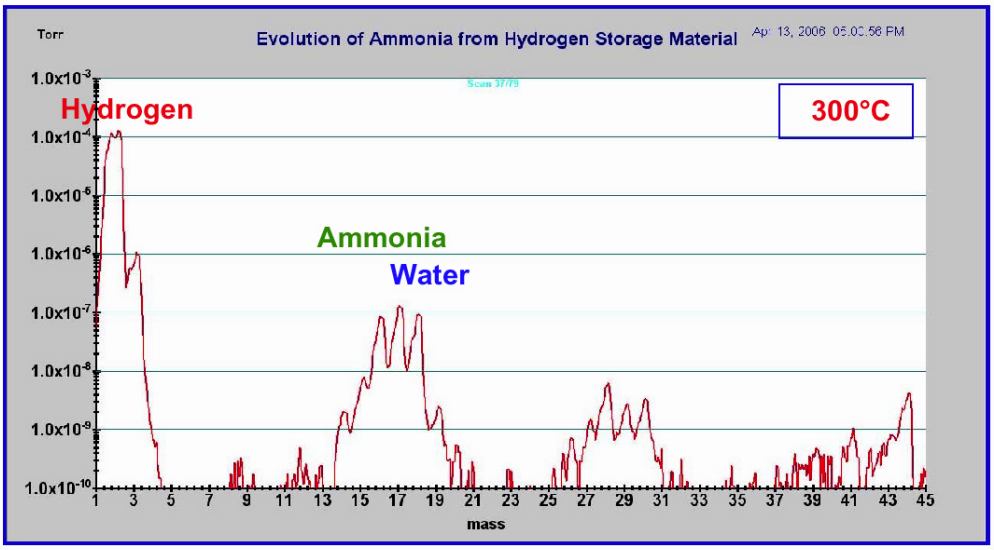

Figure 10. Residual gas analysis of an alanate-amide sample.[19]

Water is a common contaminant of hydrogen storage materials, generally due to adsorption from air due to improper sample handling prior to testing. The presence of ammonia is much more interesting in this case. Under elevated temperature, the alanate-amide mixture reacted to form ammonia although the exact mechanism for the reaction is unclear. This type of unforeseen gas evolution shows the need to account for desorbed gas composition variation to validate the assumptions inherent in the gravimetric and volumetric methods. However, unexpected gas evolution is less common in metal hydrides since the metals involved tend to be stable in metallic form after releasing hydrogen.

2.7.3 Leaks

Leaks in the connections of volumetric hydrogen storage testing equipment can be another significant cause of errors in the data. In kinetics measurements, they cause absorption or desorption profiles to appear linear in time, as opposed to true sorption profiles that usually have a curved profile. During absorption testing above ambient pressures, gas leaked to the environment is mistakenly thought to be absorbed by the sample. Leaks during sub-ambient desorption also affect the capacity by increasing the reading of the amount of gas desorbed with time. An example of this is demonstrated in Figure 11, where the expected capacity of the sample is 1.39 wt% H_2. Absorption steadily increased with a linear behavior until a fitting was tightened about 2 hours into the experiment. The potential for leaks also suggests the practice of double checking all experiments which result in an equilibrium pressure of 1 atm. While plateau pressures at exactly 1 atm are possible and even desirable, they are also unlikely.

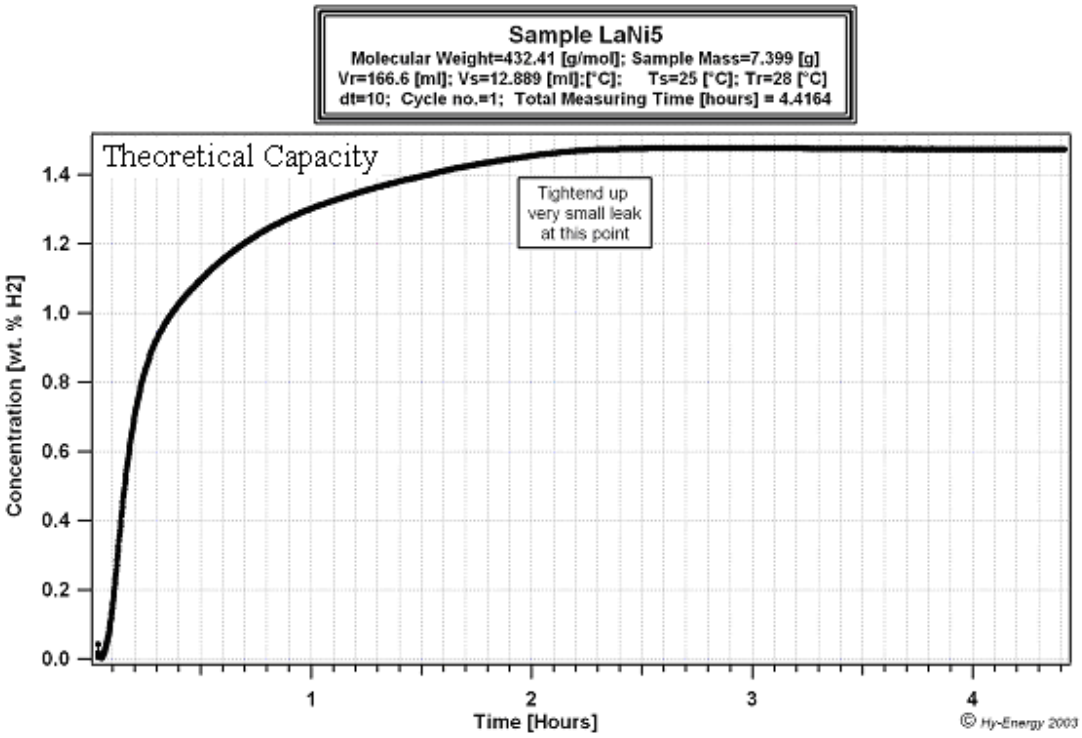

Figure 11. Example of a leak on kinetics measurement. A little after two hours into the experiment, the leak was eliminated.[19]

Absorption testing of on-board reversible materials such as most metal hydrides is often done at higher pressure where a leak might be more obvious, especially in a static measurement. However, for practical applications pressures near atmosphere are desirable for supply to a fuel cell and for safer fueling.

2.7.4 Materials Preparation and Handling

The determination of a sample's purity or at least its chemical composition is clearly important, but the impact of materials preparation and handling on chemical composition is often overlooked. For reversible materials, it is critical to measure hydrogen uptake and release over several cycles as the formation of unintended by-products or the preferential migration of elements to suboptimal sites may reduce the hydrogen storage capacity of the material.

Impurities or wholly inactive side products are unavoidable in most sample preparation techniques; it is simply a matter of reducing and understanding their impact. An inactive contaminant will simply reduce the total capacity of a material, but some impurities may have an effect on the hydrogen uptake or release capacity and/or kinetics. These additions do not necessarily produce poor results. For example, the accidental inclusion of a catalyst could enhance the kinetics of a sample. Careful sample characterization is therefore an important step in any hydrogen storage test to identify all potential impurities.

These issues are often most consequential for high-surface-area materials because the level of impurities generally scale with the amount of active surface area. Impurity issues are also most difficult to identify in high-surface-area materials because while impurities may be

present in significant quantities, they may be dispersed in only a few monolayers, present as nanoparticles, or amorphous in nature and not readily observable using common analytical methods such as X-ray diffraction.

It is also important to understand the possible reactivity of all of the intended components of a sample. For example, the presence of a catalytic metal that itself forms a reversible hydride could easily lead to unexpectedly high capacity measurements. On the other hand, the use of unstable oxides that may react with hydrogen to form water can lead to poor performance after just a few cycles. Some catalysts may be involved in even more complicated scenarios. For example, a sample of unreacted $NaAlH_4$ + $xTiCl_3$ may produce more hydrogen on its first desorption than expected from the decomposition of $NaAlH_4 \rightarrow NaH + Al + 3/2H_2$. This is because in the process of decomposition NaH may react with $xTiCl_3$ to form xNaCl releasing x/2 H_2.[20] If only one cycle was tested, the results could readily be interpreted too favorably.

Understanding the method by which impurities may be incorporated in a sample can help with their identification. For example, thin film deposition techniques such as sputtering can coat the entire deposition chamber with a thin material of the deposited material. Later depositions may cause resputtering from the walls of materials used in previous sample preparations. This is particularly important for lightweight materials such as Mg. Knowledge of previous activity in a deposition chamber can assist in the detection of unwanted impurities. Another example comes from the common practice of ball-milling to introduce catalysts, create defects, or produce nanostructured materials. The milling pot and balls themselves may introduce metals into the samples such as Fe, Cr, or W. Enhancement of the kinetics may not be coming solely from intentionally added catalysts, but rather the components of the ball mill may be participating as well.

A well-controlled series of sorption tests of the materials after exposure to known quantities of contaminants should provide insight into the sensitivity of the materials to impurities during preparation and/or testing. However, it is difficult at best to perform hydrogen sorption testing on materials in an ultra-high purity environment, and it is unlikely that in the real world application for which the materials are being developed that any hydrogen storage system will ever operate under Ultra High Purity (UHP) conditions.

2.7.5 Surface Conditions

Imperfect materials preparation and handling often has the greatest impact on the surface of the material. The most common defect is surface passivation, which is the formation of a non-reactive surface film, often either an oxide or a nitride. Oxidation may prevent the dissociation of molecular hydrogen gas to atomic hydrogen at the surface or prevent the diffusion of hydrogen from the surface into the bulk. This can be a significant problem, since many of the materials of interest, such as Mg and Li, are readily oxidized by water or oxygen. Even a thin surface oxide layer can block hydrogen diffusion into the bulk of the sample, leading to drastic reductions in the measured capacity and kinetics. Depending upon the nature of the surface coating, the effects of surface passivation can be mitigated by annealing or cycling the sample.

For fundamental studies, this problem is often mitigated by using a capping layer to protect the surface. The capping layer is typically 5-20 nm thick and composed of a material resistant to oxidation such as palladium or nickel. These materials also offer an aid studies by catalyzing hydrogen dissociation and uptake, making it possible to run experiments fundamental

studies at lower temperature and pressure. However, extreme care is still necessary to limit surface oxidation since even trace amounts of oxygen or water can contaminate the sample surface of many materials. It is also important to understand how the catalyzing effects of the capping layers might impact the results of the study.

Still, it is extremely difficult to eliminate all potential oxidizing agents. For example, thin films are often deposited in high vacuum conditions, but even at a pressure of 10^{-6} Torr the primary constituent of the residual gas in the chamber is water vapor evaporating from the chamber walls. In a worst-case scenario where all of the gas molecules in the chamber are water vapor and all impinging molecules stick to the surface, the monolayer formation time is about 3 seconds.[21] Therefore in imperfect vacuum conditions there may be some surface passivation even before the capping layer can be deposited. Similar logic also applies in the case of using glove boxes to limit exposure to an oxidizing atmosphere.

Since it is impossible to prevent all exposure to oxidizing elements, all samples should be subjected to exactly the same conditions as much as possible. This includes establishing a standard cleaning procedure for targets before deposition (e.g. sputtering for 15 seconds before opening the shutter to begin deposition), setting a standard vacuum level for deposition and exposing a sample to ambient or glove box conditions for the same amount of time.

2.7.6 Capacity and Kinetics

Ideally, capacity measurements of reversible materials should be taken at thermodynamic equilibrium, regardless of the time required to reach equilibrium. However, the amount of hydrogen absorbed or released from a reversible storage material is dependent on the kinetics of the sorption process which is strongly dependent on the type of material and the pressure and temperature conditions. While a material might demonstrate high hydrogen storage capacity, the actual amount of hydrogen practically available may be significantly less depending on the material's intrinsic kinetics as well as the system's ability to deliver hydrogen due to heat transfer, gas flow through the material and other considerations.

While total capacity is the amount of hydrogen released after an infinite amount of time at a given temperature and pressure, in reality the kinetics of many materials are so slow that one must conclude a hydrogen capacity measurement after some reasonable period of time even if equilibrium has not been reached. An example would be to take the final measurement when the material capacity has reached 95% of its asymptotically projected capacity.

Another important consideration is that the output of a measurement device tends to change or drift with time. Thus, unless these devices are continuously recalibrated in some manner, the measurement of capacity over long periods of time is more prone to errors that relatively short measurements. Since the measurement time for some experiments on metal hydrides can be on the order of months, this factor cannot be overlooked.

2.7.7 Hysteresis

Any measurement will have some hysteresis when a variable, such as temperature or hydrogen pressure, is ramped up and down. Hysteresis can be due to properties of the material, deviations from equilibrium, errors in the measurement devices, or combinations of all of the

above. Hysteresis due to measurement devices is commonly contained within the expected error of the devices, so this section will focus on the causes with more physical meaning.

The most important occurrence of hysteresis in hydrogen storage measurements is in PCT measurements where different observations are made between absorption and desorption runs. This is most often due to insufficient time to reach equilibrium, intrinsic properties of the material, or most commonly both. Both causes can lead to variations in the plateau pressure, with the observed value for absorption runs typically being higher. A variation in the hydrogen concentration at which phases changes occur has also been observed, and is more likely due to intrinsic properties.[22]

Intrinsic hysteresis is observed for nearly all metal hydrides. It is of considerable interest as it represents a loss of efficiency in energy storage and has been the focus of study since the investigation of the phenomena in the Pd-H system by Ubbelohde in 1937.[23] A number of models and theories have been proposed concerning the origin of hysteresis.[24] The most promising models focus on the variation in plastic deformation and dislocations during hydride formation and decomposition,[25,26,27,28] which is supported by experimental evidence of dislocations during both formation and decomposition reactions.[29,30]

One significant consequence of hysteresis effects in metal-hydrides is that the capacity at a given pressure will be dependent on whether one references the absorption or the desorption data. Likewise, hysteresis may have a profound effect on the actual hydrogen storage capacity of a material system for many applications. This is demonstrated in Figure 12 for a hypothetical material with a realistic amount of intrinsic hysteresis.

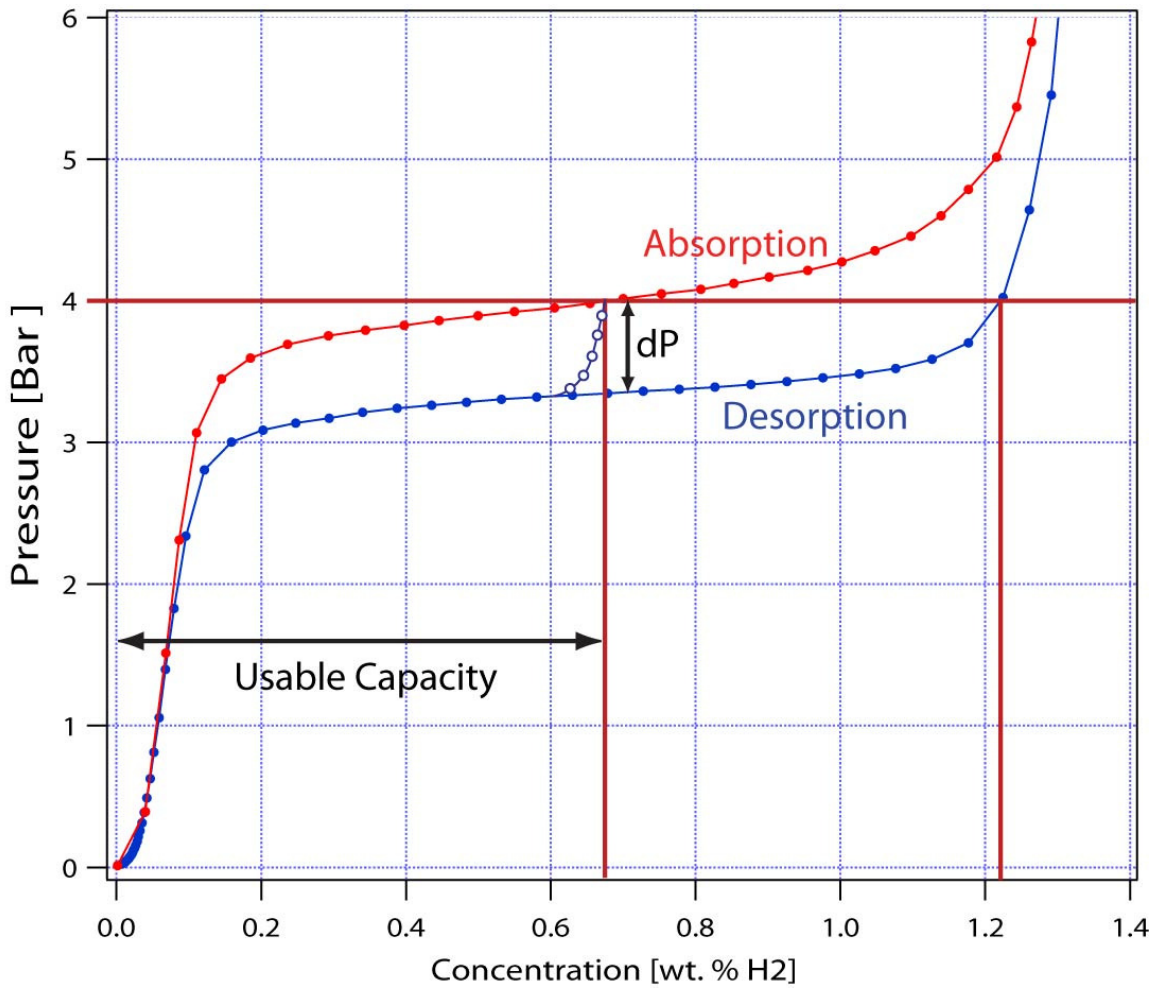

Figure 12. Depiction of absorption (red) and desorption (blue) PCT profiles for a material at one temperature. Open (blue) circles represent the effective desorption curve where the material only charged with hydrogen at a maximum pressure of 4 bar.

At a given constant operating temperature, the intrinsic material hysteresis presents itself as a difference in pressure dP between absorption and desorption PCT isotherms. This means that if the upper pressure limit of a storage system is 4 bar, the full theoretical capacity (1.2 wt.%) that could be discharged from the material could not be achieved in practice. This is because the maximum amount of hydrogen that could be absorbed before reaching equilibrium at 4 bar is only about half this capacity (~0.66.wt%). The effective desorption curve is shown as open circles. Thus, the usable capacity of such a material under these operating conditions is effectively half of its total hydrogen capacity.

From the practical perspective of the result obtained from PCT measurements it is important to understand that the difference between measured absorption and desorption pressures may be simply due to kinetic effects and the inability to reach true equilibrium at each step within a reasonable period of time. It is difficult to distinguish the two effects without looking at the time dependency of the approach to an equilibrium pressure at each data point in a PCT measurement. Ideally, one would want to have a test at each data point to ensure that equilibrium has been reached before moving on to the next data point. This is often

accomplished with automated equipment by setting a lower limit on the rate of concentration change that must be achieved before automatically moving to the next data point.

One simple approach to distinguish between hysteresis due to kinetics, i.e. a non-equilibrium measurement, and intrinsic hysteresis, a material property, is to run a series of PCT absorption and desorption isotherms for different durations of time. Other methods include using different dosing rates for volumetric measurements or different rates of increasing pressure for gravimetric measurements. An illustration of this is shown in Figure 13, which shows that as the time allowed for the absorption or desorption process is increased the plateau pressures will drop for absorption and increase for desorption. Given enough time the measurements should reach steady state equilibrium conditions such that making measurements of longer duration will no longer change the results.

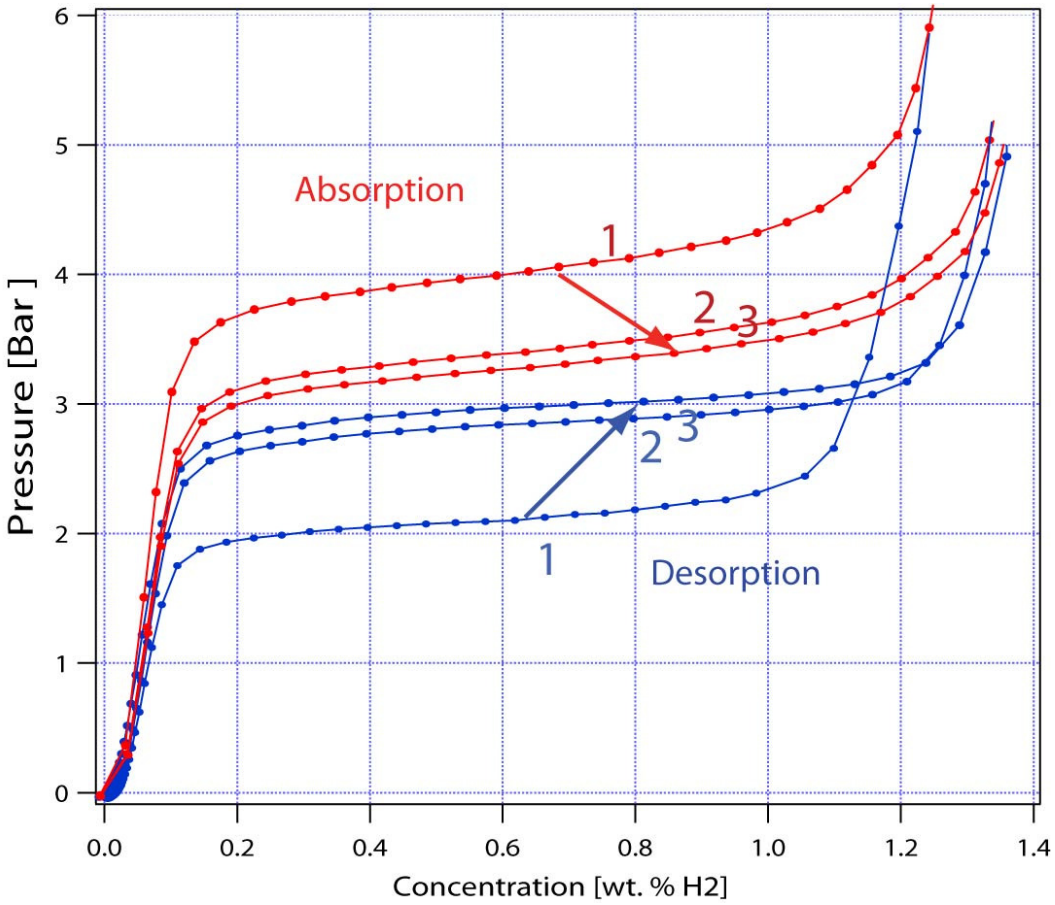

Figure 13. Depiction of absorption (red) and desorption (blue) PCT measurements made over increasingly long (1,2,3) periods of time.

In theory, it should be possible to extrapolate the time resolved pressure changes in volumetric measurements to obtain final equilibrium pressures.[31] Recent results on the hydrogenograghy of Mg-Ni-H thin films have employed such an analysis for evaluating equilibrium pressures using optical transmission measurements under controlled pressure.[32] A caveat to this is that there is some evidence that final equilibrium pressures may not be identical depending on whether hydrogen is introduced to the sample in doses or continuously.[33]

Ultimately, it is important to verify that the system has reached a close approximation to thermodynamic equilibrium when making PCT measurements. This is best achieved by observing the hydrogen concentration change vs. time during the measurement and proceeding with the measurement at a pace that is slower than required to reach 95% of the reaction at each data point if possible. However, many materials have such poor kinetics that this is not achievable in a reasonable amount of time. It is important to indicate when results represent non-equilibrium conditions that may have some impact both on the capacity of the material presented and any evaluation of thermodynamics. When it is possible to measure the relevant rates of absorption or desorption, it is highly valuable to present these values as well.

2.7.8 Activation Effects

For most reversible materials, hydrogen storage capacity is not maximized after the first absorption and desorption cycle. In both chemisorbing and physisorbing media, reaction with hydrogen can be initially obstructed by impurities caused by exposure to contaminants such as ambient air during preparation, as discussed in Section 2.7.5. Conversely, some effects will tend to degrade performance, such as catalyst migration, so capacity will not always improve with cycling.

In metal hydrides, exposure to air often leads to a natural oxide film barrier on the sample surface that inhibits hydride formation. Removing the oxide film activates the hydride and maximizes its hydrogen storage potential. Activation occurs in a two-step process: small amounts of atomic hydrogen penetrate the oxide layer to form the first hydride nuclei, after which the bulk hydride fragments into smaller particles through a process called decrepitation. Oxide layer penetration and nuclei formation can take anywhere between seconds to days and occurs at room temperature, if at all, and via a variety of different mechanisms depending on the sample.

This process of oxide film break up is referred to as decrepitation. Decrepitation is a phenomenon caused by the stresses placed on the usually brittle metal phase by the expanding hydride phase and yields a substantial increase of uncontaminated, oxide-free surface area, assuming that the material is exposed to pure hydrogen gas. Most decrepitation occurs during the first few cycles of hydrogen absorption and desorption and tails off during subsequent cycles. FeTi is an example of a metal hydride that is difficult to activate due to more passive and dissociatively inactive natural oxide films on the surface of air-exposed particles. This is partly the result of higher toughness than other intermetallic compounds. A study performed by Sandrock showed that even this difficult material showed steady improvement over the first 3-10 cycles, depending on initial oxygen content, sometimes even doubling the initial capacity value.[34]

Porous media and other physisorption materials also experience activation effects, although of a different nature than chemisorbing materials. Physisorption is dominated by van der Waals forces, which do not differentiate between potential sorbents. Physisorption samples exposed to the environment form a barrier of physisorbed air constituents, which take up surface area on the sample and must be removed before maximum hydrogen storage can be achieved. Since hydrogen adsorption is often a first step in the dissociation process before it can be absorbed into a material, adsorbed gases can also block chemisorption.

Because the physisorption mechanism weakens with increasing temperature, it is usually only necessary to heat a sample under vacuum to remove adsorbed impurities. It is best to perform the activation process *in-situ*, immediately prior to experiments so that there is no chance for contamination between the activation and the actual experiment. A "perfectly clean" surface requires ultra-high vacuum ($<10^{-9}$ Torr) and very high temperatures (>1000 K), but few materials are stable in this range. Therefore the goal of activation should be to remove most of the residual species without modifying or destroying the adsorbent itself.[35] Generally, a rough vacuum of 10 to 100 mtorr is sufficient for the degassing of most physisorption materials. In any case, the conductance through standard tubing limits the effective vacuum that can be achieve at the sample position in most experimental setups regardless of the vacuum that the pumping system may achieve (see Appendix A).

Activation effects upon repeated cycling are not guaranteed to improve performance. Specifically, in reversible chemical hydrides the hydrogen uptake and release can be strongly affected by many factors which can affect material properties both positively and negatively. Distribution of catalyst and reactants, completion of initial unstable reaction processes resulting in final reversible reactions, particle size, and morphology of the material on a macroscopic and microscopic level are just a few of the potential factors. It is important to run new materials through several absorption/desorption cycles to determine the actual steady state capacity of the material. For example, reducing grain size is a technique which has been shown to improve both the kinetics and thermodynamics of hydrogen storage systems, particularly in the Mg system. However, highly exothermic materials such as MgH_2 release enough heat during the dehydrogenation process to allow for considerable agglomeration, and the improved performance typically does not survive cycling well.

2.7.9 Effect of Sample Size

Many hydrogen storage materials require expensive or difficult preparation techniques to achieve optimal performance. Preparing small samples can reduce the cost and time of an experiment significantly, so that many more samples can be tested. Thin film and ball-milled powder samples are commonly prepared during fundamental studies of hydrogen storage materials, but the results do not always represent the system level performance of the material.

Thin films are interesting because deposition techniques such as sputtering and pulsed laser deposition (PLD) can be readily tuned to make films of varying composition to study many material compositions in one sample. Another advantage in using thin films in fundamental studies is that the effects of kinetics can be dramatically reduced in the limit of extremely thin films, shortening experiment times.

Similarly, ball-milling powders with a small of amount of catalyst is a fast and effective way of doping a sample and creating small grains. The catalyst is often well distributed and the small grain and particle sizes can again reduce the effect of kinetics on thermodynamic measurements.

It is important to maintain a focus on the goals of the experiment at hand when deciding whether to use a thin film, ball-milled powder or bulk sample. For example, it is not reasonable to spend a lot of time measuring the usable capacity of a thin film, since kinetics play such an important role in determining the usable capacity of a practical system.

Another impact of sample size arises because many potential hydrogen storage materials are strongly oxidizing, such as Li and Mg. Even brief exposure to air can lead to significant oxidation. To prevent this, sensitive samples are often capped with a non-oxidizing metal. Often these capping layers are can also serve as catalysts, Pd or Ni. This is particularly important in experiments under a limited temperature and pressure range. For example, X-Ray Absorption Spectroscopy (XAS) measurements taken at the ALS (see Chapter 3) require a sample holder which can be contained in UHV environment with a window thin enough to be transparent to x-rays, limiting the maximum pressure to only 2 atm. Additionally, while it is conceivable to add a heater to the sample holder, it would add significant complexity to the experimental setup. By capping a thin film of Mg and Ni with Pd, it is possible to observe hydrogenation at room temperature and 1 atm H_2 while taking XAS measurements.[36] However, it is important to keep in mind that a catalytic capping layer may lead to dramatic improvements in a thin film with short diffusion lengths, but may be much less effective in a bulk sample where the catalytic effect would be concentrated in a surface layer only.

2.7.10 Thermal Effects

Large temperature variations can occur locally due to exothermic or endothermic reactions and inadequate material thermal conductivity. Thermal equilibrium is extremely important in capacity measurements, particularly reversible metal hydrides which are typically largely exothermic and release a large amount of heat during hydrogen loading. Total capacity measurements should always be made under conditions as close to equilibrium as possible, but as has been stressed before, this is often difficult and time consuming.

Reversible and usable capacity measurements may be more focused on practical applications rather than maintaining equilibrium during testing. However, it is still important to consider the heat transfer effects. For example, an insulated sample may yield unrealistically high reversible capacity results due to the heating effect during absorption, whilr a practical application may result in more heat transferred away from the sample and therefore reduced performance.

2.8 Methods to Improve Hydrogen Storage Performance

There are many techniques that can be used to improve a material's storage properties, but the reported improvements can be misleading. Many of these techniques work well on a small scale, but do not translate well for system level implementation. Other improvements may be appear significant, but may be limited by the scope of the investigation. The following section is a brief discussion of some of the main issues to consider regarding the most often used material improvement techniques.

2.8.1 Catalyst Doping

Doping has been shown to be an effective way to distribute a catalyst throughout a material to make reversible hydrogen storage feasible. Bogdanovic and Schwickardi

demonstrated that doping sodium alanate with transition metals, particularly Ti, improves reaction kinetics and reduces the temperature associated with equilibrium hydrogen pressure of 1 atm. For example, by doping $NaAlH_4$ with 2% $Ti(OBu)_4$ they were able to evolve about 4.5 wt% hydrogen in 1 hr versus 22-24 hrs for the undoped sample.[7]

In most fundamental studies, small sample sizes are used. This can simplify a study significantly, but can also be misleading. For example, for a small sample, it is easy simply to deposit a catalyst on the surface, since diffusion lengths are typically small and the catalytic effect should work on most of the sample. However, this principle does not apply very well to a bulk sample, where the surface area to volume ratio is much less advantageous. It is often necessary to distribute a catalyst throughout a bulk sample to achieve full effectiveness. This may add significant difficulty to the manufacturing process of a large system, as required for implementation in a fuel cell vehicle. Additionally, the improvements may not stand up well to cycling due to catalyst migration.

2.8.2 Grain/particle Size Effects

Decreasing the grain or particle size in a potential hydrogen storage material can lead to a significant increase in kinetics due to the increase in grain boundaries and therefore an enhancement of hydrogen diffusion throughout the sample.[37] For sufficiently small grain sizes, it is even possible to improve the thermodynamic performance through reduction of the enthalpy of formation. Calculations have shown that significant excess energy can be introduced due to increased grain boundary area. High energy ball milling processes can produce further excess energy by creating strained regions of excess volume.[38] If the energy of the hydrided state increases more than the unhyrided state, then the enthalpy of formation will decrease, as shown in Figure 14.

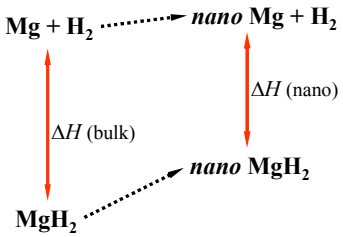

Figure 14. Illustration of how destabilization of both the hydrided and unhydrided state can lead to a reduction in the enthalpy of formation.

This reduction is attributed in part to increased grain boundary area. If the surface energy of the hydride phase is higher than that of the metal phase, increasing the surface area will decrease the difference in energy between the two phases. Most metals expand upon hydrogenation, enhancing this effect with a natural increase in surface area. The Mg-MgH_2 system is a good example of this. Mg has a surface energy of 0.55 J/m^2[39] and expands by 34% upon hydrogenation to MgH_2,[40] which has a surface energy of 2.08 J/m^2.[41] Taking into account the volume expansion, the surface energy of MgH_2 is larger by about 2 J/m^2.

This effect is negligible in a bulk sample, but similar logic can be used to generate a maximum estimate of the change in enthalpy of formation in samples with small grain sizes. Grain boundaries can be approximated as surfaces by neglecting the reduction of energy due to

planar bonding. The difference in surface energy between Mg and MgH_2 grains is then also 2 J/m^2. Calculations predict the maximum change in enthalpy of formation for MgH_2 based on these assumptions to be 9-10 kJ/mol H_2 for a sample with grain sizes on the order of 7-9 nm.[38]

Additional reductions in enthalpy of formation can be expected in the case of small grain sizes attained through high energy processes such as ball milling. High energy ball milling can lead to regions of lattice distortions which can cause the actual volume of a material to be greater than its standard value. Equations of State for solids such as the Universal EOS and the 2nd and 3rd order Birch-Murnaghan EOS show a wide range of applicability across metals and insulators,[42,43] and therefore are a good choice for examining a system under transition from a metallic to a semiconductor state.

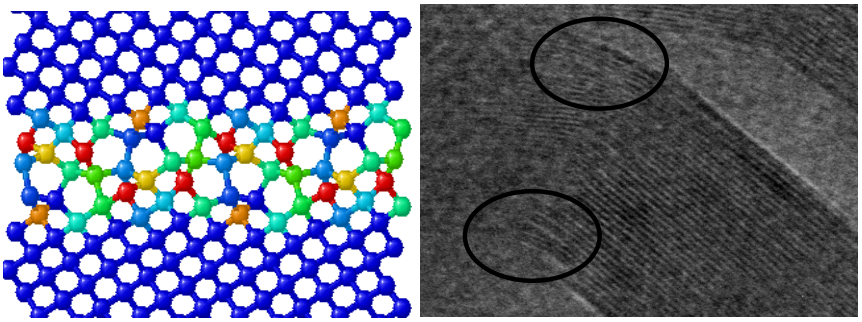

Figure 15. Illustration of excess volume in a crystal structure due to high energy ball milling or other high energy processes showing (a) a theoretical representation and (b) SEM images of regions of excess volume in a real material.

2.8.3 Alloying

Many potential materials for on-board reversible storage, such as MgH_2 and LiH, have favorable total capacity statistics, but are too thermodynamically stable for practical applications. It is impossible to overcome thermodynamic barriers by addressing the kinetics alone, so much research has been focused on reducing the thermodynamic stability of materials with a high total capacity. One technique is to alloy the stable metal with a metal that forms a less stable hydride such as Ni or Al. For example, Mg_2NiH_4 has an enthalpy of formation of -65 kJ/mol H_2,[44] compared to -75 kJ/mol H_2 for MgH_2.[45,46,47,48] However, the addition of nickel leads to a significant reduction in total capacity (down to 3.6% from 7.7%), while still falling short of the ideal enthalpy of formation of -39.2 kJ/mol H_2.[10] The ideal enthalpy of formation in this case is determined as the value that would lead to an equilibrium hydrogen pressure of 1 atm at 100 ^oC as determined by the Van't Hoff equation.

2.8.4 Capping Layers

Capping layers can be very useful in preventing oxidation and as a simple catalyst layer for fundamental studies. This can speed up the search for potential materials, but does not necessarily translate into good system level performance. Many of the commonly used materials, such as Pd, are heavy and expensive, and therefore not practical for real applications. In addition, a capping layer will be much more effective on a thin film than a bulk sample.

Optimization of capping layers to provide sufficient protection from oxidation with minimum impact on measurements is a difficult problem that is discussed further in Appendix B.

Chapter 3: Study of Hydrogen Storage Materials Using Synchrotron Radiation

3.1 Introduction

Magnesium based hydrogen storage materials have generated a significant amount of interest. This is because magnesium hydride (MgH_2) has a theoretical storage capacity of 7.7%, above the DOE target presented in Table 1. Mg is also a relatively cheap and abundant material, making it a viable candidate for mass production. The biggest drawback is that the dissociation temperature of MgH_2 is greater than 280 ^oC, far above the DOE target of 85 ^oC. Additionally, Mg is strongly oxidizing, making it difficult to work with.

As discussed earlier, the dissociation temperature is high because the dehydrogenation reaction of MgH_2 is strongly exothermic at -75 kJ/mol H_2.[45-48] A significant amount of research has gone into alloying Mg with destabilizing elements such as Ni and Al,[10,49] but the destabilizing properties of these materials are still not well understood. A fundamental study of the electronic structure is useful in understanding the process and can enable the design of more effective systems. The core electronic structure is particularly interesting because it is element specific and can therefore give information on the behavior of each individual element. For example, it is possible to separate the effects of hydrogen absorption on the electronic structure of Mg and Ni in a Mg_2Ni sample.

3.2 Synchrotron Radiation

Synchrotron radiation results from the fact that a charged particle emits radiation when it is accelerated, as is required to maintain conservation of momentum. For example, when an electron travels at constant speed along a curved trajectory, radiation is emitted tangential to its path, or perpendicular to its inward acceleration. When the electron is travelling at relativistic speeds, the radiation is condensed into a small cone of angle $1/\gamma$, where γ is the Lorentz contraction factor, given by Equation 11.

Equation 11

$$\gamma = \frac{1}{\sqrt{\left(1 - \frac{v^2}{c^2}\right)}}$$

Here v is the speed of the electron and c is the speed of light. The spectrum of light emitted in this process can be very broad. When the acceleration is due to a magnetic field, the maximum intensity occurs at the critical photon energy, E_c, given by Equation 12, where B is the magnetic field strength in Tesla.

Equation 12

$$E_c = \frac{3e\hbar B\gamma^2}{2m}$$

Significant photon flux can be obtained from about 0.1% of E_c to $4E_c$.[52] The high intensity of light in this range means that only a fraction of the beam's bandwidth is necessary to

achieve a strong signal, allowing high spectral resolution and the observation of fine structure. This fact in combination with improved optics and tunable monochromators have led to increasingly refined excitation energy selection, adding another degree of freedom to X-ray Emission Spectroscopy (XES) studies.[50]

3.2.1 Sources of Synchrotron Radiation

Useful radiation is generated from three main sources in a synchrotron facility, bending magnets, undulators and wigglers. The primary function of bending magnets is to guide charged particles along the designated path. Synchrotron radiation was initially observed as an energy loss in particle accelerators used to study particle physics, and bending magnets were originally designed to minimize these losses. Once the usefulness of the radiation was realized, ports were built off of the bending magnets to capture the radiation and use it for scientific purposes. Now bending magnets are designed both to provide useful radiation and guide electrons in the storage ring.

In a bending magnet, the electron follows a curved path, producing a sweeping beam of radiation of which only a portion is captured. The energy of the beam is characterized by Equation 12 above. The desired energy is then selected using beamline optics such as a monochromator. Bending magnet radiation is characterized by a broad spectrum which good brightness and cheap maintenance.

The main distinction of a third-generation synchrotron light source is the incorporation of a series of straight sections fitted with undulators or wigglers. These are periodic magnet structures which provide a tunable spectrum of high brightness photons. X-rays are generated as the magnets accelerate the electrons in the storage ring perpendicular to their direction of travel, emitting dipole radiation along the direction of travel. The periodic structure serves to enhance the brightness of the radiation and keep the electrons travelling along their path. The main differences between a wiggler and an undulator are the number of periods and the strength of the magnets. The magnet strength is usually presented in terms of the non-dimensional magnetic deflection parameter, K:

Equation 13

$$K = \frac{eB_0\lambda_u}{2\pi mc}$$

where e is the charge on an electron, B_0 is the maximum magnetic field strength in Tesla, λ_u is the period of the magnets, m is the mass of an electron and c is the speed of light.

An undulator has many magnets with a relatively low K value. This creates a high intensity beam with a narrow bandwidth which is tunable by adjusting the gap between the magnets, effectively adjusting the K value. The oscillations also have many harmonics at higher energy which can be exploited to give undulators a large range. Only the odd harmonics produce beams on-axis, and they get progressively weaker, so that usually only the 1^{st}, 3^{rd} and 5^{th} harmonics are useful. For example, a typical undulator at the ALS has 89 periods, each 5 cm long, and can produce x-rays with energies from 100 to 1000 eV.

The small oscillations in an undulator create radiation with a very narrow relative spectral bandwidth, given by

Equation **14**, Where $\Delta\lambda$ is the spectral resolution, λ is the wavelength of the selected radiation, and N is the number of periods in the undulator.

Equation 14

$$\frac{\Delta\lambda}{\lambda} = \frac{1}{N}$$

Similarly, the radiation is focused in a narrow cone with the halfwidth, θ_{cen}, given by Equation 15.

Equation 15

$$\theta_{cen} = \frac{1}{\gamma\sqrt{N}}$$

A wiggler tends to have fewer magnets with a higher K value. This creates larger oscillations, and correspondingly stronger harmonics. For large enough K, the harmonics blend into a continuous spectrum similar to that of a bending magnet.

3.2.2 Terminology in X-Ray Spectroscopy

In traditional quantum physics, the energy levels of electrons are defined to be in a series of orbits labeled by a number corresponding to their principal quantum number, n, and a letter corresponding to the orbital angular momentum quantum number, l. For example, an electron orbit with n=1 and l=0 is called 1s, while an electron orbit with n-2 and l=1 is called 2p. The spin quantum number of ± ½ is sometimes also included to distinguish between states such as $2p_{1/2}$ and $2p_{3/2}$. In x-ray spectroscopy, the groups of electron orbits, termed shells, are labeled by a letter corresponding to the principal quantum number. Each orbit within the shell is assigned a number in order from the lowest energy to the highest. For example, the K-shell corresponds to 1s electrons only, while the L-shell consists of 2s and 2p electrons and the M-shell consists of 3s, 3p and 3d electrons. The shells are further split into subshells, or absorption edges, corresponding to the binding energies of the electrons in the shell in order from highest to lowest so that the L_1 edge corresponds to the 2s electron orbit, L_2 to $2p_{1/2}$ and L_3 to $2p_{3/2}$.

3.3 X-ray Absorption Spectroscopy

X-ray Absorption Spectroscopy (XAS) probes the unoccupied states of the conduction band through excitation of core elections. For a given element, the energy levels of the core electrons are distinct enough to distinguish between the excitation of individual electron energy states. A typical XAS experiment focuses a soft x-ray beam on a target and scans across a range of energies to cover one or two absorption edges. X-ray Absorption Near Edge Spectroscopy (XANES) is a technique where light with extremely fine energy resolution is used to scan the material near a specific edge, usually within 100 eV. XANES can give specific information on the chemical bonds within a material, such as the degree of charge transfer between ions in a compound. XANES is sometimes referred to as Near Edge X-ray Absorption Fine Structure (NEXAFS) when it is applied to surface and molecular science.

Extended X-Ray Absorption Fine Structure (EXAFS) is a similar technique, except that the energy is scanned over a larger range often of about 500-1000 eV. EXAFS spectra typically have oscillations at energies more than 100 eV above the absorption edge due to interference between neighboring atoms, and can be used to determine aspects of the atomic structure such as the degree of local and long range order.

There are many different ways to detect and measure absorption events, but the most common are Total Electron Yield (TEY), Fluorescence Yield (FY) and Transmission Yield

(TY). In most cases, the absorption of a photon does not lead directly to the emission of an electron, but rather excites an electron to an unfilled energy state in the conduction band. An electron from the conduction or valence band then relaxes to fill the hole vacated by the excited electron. The energy balance is satisfied either by the emission of a photon or an electron. The latter process is termed the Auger Effect. Just as a given element will have a characteristic emission spectrum, the kinetic energy of the Auger electrons will form a characteristic distribution of discrete values.

The TEY signal is measured by attaching a grounded wire to the sample. The wire supplies electrons to fill the holes left by the Auger electrons that are excited out of the sample. Only electrons within a distance on the order of their mean free path from the surface will leave the sample. The current in the wire is then directly proportional to the number of excitation events leading to the emission of an electron. Typical electron mean free paths are in the range of 5-50 nm at soft x-ray energies, making this a surface sensitive technique. With careful tuning, it is possible to differentiate between the spectra generated by the different surface atomic layers using the TEY measurement technique.

The FY technique detects the emitted photons generated by the relaxation of excited electrons to fill the core holes left by the excitation process. The number of photons generated by these relaxations will therefore be directly proportional to the number of excitation events. The photons from these relaxations are emitted in all directions, so it is important to optimize the placement of the photodiode or other photon detection device for maximum solid angle without interfering with other aspects of the experimental set up. Since it is generally possible to intercept only a small fraction of the total solid angle, the FY signal is often many orders of magnitude below the intensity of the incident photons and therefore requires significant amplification for a detectable signal. Since FY measurements detect emitted photons rather than electrons, the absorption length of photons is the critical measure for determining the depth sensitivity. FY measurements are generally considered bulk sensitive, as emitted photons can be detected from as deep as 200 nm or more.

It is not always possible to collect both the FY and TEY signals for a given material, since the ratio of auger electrons to emitted photons is strongly dependent on the atomic number Z and the primary quantum number n. The auger process dominates at low Z and low n, while fluorescence dominates at high Z and high n. For example, the Auger process dominates for $Z < 30$ for K shell electrons, but it dominates for $Z < 90$ for L shell electrons.[51] Most of the experiments presented here are on the L shell of Ni, with $Z = 28$, making it difficult to collect a clean FY signal.

To collect a TY signal a photodiode is oriented behind the sample in the incident beam path to detect all photons that are transmitted through the sample. The intensity of the transmitted beam is compared with the intensity of the incident beam to determine the proportion of photons absorbed by the sample. Clearly this technique can only be used with thin samples on transparent substrates, but it is truly bulk sensitive. It also measures all absorption events, and therefore is less sensitive to atomic number constraints.

3.4 X-Ray Emission Spectroscopy

X-ray Emission Spectroscopy (XES) is a powerful technique which can be used to probe the occupied states of the valence band. When core electrons are excited to the conduction band,

the holes are selectively filled by electrons from the conduction or the valence band, often emitting a photon as discussed in reference to FY measurements above. Since the binding energy of the core electron is known, the energy of the relaxing electrons can be determined by measuring the energy of the emitted photon. This means that a very sensitive spectrometer is required for XES measurements, as opposed to the simple photodiode used to collect the FY signal.

When the incoming photons are tuned to the binding energy of the core electron, the technique is referred to as resonant x-ray emission spectroscopy. Recent advances in beam intensity and beamline optics have led to the development of a more interesting technique call Resonant Inelastic X-Ray Scattering (RIXS). In RIXS, the excitation energy is chosen from a set of points of interest determined by XANES spectra of the sample. Photons emitted from relaxing electrons map the valence bend, while the change in the spectra with different excitation energies gives even more specific information.

3.5 Experiment Setup

All experiments presented in this chapter were conducted on Beamline 7.0.1 of the Advanced Light Source (ALS) at the Lawrence Berkeley National Laboratory. The ALS is a third-generation synchrotron light source, providing an extremely bright source of soft x-ray photons. The ALS consists of a linear accelerator (linac) to provide initial acceleration of electrons, a booster synchrotron to increase the electron energy to 1.9 GeV and a main storage ring where the electrons are accelerated through various magnets to generate x-rays in the energy ranges of interest. Each straight section incorporates either a wiggler or an undulator to provide tunable x-ray sources for a beamline or the radiofrequency accelerator (RF) which is used to restore any energy lost by the electrons in the circuit of the main storage ring. [52]

3.5.1 Beamline 7.0.1 Setup

A schematic of Beamline 7.0.1 is presented in Figure 16. The beamline is supplied with x-rays generated by an undulator with a 5 cm period and a monochromator which can deliver light in the range of 60–1200 eV. Depending on the experiment, data is collected either through the TEY detector, photodiodes to measure the fluorescence yield (not shown), or in the case of emission studies through the soft x-ray spectrometer. The beam energy is selected by tuning the undulator period, as discussed above.

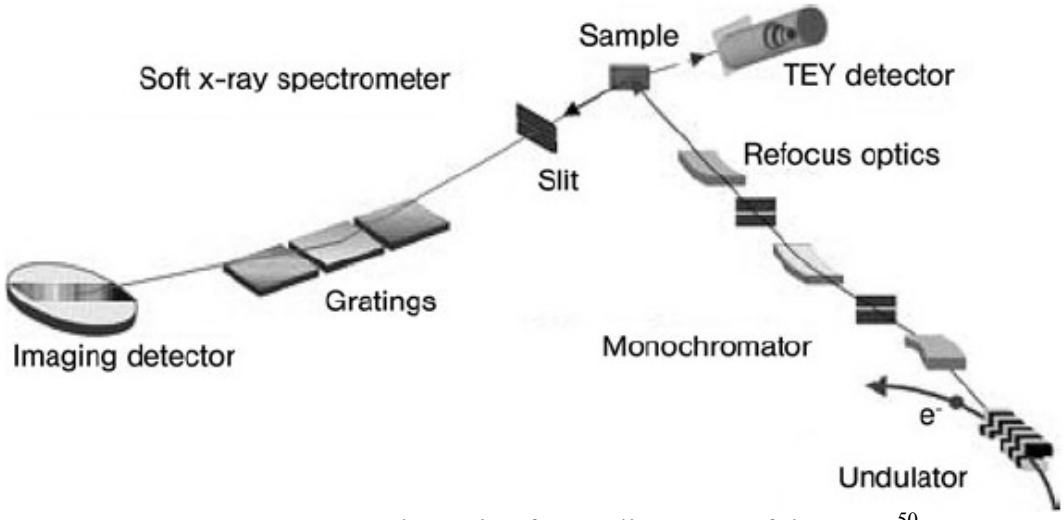

Figure 16. Schematic of Beamline 7.0.1 of the ALS.[50]

Basic x-ray absorption and emission measurements were conducted in the main experimental chamber. The main chamber has three stages of pumping. A mechanical roughing pump is used to reach the millitorr pressure range. At this point, the mechanical pump becomes a backing pump for a turbomechanical pump, which can achieve pressures down to 10^{-7} torr. Most experiments require even higher vacuum, so an ion pump is then turned on, which can drive pressures down to Ultra-High Vacuum (UHV) pressures on the order of 10^{-9} or 10^{-10} torr.

The chamber is equipped with a Residual Gas Analyzer (RGA) to determine the components of the gas inside the chamber. This is useful to determine whether poor vacuum levels are due to water evaporating from the chamber walls, a small leak, or outgassing from the sample. The surface water and other contaminants can be removed by baking out the system under vacuum at the highest temperature the components can withstand, usually about 300 ^{o}C. The RGA can also be used to determine the location of the leak by directing a small flow of helium near all potential leak sites. When the RGA shows a spike at mass 2, then you have found the leak. Outgassing samples are the most difficult problem to solve. If the samples are small, then it may be possible to wait for equilibrium to be established. Otherwise it is necessary to contain them in a wet cell. The wet cell is a sample holder with a rubber gasket and a 100 nm thick 3mm x 3mm silicon nitride window. Silicon nitride is used because it is mostly transparent to soft x-ray light, and the window is kept small so that it can withstand UHV conditions despite being only 100 nm thick.

Even after a bake out to remove all surface and water contaminants, the pump down procedure takes approximately 1 day. The chamber is equipped with a small loading lock so that it is not necessary to break the vacuum and pump down the entire chamber every time a new sample is loaded. The load lock can be pumped down while measurements are being taken in the main chamber so that no experimental time is lost.

3.5.2 In Situ Gas Reaction Chamber

The simplest experiment on hydrogen storage materials using synchrotron radiation is to take XAS or XES measurements before and after hydrogenation with the sample held in the

vacuum of the main chamber. However, it is also interesting to take measurements under hydrogen pressure. We developed a small reaction chamber which could be sealed off from the main vacuum chamber but connected to a hydrogen supply line, making it possible to track the hydrogenation reaction from beginning to end.

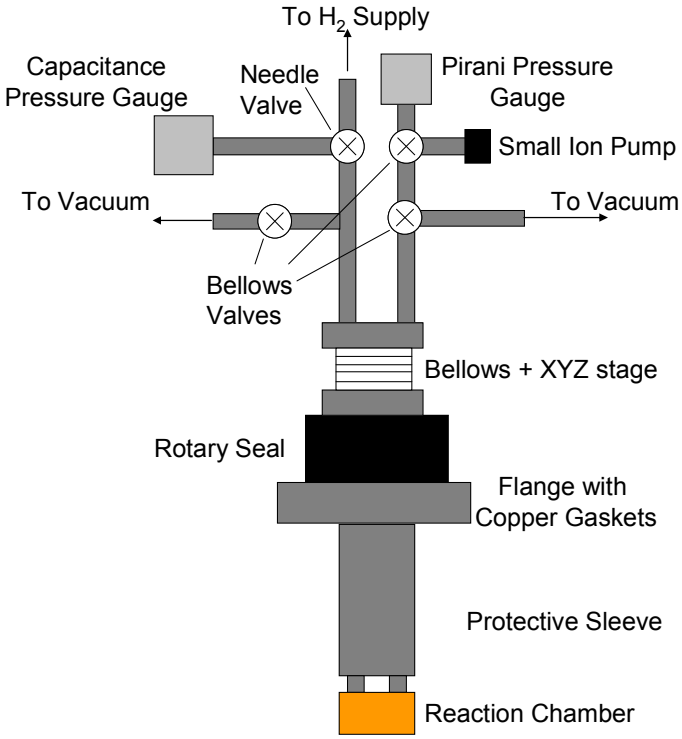

Figure 17. Schematic of the reaction chamber configured for XAS and XES measurements of samples under gas pressure taken inside the auxiliary vacuum chamber.

Figure 17 is a rough schematic of the reaction chamber setup. The basic structure consists of stainless steel tubing connected to both sides of a 2 ¾" Del Seal™ flange which seals to the main vacuum chamber with a copper gasket. Two 1/8" stainless steel tubes were welded to the vacuum side of the flange and surrounded with a stainless steel protective sleeve to reduce jostling during installation and removal from the vacuum chamber. Two ¼" Swagelok fittings were welded to the air side of the flange. The Swagelok fittings were used to attach a tubing manifold to the flange which could control and measure the vacuum level and hydrogen pressure in the reaction chamber.

The reaction chamber was attached to the 1/8" tubing via a custom designed clamp. The clamp fits around small flanges which were welded to the tips of the tubes. The clamp is then screwed onto the reaction chamber, causing the small flanges to compress rubber O-rings, forming a seal which can withstand UHV conditions on one side while maintaining up to 2 bar H_2 pressure on the other.

Pumping systems are attached to both sides of the tubing manifold at the top of the setup. On one side the tubing is connected to a turbopump reserved for use only on the hydrogen supply lines. On the other side the tubing is connected to the main vacuum chamber, so that the main chamber turbopump can be switched to pump on either the chamber or the supply lines. The vacuum level in the tubes does not approach the UHV conditions of the main chamber, so the system is never set up to pump on both the chamber and the tubes simultaneously. Instead, the

ion pump in the main chamber is used to maintain UHV conditions while the turbopump is used to pump down the tubes. A separate small ion pump is also attached to the hydrogen supply lines when additional pumping is required. It is important to note that the long, thin tubing separating the vacuum pumps from the sample holder significantly limits the achievable vacuum in the reaction chamber due to vacuum capacitance constraints. For further discussion, see Appendix A.

Both sides of the hydrogen supply lines are also equipped with pressure gauges to determine the vacuum level in the tubes. The capacitance gauge operates from atmospheric pressure down to millitorr. The pirani gauge measure pressures from atmospheric pressure down to 10^{-4} Torr with better accuracy than the capacitance gauge, as long as the chamber is clean and the residual gas is mostly made up of nitrogen and residual water vapor. While there is no pressure gauge directly measuring the pressure inside the reaction chamber, it is possible to approximate the pressure by sealing one side of the tubing while pumping on the other and averaging the two pressure readings.

The pirani gauge pressure measurement is based on the thermal conductivity of the atmosphere surrounding a metal filament, usually made of platinum. An electric current runs through the filament and heats it. The heat loss to the environment and the resulting temperature of the filament is a function of the thermal conductivity of the surroundings, which largely depends on the vacuum level of the surroundings. However, the chemical makeup of the surroundings is also important. In general, the pirani gauges attached to the chamber and pumping lines are calibrated to nitrogen gas, since the chamber and lines are purged with nitrogen when opened to reduce water contamination. It is possible to use a correlation from the gauge manual to determine the real pressure if the gauge is in a different gas environment, such as hydrogen, but the correlation only works over a limited pressure range and some accuracy is lost.

A capacitance gauge consists of a diaphragm and a plate set up to act as a capacitor. The capacitance of two parallel plates is given by Equation 16:

Equation 16
$$C = \varepsilon \frac{A}{d}$$

Here C is the capacitance, ε is the relative permittivity, A is the area of the plates and d is the separation between the plates. The diaphragm is oriented on the side of the gauge on which the pressure is measured. By measuring the capacitance, the distance between the plates can then be calculated, which is directly related to the deflection of the diaphragm and therefore the pressure. The capacitance gauge was used to measure the hydrogen pressure during experiments since this method is independent of the composition of the gas.

The entire system of tubing and pressure gauges was mounted on a rotary seal and an XYZ stage. Since the beam spot location varies slightly depending on its energy, it is necessary to have the ability to move the sample in the vacuum to position the beam directly on the sample at all times. The rotary seal adds a fourth degree of freedom by allowing us to rotate the sample. This is useful because the photodiodes used to collect the FY data are fixed in space. By rotating the sample we are able to maximize the solid angle.

The reaction chamber consists of a main plastic piece with a threaded center, a groove for a rubber gasket and a hole in the back for a TEY connection (see Figure 18). Two holes are drilled in the side of the chamber for the gas input and output connections. A wire was threaded through the back hole and then coiled into a spring. The sample is placed on a plug which is

screwed into the threaded center hole, compressing the spring to ensure a good electrical contact. EccoBond® epoxy was used to seal the hole around the TEY connection. It was chosen since it is suitable for both electronic and vacuum applications. A detachable electrical connection was then made on the back side of the cell.

a) b) c)

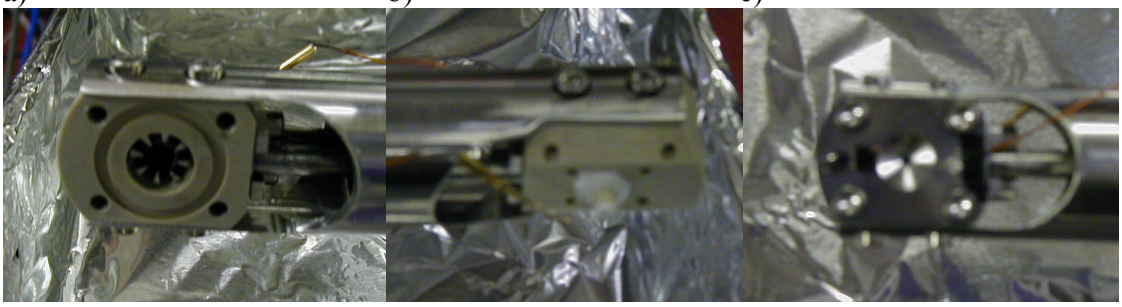

Figure 18. Images of the plastic reaction chamber of the in situ hydrogenation setup showing a) the opened gas cell with a carbon nanotube sample on the screw plug, b) the back of the reaction cell with the TEY connection coming out and c) the front of the cell with two reference samples attached to the cover plate and a second wire to collect a TEY signal from the cover plate.

The cover plate is made from stainless steel and has a conical groove with a hole in the center where x-rays pass through to the sample. The groove limits shadowing effects of both incoming and outgoing photons while maintaining a sufficient plate thickness to prevent warping near the screws and along the O-ring seal. Incoming photons could be blocked for samples where the angular dependence is tested and a wide range of rotation is used. Maximizing outgoing photons enables better FY signal collection. The hole is covered with a 100 nm thick 3mm x 3mm silicon nitride window which is transparent across most of the soft x-ray spectrum. The window is integrated in a small square of silicon, which was glued to the cover plate using EccoBond® epoxy for a good seal. The windows were shown to withstand pressures up to 2 bar in a surrounding UHV environment as long as the pressure was ramped up slowly.

3.5.3 Sample Preparation

All the samples tested by XAS and XES were thin films prepared using Pulsed Laser Deposition (PLD). PLD was chosen over more standard thin film deposition techniques such as ion beam sputtering because recent research in our laboratory has shown that by controlling the deposition parameters it is possible to control the particle size of ablated material.[53] If the substrate is not heated, the particles condense on the substrate and form a film with a very fine grain structure.

Small grain sizes have been shown to enhance hydrogen absorption kinetics.[54,55] Extremely small particle sizes created by high energy ball milling have been shown to reduce the enthalpy of formation.[56] Theoretical calculations predict that the increased proportion of grain boundaries can reduce the enthalpy of formation by as much as 10 kJ/mol H_2, while excess volume in the sample due to the stress from high energy ball milling could reduce it by another 2-7 kJ/mol H_2.[38] A thin film deposited by PLD will have similar grain boundary structure and will be faster and simpler to prepare with better control over particle size.

PLD was performed using an LPX 200 Lambda Physik Excimer laser at 248 nm. The laser light is directed through a series of mirrors and focused through a quartz window into a

vacuum chamber. The pumping system, consisting of a mechanical pump and a turbomechanical pump, can achieve vacuum levels down to 2x10-7 Torr. The background pressure can also be adjusted using an Ultraflow Vacuum General flow controller. By varying the background pressure and the laser fluence, it is possible to control the particle size in the deposited films.

The targets are mounted on a rotating piece to avoid continuous deposition from one crater. Complex films can be created by taking advantage of the rotating targets. After the deposition rates of various target materials are calculated using a Quartz Crystal Monitor (QCM), the targets can be arranged to intercept the appropriate fraction of the beam path to create a mixed sample. A QCM measurement consists of tracking the change in resonant frequency as a thin film is deposited on its surface. The change in resonant frequency can be correlated to the additional mass on the crystal surface, and therefore to the film thickness as a function of time.

To prepare a sample with multiple distinct layers, such as a bulk metal hydride with a Pd capping layer, the two targets are arranged concentrically. By changing the focus of the beam, we can choose the appropriate target. This technique was combined with the mixed targets technique described above to create a sample with an Mg_2Ni layer capped with Pd.

Most samples were deposited on a Si substrate, since it was readily available and provided a good electrical contact for the TEY signal. However, TEY is a surface sensitive measurement, detecting a signal only from atoms in the first 5-20 nm of the sample. A capping layer of more than 5 nm of Pd is required to prevent oxidation,[57] making it difficult to detect the TEY signal through the capping layer side of the sample. To address this issue, some samples were deposited directly on the silicon nitride window of the gas cell. When oriented properly, the light then strikes the substrate side of the sample first, so the surface sensitivity of the TEY signal is not a problem.

Mg-Ni samples prepared for before and after XAS and XES experiments were cut into small pieces after deposition. Half of the pieces were hydrogenated at 20 bar H_2 and 350 ^oC for 12 hours. The other half were unchanged and used for the "before" measurements so that they could be taken at the same time with the same beam calibrations.

3.6 Experimental Results

Initial tests were performed on thin films composed of 500-1000 nm thick films composed of Mg and Ni. In the first runs, PLD was performed on targets made from pressed powders of Mg and Ni. Since Mg and Ni have different ablation thresholds and therefore different deposition rates, a 1:1 target ratio does not lead to a 1:1 ratio of Mg to Ni in the deposited film. The EDX measurements presented in Table 3 show films deposited from a target composed of 2:1 Mg to Ni. The actual atomic ratio in the films is approximately 4:1 Mg to Ni. There is also a large amount of oxygen present in these films. The substrate Si signal is strong, so the possible sources of oxygen are from oxidation of Mg, Ni or Si. There must be at least some substrate oxidation contributing to the measured oxygen content, since even if all of the Mg and Ni were oxidized to MgO and NiO respectively that would only account for an atomic percentage of roughly 22%, while the measured value is actually greater than 35%. It is impossible to determine additional chemical information from EDX measurements, but XAS measurements will be presented shortly to clarify this point.

Element	Wt%	At%
Mg	18.34	18.21
Ni	8.26	3.39
O	23.62	35.62
Si	49.78	42.78

Table 3. EDX results for a thin film deposited from a target with a 2:1 ratio of Mg to Ni.

A target with a 1:1 ratio of Mg to Ni was created to achieve the appropriate ratio for the formation of Mg_2Ni in the film. EDX results confirmed this, but still showed a strong oxidation signal. The XAS measurements subsequently confirm that even the Ni was oxidized. Even samples deposited from the pressed powder targets and capped with Pd while still in vacuum have large oxygen content. This shows the drawback of the pressed powder method, since the components are likely to oxidize before the target is formed. It is therefore impossible to clean the surface of the target to reach clean material underneath.

New samples were prepared from bulk targets using the mixed targets technique described above. The XRD measurements presented in Figure 19 show that the film formed the intermetallic compound Mg_2Ni, rather than just a simple mixture of the two elements. In addition, no signal from NiO or MgO is present.

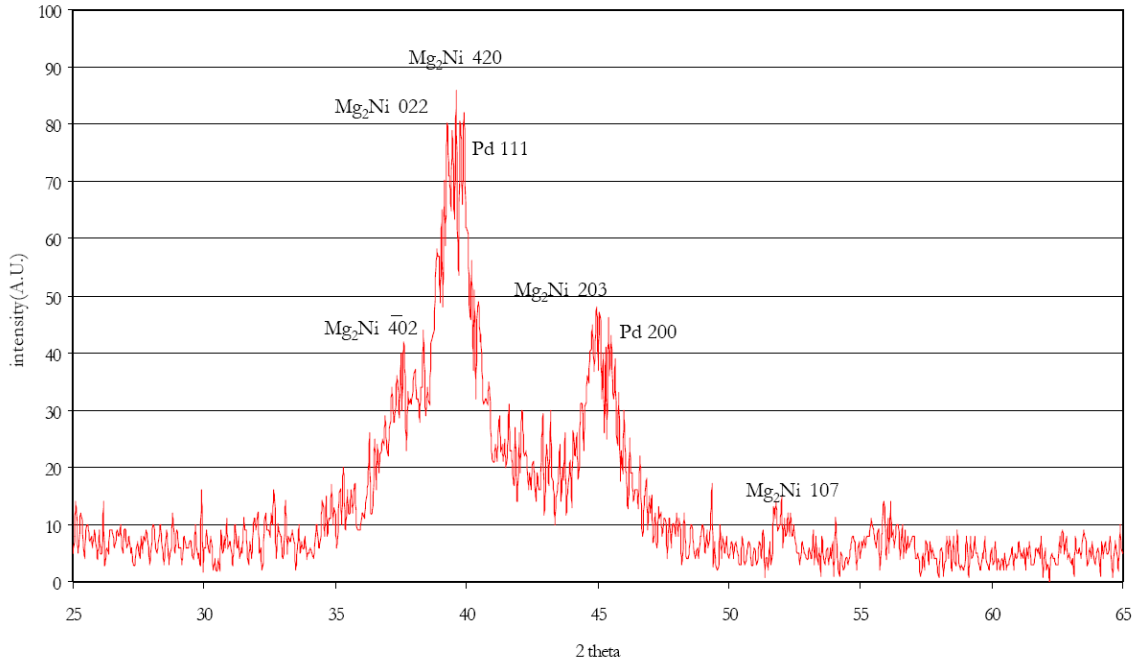

Figure 19. XRD results of a film deposited from bulk Mg and Ni targets. The intermetallic compound Mg_2Ni is clearly formed.

In all experiments, both TEY and FY signals were collected. Only TEY results are reported, due to the many complications in collecting a significant FY signal. This is in part due to the small size of the photodiodes used to collect the FY signal, and the corresponding small solid angles. Even more importantly, Mg and Ni are low Z elements, and therefore the Auger process dominates the emission of photons, especially in the L-shell. Finally, Ni made up only a fraction of all the samples tested, reducing the photon yield even further.

3.6.1 Mg_2Ni Samples Before and After Hydrogenation

XANES measurements were taken across a 50 eV range near the Ni L-Edge, from approximately 835 eV to 885. Previous studies have shown a substantial shift in both the L_2 and L_3 edges when hydrogen was added to Mg_2Ni films prepared by ion-beam sputtering.[36] Data collection was started 20 eV below the L_3 edge. This section was used to define a flat line to adjust the tilt of the spectra, eliminating error due to background drift in the measurement equipment. All spectra were also normalized against this baseline and the maximum at the L_3 peak. A pure Ni sample was measured at least once during each 12-hour set of beam time to determine any drift in the undulator energy. The energy of the L_3 edge was used to adjust all subsequent readings and was usually within 0.5 eV of the expected value.

Figure 20 displays the XANES spectra of two standard samples of bulk Ni and NiO compared to a sample composed of roughly 4:1 Mg to Ni. The Ni L-edge spectrum in the sample clearly shows the splitting at both the L_3 and L_2 edge indicative of oxide formation.[58] The small splitting at the L_2 edge of the "pure" Ni standard is likely due to a small surface layer of oxide, but the almost perfect match of the MgNi and NiO indicates that all of the Ni in the deposited sample is oxidized. Therefore the oxygen detected in the EDX results presented in Table 3 is not due only to a native oxide on the Si substrate.

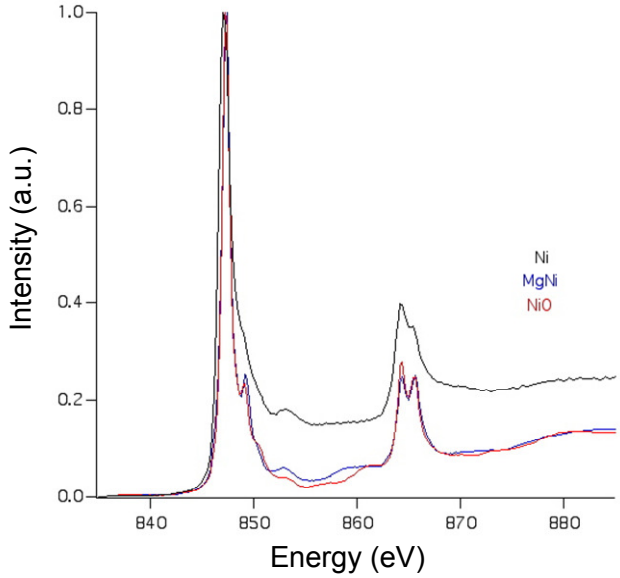

Figure 20. XANES spectra of standard samples of Ni and NiO compared to the deposited film of MgNi. The MgNi sample shows a strong degree of oxidation as it matches the NiO spectrum much more closely.

It is important to note that the X-axis of Figure 20 is the amount of energy absorbed by the electron as it transfers to a valence state. A higher energy electron state will required a lower energy photon to transfer to the bottom of the valence band, so the L_3 edge, corresponding to the $2p_{3/2}$ to 3d transition, is the left peak and the L_2 edge, corresponding to the $2p_{1/2}$ to 3d transition, is the right peak.

Oxidation of the sample serves as a barrier to hydrogenation, but it is still possible to form the metal hydride phase under sufficient heating and hydrogen pressure. Figure 21 is a

comparison between the XANES spectra of two pieces of the same thin film sample deposited by PLD from a target of pressed Mg and Ni powders. One sample (MgNi) was kept as is and the other was hydrogenated at 350 ^{o}C and 20 bar H_2 (MgNi-H). There is a clear growth of the satellite at the L_3 edge relative to the main peak. This is consistent with a mixture of a small amount of Mg_2NiH_4 in a larger background of unreacted Mg_2Ni. However, it is difficult to distinguish between this result and the split peaks due to oxidation of the sample. One distinction is that the satellite due to NiO formation is expected at 2 eV above the L_3 edge,[58] while Mg_2NiH_4 formation leads to a shift of the entire spectrum up 2.5 eV.[36] Figure 21b is an enlarged section of the L3 edge showing the small spread between the L_3 satellite before and after hydrogenation. The spread is on the order of the resolution of the experiment at about 0.2 eV.

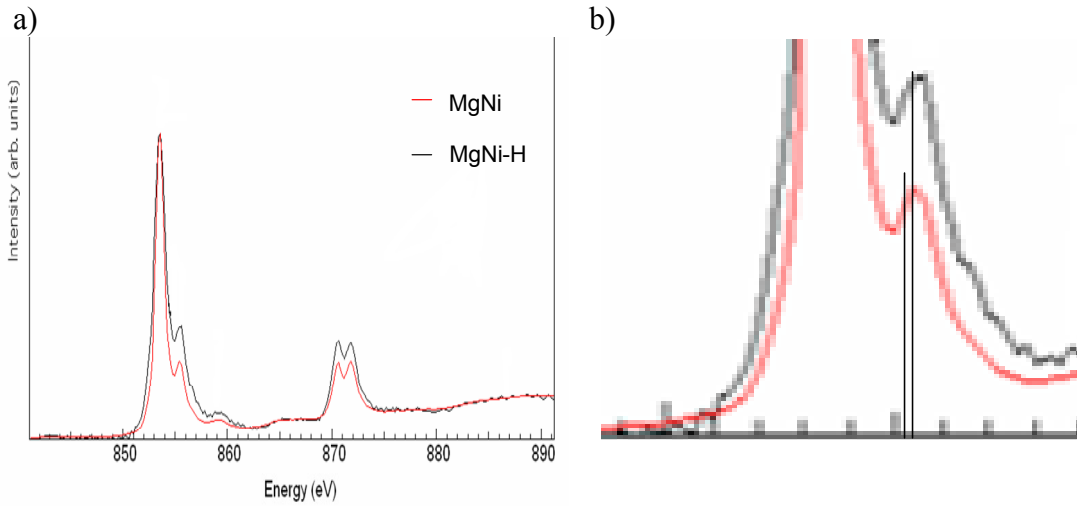

Figure 21. XANES spectra of two sections cut from one sample deposited from an Mg-Ni pressed powder target. The spectra in a) show the beginning of the change expected during the hydrogenation reaction, but it is difficult to distinguish from the oxide splitting, b) is a blown up section of the L_3 edge showing that the MgNi-H curve is at a slightly higher energy, indicating the likely formation of a small portion of Mg_2NiH_4.

Sample oxidation is the largest barrier to completion of the hydrogenation reaction, and therefore the largest barrier to our successful completion of our study. The next set of experiments show the approaches taken to prevent oxidation while still achieving good resolution.

3.6.2 Mg-Ni Samples with Pd Capping Layer

There are two potential methods to prevent sample oxidation after the deposition stage. The first is to prevent all contact with air or oxygen between deposition and measurement. The second is to cap the sample with a protective layer that is not sensitive to air. The first method normally requires extensive planning prior to the installation of equipment and can lead to a significant increase in the complexity of experiments. Additionally, such preparation is not always possible. In this case, it is possible to achieve some protection from air through the use of a glove bag. A glove bag is effectively a portable glove box which can be purged of air and filled with nitrogen. They typically fit around deposition chamber ports so that samples can be removed, transported between sites, and installed in an experimental chamber without exposure to air. Glove bags are typically less effective than glove boxes, because without a portable source of an inert gas such as nitrogen or argon, they cannot easily be maintained under pressure.

Due to advantages of simplicity and effectiveness, we chose the second method and protected our samples with a capping layer of Pd. The biggest disadvantages of capping layer systems are expense and potential interference in measurements. For example, Pd acts as a strong catalyst for dissociation of hydrogen molecules. This should not affect the fundamental changes to electronic structure that we are measuring in this experiment, but must be considered in other applications. Other experiments have been performed with Ni as a capping layer, but this would clearly dilute the information obtained from XAS measurements of the Ni L-Shell.

Capping layers are often kept as thin as possible to limit their impact on measurements. A layer as thin 5 nm can prevent oxidation, while thicker layers will inhibit the TEY signal. Below 5 nm, the film of Pd breaks up into islands and it no longer provides complete protection from oxidation.[57] The mechanism for the film breakup is unclear, but one likely explanation involves surface energy considerations similar to capillary instability in thin liquid films. Further discussion of this process is Provided in Appendix B.

The Pd capping layer thickness was determined by RBS measurements, as shown in Figure 22. For the sample shown, the Pd capping layer was less than 1 nm thick. Significant oxygen content is also shown, proving that this capping layer was not sufficient to block oxidation.

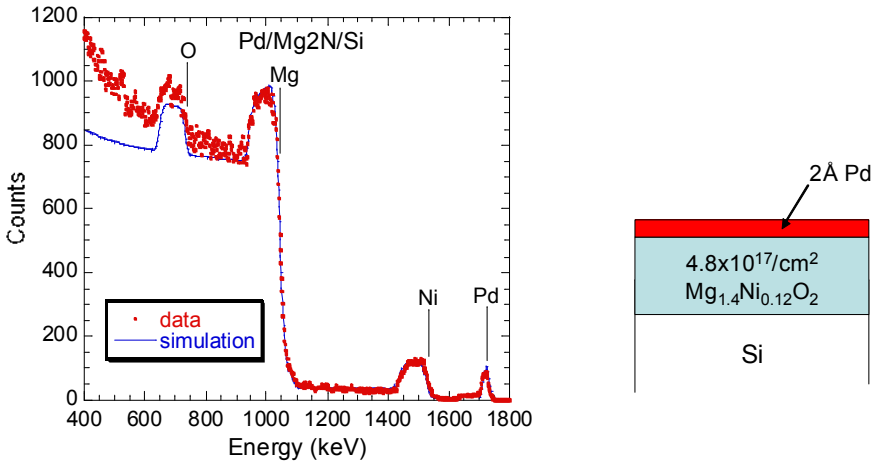

Figure 22. RBS results for an Mg-Ni sample showing a thin capping layer and significant sample oxidation.

XAS measurements taken on Mg_2Ni samples with varying Pd thicknesses are presented in Figure 23. The thick capping layer sample showed a very weak TEY signal, indicating that the capping layer was too thick for useful measurements. The thin capping layer sample showed a stronger signal, even though measurements were taken during 2 bunch mode operation at the ALS, where the beam intensity is only a fraction of the standard operating condition. The RBS results shown in Figure 22 indicated that the sample with a thin capping layer was oxidized, so no experiments were conducted under regular light conditions. The XAS spectrum from a pure Ni sample taken under regular light conditions is included for comparison.

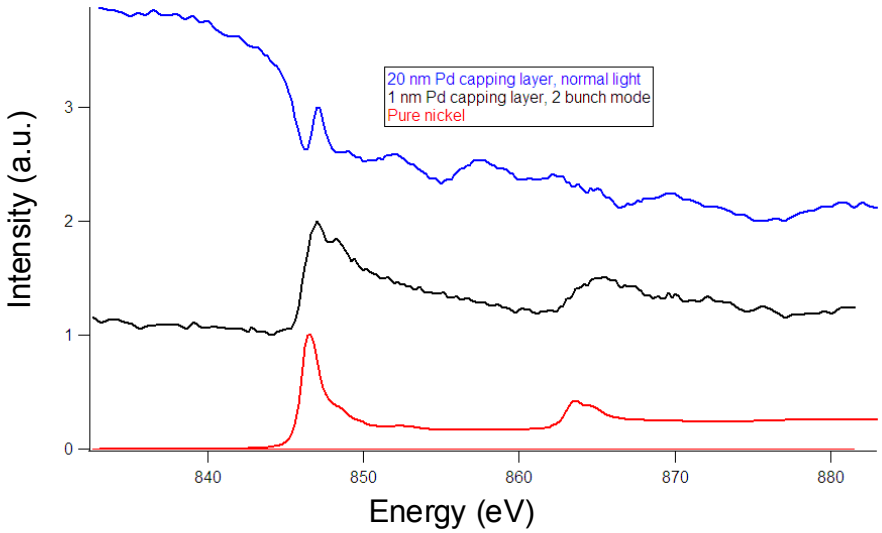

Figure 23. XAS spectra of Mg-Ni samples with Pd capping layers compared to a pure Ni sample with no capping layer.

The results shown above indicate that the optimal Pd capping layer thickness lies in the 5-10 nm range, which should be thick enough to prevent oxidation but thin enough to allow TEY measurements. An additional concern is that the low Ni content shown in the RBS results could reduce the TEY signal strength. Future depositions were controlled to include larger ratios of Ni, but the Pd capping layer thickness was difficult to control. To solve this problem, future samples were deposited directly onto the silicon nitride window. The window is aligned in the sample holder so that light strikes the transparent substrate side of the sample first and the effects of the Pd capping layer thickness are removed.

3.6.3 Mg-Ni Samples on Silicon Nitride Window Substrates

Mg-Ni samples deposited on silicon nitride windows were tested in the in situ gas reaction chamber described in Section 3.5.2 above. Multiple window samples were deposited simultaneously. Tests were performed with incident light on the Pd side and the substrate side for comparison (see Figure 24).

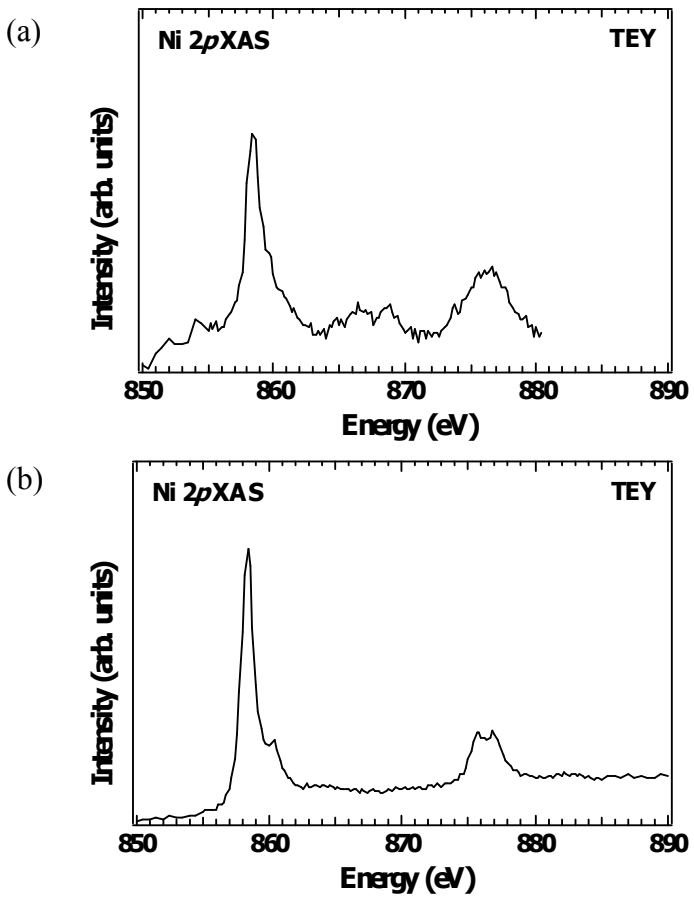

Figure 24. XAS results for Mg-Ni samples deposited on a silicon nitride window. Window was oriented for light to shine through (a) the Pd capping layer and (b) the window side, bypassing the Pd capping layer.

Tests with incident light on the Pd capping layer showed a noisy signal as before. Figure 24b shows that it is possible to get a clean signal from the window deposited samples by measuring the TEY signal with light incident on the substrate side of the sample. There is a clear indication of sample oxidation in the split peaks at the L_2 and L_3 edges, indicating the Pd capping layer was still insufficient. Since it was still thick enough to hinder the TEY signal, this implies that the only way to successfully make XAS measurements using the TEY signal is to use a sample with a thick Pd capping layer and light incident on the substrate side of the sample.

3.7 Conclusions

A portable reaction chamber was developed in which soft x-ray absorption and emission measurements can be taken of a sample in a gaseous environment at beamline 7.0.1 of the ALS. This was a significant improvement, enabling time sensitive measurements to analyze the changes in electronic structure as a reaction progressed. Previously, it was only possible to take before and after measurements, since all reactions had to be carried out prior to insertion in the experimental chamber.

The usefulness of the gas reaction cell was demonstrated on Mg-Ni samples, but sample oxidation proved to be a significant problem in studying Mg systems and can severely limited experimental results. For example, a bulk target of Mg can be stored easily as long the surface is cleaned sufficiently before each use, but pressed powder targets will become useless after even the briefest exposure to air. Significant steps were taken to reduce sample oxidation, such as implementing a Pd capping layer and transparent substrates, but accurate measurements still proved difficult to obtain. Further improvements in the sample preparation process are required before conclusions can be drawn about changes to the Ni L-Shell electrons during hydrogenation of Mg-Ni mixtures.

Chapter 4: Gravimetric Analysis of TiO_2 as a Catalyst for Borohydride Systems

4.1 Introduction

Borohydrides were introduced as a subset of complex metal hydrides in Section 1.4.2.1 of Chapter 1. As the group of metal hydrides with the highest theoretical storage capacity, they merit further discussion and investigation. Table 4 shows some of the properties of borohydride materials as compared to other commonly studied hydride materials. The theoretical capacity is simply the amount of hydrogen stored in the compound based on the molecular formula. The maximum reversible capacity is more interesting, as it is a measure of the amount of hydrogen available from the least stable reactions. The reported enthalpy of formation values are also for the least stable reaction. Slightly higher temperatures would be required to achieve the maximum reversible capacity, and significantly higher temperatures are needed to achieve values close to the theoretical capacity.

Material	Theoretical Capacity (wt%)	Maximum Reversible Capacity (wt%)	Enthalpy of Formation (kJ/mol H_2)
$NaAlH_4$	**7.5**	**5.6**	**-27**[59]
MgH_2	**7.6**	**7.6**	**-75**
$NaBH_4$	**10.6**	**8**	**-183.3**
$LiBH_4$	**18.3**	**13.9**	**-184.5**

Table 4. Comparison of various metal hydride materials of interest for hydrogen storage.

While the weight capacity of most borohydride materials is higher than any other metal hydrides currently being considered, the high enthalpy of formation, along with typically slow kinetics, leads to poor performance when all factors are considered. Still, the success of Ti compounds as a catalyst for $NaAlH_4$ generates optimism about the potential to find similar catalytic effects for borohydride materials.

The most common method to recover hydrogen from $NaBH_4$ is hydrolysis, described by the reaction in Equation 17.[60] However, the byproduct sodium metaborate ($NaBO_2$) requires further processing to be returned to $NaBH_4$. For example, regeneration of $NaBH_4$ can be achieved by annealing a combination of $NaBO_2$ and MgH_2 or Mg_2Si at high temperature (3550-750 ^oC) and high H_2 pressure (0.1-7 MPa) for 2-4 hours.[61] This is clearly not practical for application in an onboard storage system.

Equation 17 $$NaBH_4 + 4H_2O \rightarrow NaBO_2 \cdot H_2O + 4H_2$$

The research presented in this chapter focuses on finding a simpler process for releasing the hydrogen stored in $NaBH_4$ and its subsequent regeneration. A material cycle involving only heat and hydrogen pressure is desirable, as it has the potential to be much simpler and cheaper.

The methods discussed earlier for studying gas phase hydrogen absorption are therefore appropriate to test the benefits of various catalysts and destabilizing elements.

4.1.1 Gravimetric Method to Study Borohydride Materials

Chapter 2 provides a general discussion of conducting good research on improvements to kinetic and thermodynamic properties of hydrogen storage materials. This chapter provides an example of a study on a specific material system incorporating many of the concepts required for reporting consistent results discussed previously. The focus is on gravimetric analysis of TiO_2 as a catalyst for $NaBH_4$.

The gravimetric method is often used for studies of new material systems, particularly those with complicated, low yield preparation processes such as PLD and ball milling. Continued improvements in the accuracy of gravimetric systems allows for the measurement of ever smaller samples, even down to 10-50 milligrams. Small sample sizes offer some advantages as well, such as smaller volume changes reducing buoyancy effects, one of the largest sources of error in gravimetric studies of larger samples.

There are also some difficulties involved in studying borohydride materials with gravimetric systems. Of particular importance is the slow kinetics of most borohydrides, which can lead to extremely long experiment times, since equilibrium is required for each point and a minimum of 20 points is typical for even a short experiment. Many points are required in order to establish a clear pressure plateau in a PCT plot, and many pressure plateaus are required to extract thermodynamic data. Most borohydride materials are also highly reactive with air and water, which increases the difficulty of every step in the preparation and experiment process. For this reason, our initial studies on borohydride materials focus on $NaBH_4$, which is commercially available and more stable compared to other materials such as $LiBH_4$, which has a higher theoretical storage capacity and may be more promising in the long run. The basic results on one borohydride system are likely to be applicable across others.

4.1.2 Use of Ti Compounds to Improve Kinetics and Thermodynamics

Many studies have been performed to show that Ti compounds have a catalytic effect on absorption and desorption of hydrogen by sodium alanate, $NaAlH_4$. Doping with elemental Ti has less of an effect, especially on the desorption reaction.[62] The dopants $TiCl_3$, $Ti(OBu)_4$,[7] TiF3,[63] and TiN[64] have been shown to be particularly effective, reducing the desorption temperature of $NaAlH_4$ by up to 100 ^oC. A variety of wet chemical methods have been used to achieve doping with Ti compounds, but one of the most effective doping techniques is mechanical milling a small amount of dopant together with the original compound.[65,66] This is most likely due to activation from the reduction in average particle size and may lead to improved thermodynamics. The research presented here focuses on the use of TiO_2 as a catalyst as it is a well known material that is simple to prepare and work with. A recent patent focusing on destabilization of borohydrides, specifically $LiBH_4$, confirms that TiO_2 can be an effective catalyst.[67]

The catalytic effects of Ti compounds are not limited to $NaAlH_4$, but have a similar effect for most alanates. In fact, the catalytic effects of Ti were first reported for $LiAlH_4$[68] and have

also been reported for more complex systems such as $Mg_2Cl_3AlH_4$.[69] It is reasonable to assume that a similar catalytic effect could be found to apply across borohydride materials as well.

The exact role of Ti dopants in improving performance is not clear. It can be difficult to distinguish between kinetic enhancement that speeds up a thermodynamically allowed reaction at lower temperature and a decrease in the enthalpy of formation that lowers the temperature at which a reaction is thermodynamically favored. PCT measurements can be used to distinguish between these two effects. If enough time is allowed for a material to reach equilibrium at each point, then the plateau pressure is a purely thermodynamic measurement. The amount of time required to reach equilibrium gives information on the kinetics of the material. Of course, in many real experiments the kinetics are so slow that true equilibrium is never reached, so careful interpretation of the results is required. Due to these difficulties, we will focus mainly on kinetics here, since significantly faster kinetics are required before accurate thermodynamic results can be compiled in a timely manner.

4.2 Experimental Method

$NaBH_4$ powder of >98% purity was purchased from Sigma-Aldrich®. Pure $NaBH_4$ samples were tested without any further treatment. TiO_2 powder was prepared from a common sol-gel process[70] and purified by heating at 1000 ^oC for 6 hr in air. The $NaBH_4$ and TiO_2 samples were then mixed on a 10:1 mass ratio and ball-milled together in an argon environment for 24 hrs at room temperature.

Gravimetric measurements were performed on a Hiden Intelligent Gravimetric Analyzer (IGA). The IGA consists of a stainless steel sample holder and hangdown, a microbalance, a tare, a series of electronically controlled valves to control the hydrogen pressure, a vacuum pumping system, a metal sheath to protect the sample and a furnace which fits around the metal sheath. The sample holder and hangdown are not attached directly to the microbalance, but hang from a magnet inside a chamber which can be pressurized with hydrogen. The microbalance is attached to a magnet that sits just on the other side of the chamber, but is never exposed to the pressurized gas, leading to more accurate measurements. The metal sheath fits around the sample holder and hangdown and is sealed with a copper gasket to withstand high temperatures. When heating is required, the electric furnace is fitted around the metal sheath. Thermocouples measure the temperature inside the metal sheath and inside the furnace. At steady state in vacuum, the sample temperature is typically about 50 ^oC below the furnace temperature, so while the maximum furnace temperature is 500 ^oC, the maximum achievable experimental temperature is around 450 ^oC. When hydrogen pressure is added, the additional heat transfer due to conduction through the gas brings the furnace temperature and sample temperature much closer.

Each sample was approximately 50 milligrams, providing a good compromise between the accuracy limits of the equipment and the time required to reach equilibrium. The small sample sizes also limit the error due to buoyancy effects, as discussed in Section 2.5.2. The volume of the sample is negligible compared to the sample holder and hangdowns, so buoyancy effects in these experiments are due mainly to the sample holder and hangdowns. Buoyancy effects are mitigated in the IGA through a tare made of stainless steel. The IGA is equipped with software to calculate the buoyancy force at each point based on an appropriate equation of state. Finally, since the samples used are near the accuracy limits of the microbalance, tests were also

run with an empty sample holder to gauge the measurement error under the large temperature and pressure variations of the experiment.

Samples were transported from the ball miller to the IGA with minimum exposure to air to maintain purity. All samples were initially pumped down to vacuum below 1 millibar at room temperature and held for 24 hrs or until outgassing was determined complete from a steady mass reading. This was then recorded as the starting dry mass of the sample, which is used to determine the wt% of hydrogen desorbed.

Hydrogen desorption was achieved by gradually heating the sample under dynamic vacuum. Heating was conducted at a ramp rate of 3 ^{o}C/min and was stopped at 50 degree intervals up to a sample temperature of 450 ^{o}C to record the kinetics of hydrogen desorption at various temperatures. At each fixed point, the temperature was held constant until the mass reached an equilibrium value.

After equilibrium was reached at the highest temperature, the temperature was reduced to the minimum isotherm temperature and PCT data was collected using the automated software. Data was collected for up to 20 pressure points between 12 millibar and 20 bar for each isotherm. A point below 1 millibar hydrogen pressure was also recorded, but the results were discarded due to large temperature fluctuations between the first and second points, leading to unreliable results. This temperature instability is due to poor conduction heat transfer in the vacuum environment, as mentioned above. This is not expected to introduce significant error, since minimal hydrogen absorption is expected below 12 millibar.

All PCT measurements began with an absorption run followed immediately by a desorption run at the same pressure points. This uniformity is required to ensure that the intrinsic hysteresis effects are consistent across all experiments. Multiple PCT tests were run for each isotherm to confirm the results.

4.3 Results and Discussion

The $NaBH_4$, TiO_2 and ball milled mixture powders all started out pure white in color. After testing and removal from the IGA, powders ranged from gray to black in color, as shown in Figure 25. The TiO_2 powder is not shown, but was not significantly different from the unmodified $NaBH_4$ powder in appearance and therefore did not change the sample appearance after ball milling.

Figure 25. Pictures of samples before and after testing. From left to right: unmodified $NaBH_4$ after testing, unmodified $NaBH_4$ before testing, $NaBH_4$ ball milled with 10 wt% TiO_2 after testing. TiO_2 powder is not shown, but looks similar in appearance to the unmodified $NaBH_4$ before testing.

Figure 26 shows the percentage weight loss of the pure $NaBH_4$ and TiO_2-doped $NaBH_4$ samples. The weight loss is assumed to be mostly due to hydrogen desorption, especially at lower temperature. However, since the total weight loss in both cases is approximately double the theoretical capacity, there is likely some evaporation of Na from the sample in its decomposed state. The melting point of $NaBH_4$ is 400 ^oC, so while there is some potential for melting at the highest experimental temperature, significant evaporation is not expected. The black color of the samples after removal from the testing chamber, as seen in Figure 25, also indicates a higher proportion of B in the final sample composition.

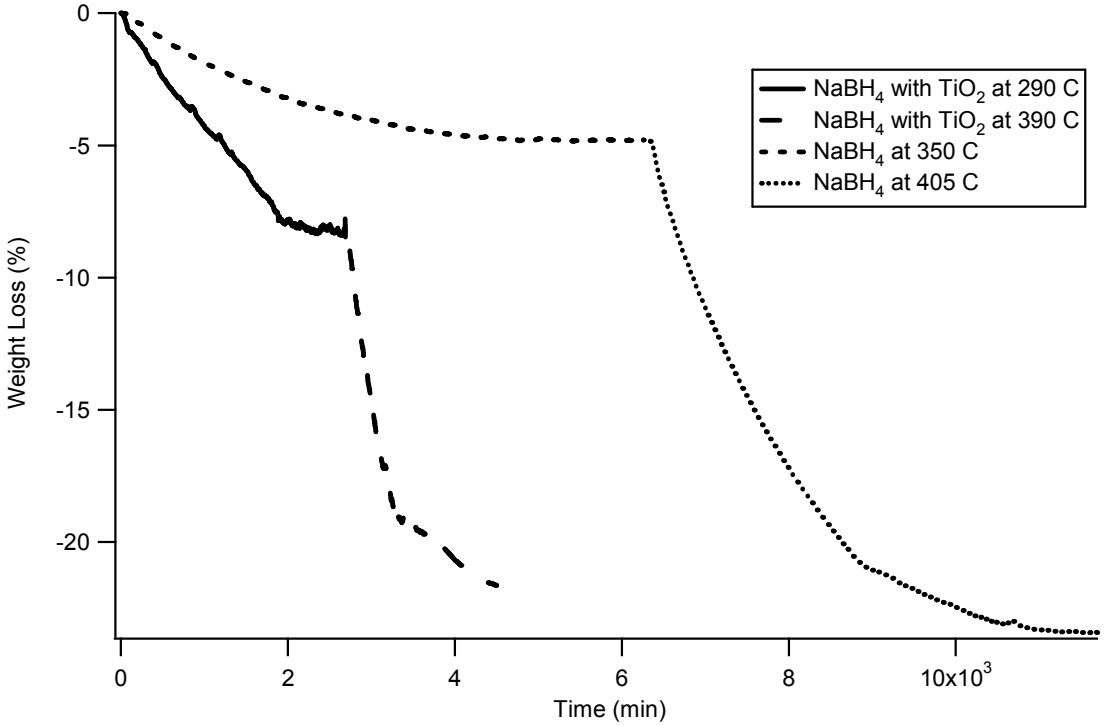

Figure 26. Weight loss plots of $NaBH_4$ and $NaBH_4$ with 10% TiO_2.

For both cases presented in Figure 26, two temperature points are recorded. The first point is the temperature at which weight loss was initially observed, and the second temperature is the temperature at which weight loss stabilized. The first step in both cases lead to the loss of 5-8 wt%, with the final step resulting in 22-25% weight loss. This corresponds to the expected two step desorption process reported for most borohydride materials as shown in Equation 18, corresponding to a weight loss of 8% as the hydrogen is released, and Equation 19, corresponding to the release of the final 2.7 wt% of hydrogen.[71]

Equation 18 $$NaBH_4 \rightarrow NaH + B + {}^{3}\!/_{2}\, H_2$$

Equation 19 $$NaH \rightarrow Na + {}^{1}\!/_{2}\, H_2$$

The weight loss at lower temperature corresponds well with the expected result, but the second step leads to a much larger weight reduction than can be explained by the second reaction. This is a further indication of the two step reaction presented above, since NaH does not melt below 800 ^{o}C, but Na melts at 100 ^{o}C and some evaporation may be expected.

A clear enhancement of the kinetics can be observed in Figure 26. The $NaBH_4$ powder ball milled with TiO_2 requires roughly half the time to release a similar amount of hydrogen at both temperature steps. Furthermore, the two weight loss steps are achieved at 60 ^{o}C and 15 ^{o}C lower temperatures, respectively. It is possible that there is some thermodynamic contribution to the reduced desorption temperature, but this cannot be confirmed from a weight loss measurement. Most importantly, 8% weight reduction in the catalyzed $NaBH_4$ sample, presumably attributable to hydrogen desorpbtion, was achieved without hydrolysis. However, the process still took almost 2000 minutes and a temperature of 290 ^{o}C, so much further improvement is still required.

Figure 27 shows the results of hydrogen absorption measurements before on unmodified $NaBH_4$ powders compared to an empty sample holder under similar conditions. It should be noted that since these results are being used to analyze kintecs rather than thermodynamics, the x- and y-axes have been flipped from the standard presentation of PCT plots.

In Figure 27 The empty sample holder shows a change in mass on the same order as that recorded for $NaBH_4$. However, there is no hysteresis in the measurements done on the empty sample holder, while there is significant hysteresis similar to that discussed in Section 2.7.7 observed in the two isotherms shown for the $NaBH_4$ sample. This indicates that while hydrogen uptake was small, it was still present in the samples even without TiO_2 doping. The small uptake is most likely due to sample degradation from the high temperatures required for complete desorption and the corresponding Na loss. The fact that some rehydrogenation was observed is an indication that the sample did not decompose completely, as boron is not expected to react directly with hydrogen. Still, the loss of Na means that the sample will exhibit poor cycling at best if the second decomposition step is allowed. For this reason, only the first dissociation step presented in Equation 18 is truly available for reversible hydrogen storage processes.

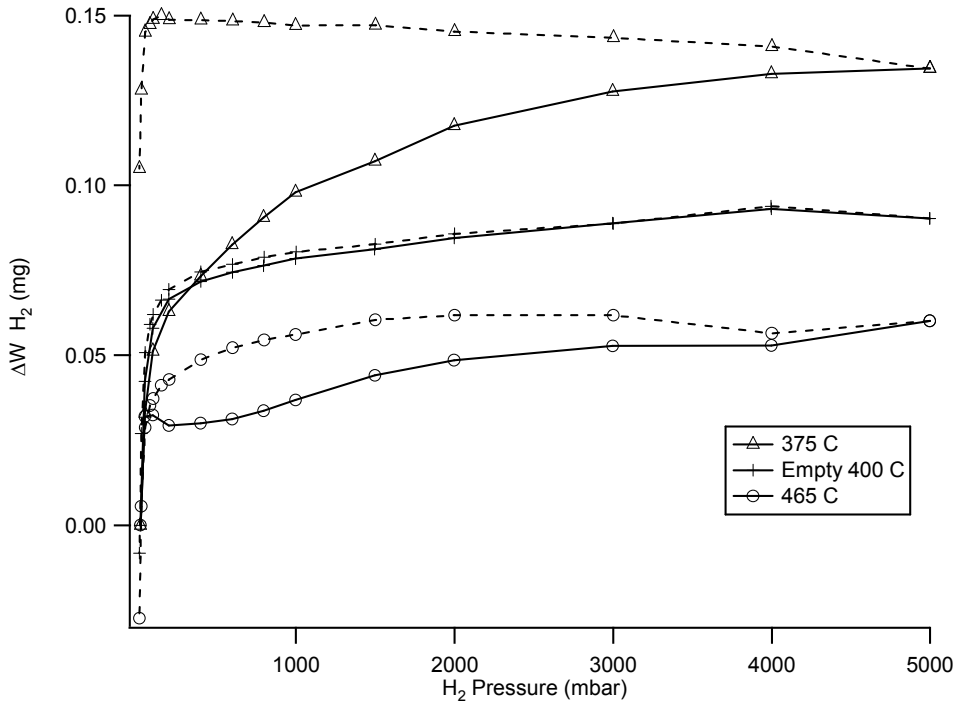

Figure 27. Hydrogen absorption/desorption results for pure NaBH4 powder at two temperatures compared to one measurement on an empty sample holder. Solid lines represent adsorption measurements and dashed lines represent desorption.

Another unexpected result shown in Figure 27 is that the isotherm at lower temperature shows a larger absorption of hydrogen than at higher temperature. This can be explained by up to three different causes. The first is that there is likely some error due to neglecting the first point that was measured in vacuum. It is possible that at higher temperature the kinetics were improved, and more hydrogen was absorbed in that first step even at low hydrogen pressure. This is probably the most significant contribution, since the higher temperature isotherm showed twice the hydrogen absorption in the first discarded step than at lower temperature. The second possible contribution is that not all of the absorbed hydrogen was released during the desorption phase of the experiment. As shown in Figure 27, the samples typically do not release hydrogen until pressures below 500 mbar are reached. The extremely slow kinetics of $NaBH_4$ could mean that some of the absorbed hydrogen remained even after the many hours required to heat to the next isotherm. The final contribution is simply the large degree of error as observed in the empty sample holder measurement.

Figure 28 shows a comparison of absorption and desorption measurements between $NaBH_4$ with and without the addition of TiO_2 powder. The catalyzed samples show larger hydrogen uptake at lower temperatures than the unmodified samples. The measurement error as calculated from the empty sample holder is on the order of +/- 0.4 wt% H_2. Taking this error into account, the catalyzed sample shows an improvement of at least 1 wt% H_2 at 364 ^oC and at least 1.5 wt% H_2 at 405 ^oC when considering the absorption measurements over the same pressure range. The catalyzed sample showed a maximum storage capacity of 5.3% at 405 ^oC and 20 bar H_2. This comes close to the maximum theoretical storage capacity of 7.2% for the reaction presented in Equation 18 when the additional weight of the TiO_2 is accounted for.

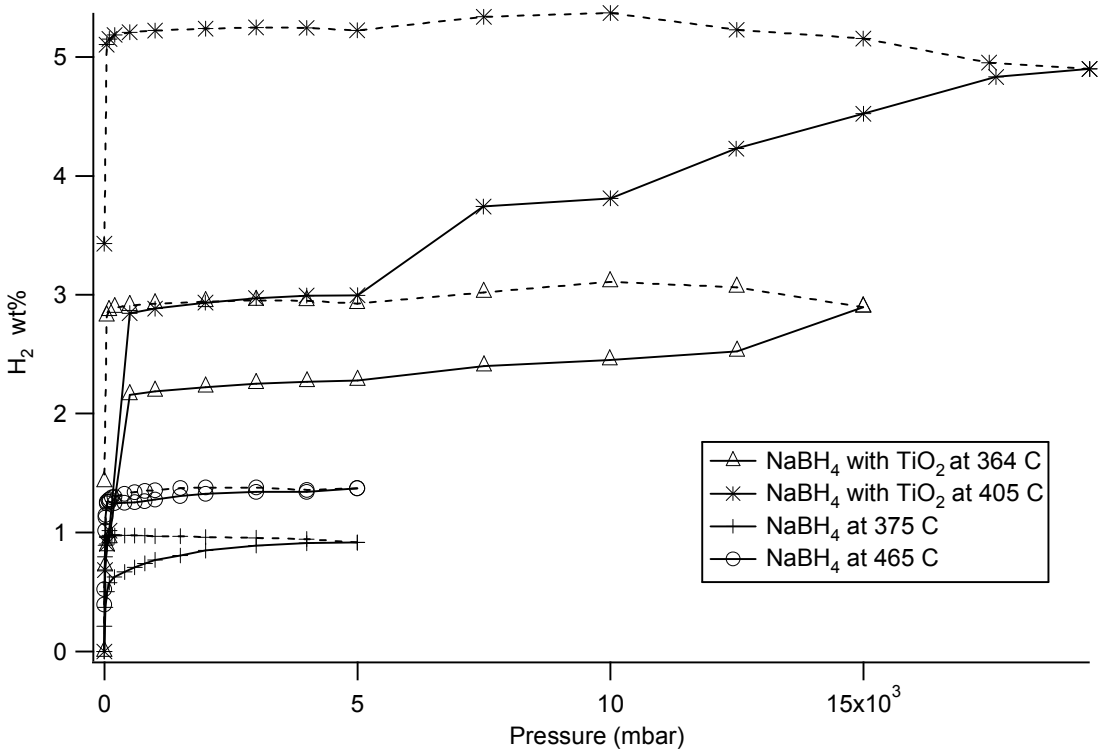

Figure 28. Hydrogen absorption/desorption measurements performed on unmodified $NaBH_4$ powder and $NaBH_4$ powder ball milled with TiO_2 powder at two temperatures. Solid lines represent absorption measurements and dotted lines represent desorption measurements.

Similar hysteresis is observed across both materials and all temperatures and no hydrogen is desorbed above 100 mbar. Hysteresis is due to a combination of measurement error, insufficient time to reach equilibrium and intrinsic material properties such as variations in plastic deformation during absorption. The most likely cause in this case is poor equilibrium due to the slow kinetics of borohydrides, as shown in Figure 26. These slow kinetics limit the potential thermodynamic analysis of the results, since it is impossible to allow enough time for equilibrium at each point in a timely experiment.

Another interesting feature of Figure 28 is the kink in the curve at a pressure of 5 bar. This could be the formation of a pressure plateau, indicating a second phase of the reaction. Recall that a pressure plateau in this plot would be vertical rather than horizontal. The sloping plateau is consistent with a material with poor kinetics. A similar plateau is potentially present in the catalyzed sample at lower temperature, but it is well within the potential error in the experiment. However, it is possible that the ball-milled samples are amorphous enough to prevent the formation of a pressure plateau even under ideal conditions.

4.4 Conclusions

Mixtures of $NaBH_4$ powder ball milled with TiO_2 powder were shown to have substantial improvements in kinetics over unmodified $NaBH_4$ powders. The initial desorption temperature was lowered by 50 ^oC, and the time to reach complete desorption was cut by 50%. Furthermore, hydrogen storage capacity was enhanced by at least 1% and 1.5% at 364 ^oC and 405 ^oC

respectively. A maximum storage capacity of 5.4% +/-0.4% was observed after exposure to 20 bar H_2 pressure at 405 ^{o}C. The slow kinetics of the reactions was a severe limitation in determining thermodynamic properties, even in the catalyzed samples.

These results are a substantial improvement over uncatalyzed $NaBH_4$ powder, but are still not sufficient to meet the performance metrics outlined in Chapter one. Further work to improve the kinetics and thermodynamics of $NaBH_4$ is required before it can become an effective hydrogen storage material.

Chapter 5: High Throughput Optical Characterization of Potential Hydrogen Storage Materials

5.1 Introduction

Metal hydrides have received significant interest as hydrogen storage media, but there is still no material that meets all of the criteria listed in Table 1 on the first chapter. The Mg-Ni system studied in Chapter 3 is of interest mainly to discover how similar improvements could be implemented in similar systems with higher theoretical capacities but similar kinetic and thermodynamic limitations. However, it is possible that the right combination of catalysts and destabilizing materials exists to create a Mg-based system with optimal properties. This becomes even more true if no material is found that can perform better, and some of the criteria in Table 1 are relaxed as the demands for viable hydrogen storage techniques become stronger.

A method for rapidly screening the vast array of potential material combinations would assist the discovery process significantly, both of materials to improve mg-based systems or of new materials systems entirely. The clearest way to achieve this is to develop a sample composed of a variety of material compositions which can be tested simultaneously. Chapter 5 is a discussion of the method we developed to screen all interesting combinations of specific material sets with the goal of speeding the search for the optimal hydrogen storage medium. Results are presented for a variety of materials to prove the concept and test out promising new systems.

5.1.1 Experiment Motivation

There are an almost limitless number of potential material combinations with attractive hydrogen storage properties. Most of these are modifications of simple systems such as MgH_2 which have a high hydrogen storage capacity but poor kinetics and a high temperature of reaction. Alloys and intermetallic compounds often show more promise, as it is possible to mix different materials to achieve improved performance. For example, the intermetallic compound Mg_2Ni forms a promising hydride, Mg_2NiH_4 which releases hydrogen at 220 ^oC, about 100 ^oC lower than MgH_2.[72] However, Mg_2NiH_4 has a theoretical storage capacity of only 3.6 wt% H_2, and therefore could never reach the DOE standards. There is likely some optimum combination of Mg and Ni with both high storage capacity and a reduced desorption temperature. It is a large project to consider testing all potential material combinations between Mg and Mg_2Ni, but it becomes much simpler if you consider using a gradient film.

Improved performance can also be achieved with the addition of a third element. Experiments on Mg-Ni-Ti mixtures have shown improved performance over Mg-Ni alloys.[10] This makes the challenge even greater as it would be impossible to test all relevant material combinations separately. Instead, we created samples with a composition gradient in three different materials, each with a maximum concentration at a different corner of a triangle. This allows us to test a wide range of material combinations in a single sample.

5.1.2 Detection of Hydrogenation

The optical properties of metals often change significantly during the metal-metal hydride transition.[73,74] In general, metals or alloys have a large reflectance at infrared wavelengths. During the transition from a metallic phase to the insulating or semiconducting phase of most metal hydrides, the optical reflectance decreases while the transmittance increases.[57,74,75] This is partially due to the opening of an electronic energy band gap when the hydride phase is formed. For example, some of the most favorable materials, MgH_2 and Mg_2NiH_4, have band gaps of 5.6 and 1.75 eV respectively.[76] This is somewhat more complicated in the study of boron-based hydrides, since B is not a shiny metal, but rather a black metalloid. Therefore combinatorial samples are typically dark in the B region. Still, the more reflective metallic parts of the sample tend to undergo a large transition. The studies presented below focus on changes in reflectance rather than transmittance. The reflectance change is observable across all material systems and thicknesses, while measuring changes in transmittance introduces more complexity than is required to draw the most interesting conclusions.

By monitoring the optical reflectance of a material before, during, and after hydrogenation, it is therefore possible to study the kinetics of metal-metal hydride phase transition. The use of optical properties also makes it possible to analyze all material combinations simultaneously from one captured image, greatly enhancing the speed of the materials discovery process.

5.1.3 Detection of Solid-Solid Phase Changes

It is also possible to use well-established optical properties of better known materials to track phase changes in the materials of interest. For example, the Mg_2Ni system is known to exhibit a "black state" during the transition from the α-phase to the β-phase hydride. The α-phase hydride, $Mg_2NiH_{0.3}$, consists of hydrogen dispersed in solid solution in Mg_2Ni, and therefore still exhibits metallic properties. The growth of the β-phase, Mg_2NiH_4, involves the development of a complex hydride, opening up a band gap as described above. When appropriately layered the reflective α-phase and the highly absorbing β-phase lead to a state with low reflectance and transmittance referred to as the "black state".[77] Using this property of the Mg_2Ni system, it is possible to track potential phase changes during the hydrogenation reaction to determine whether Mg_2NiH_4 is formed or simply MgH_2 with catalytic effects from Ni and Al. Knowledge that the material is in the β-phase is good evidence that the film has absorbed a large amount of hydrogen.

Observation of the "black state" in the Mg-Ni system is dependent on the sample orientation. It has been shown that the β-phase nucleates first at the film-substrate interface rather than the film-hydrogen interface as might be expected. This is most likely due to the typical columnar structure of Mg_2Ni with a finer grain structure near the substrate surface.[76] It has been shown that a simple model assuming two separate regions of α-phase and β-phase hydride cannot account for the observed black state. Rather, it is necessary to calculate the complex dielectric function from the volume fraction of each phase and the corresponding dielectric function using[78]

Equation 20

$$f_\alpha \frac{\tilde{\varepsilon}_\alpha - \langle\tilde{\varepsilon}\rangle}{\tilde{\varepsilon}_\alpha + 2\langle\tilde{\varepsilon}\rangle} + f_\beta \frac{\tilde{\varepsilon}_\beta - \langle\tilde{\varepsilon}\rangle}{\tilde{\varepsilon}_\beta + 2\langle\tilde{\varepsilon}\rangle} = 0$$

where f is the volume fraction of each phase and $\tilde{\varepsilon} = \varepsilon_1 + i\varepsilon_2$ is the complex dielectric function. This leads to the conclusion that when the "black state" is observed, there is a mixture of β-phase and α-phase hydride concentrated near the substrate side of the sample, while the rest of the sample is α-phase. Westerwaal et al. refer to this as a double-layered structure.[76] Therefore the "black state" occurs in a region near the substrate-sample interface, and can only be observed by reflection measurements taken through a transparent substrate.

Calculations based on Equation 20 show that the "black state" consists of a reflectance minimum at a ratio of approximately 80% Mg_2NiH_4 to 20% $Mg_2NiH_{0.3}$. Upon further hydrogen uptake, the β-phase replaces the remaining α-phase and the reflectance increases again to some intermediate level.[76]

5.2 Experimental method

All samples were prepared and optical testing was performed at Intematix. Samples were moved directly from the deposition chamber to a glove box where they were loaded into the reaction chamber to limit exposure to air. Some samples were later transported back to the Lawrence Berkeley Laboratory for further characterization. This could have lead to some oxygen contamination of the samples and is noted where necessary.

5.2.1 Sample Preparation

We fabricated continuous ternary materials libraries in the form of gradient films, which were deposited on both silicon and silica substrates by ion-beam sputtering. The deposition system was loaded with three elemental targets which could be rotated, making it unnecessary to break the vacuum after deposition began.

Many of the elements of interest, such as Mg and Ca, oxidize rapidly with even the slightest contact with air or moisture. To ensure pure material deposition, multiple cleaning steps are required for the sensitive targets. First, all targets were polished to remove surface contaminants and native oxide layers prior to loading in the chamber. The surface layers of the targets were removed after loading in the deposition chamber by briefly sputtering with a shutter protecting the substrate to eliminate any oxide layers formed during the target loading procedure.

Elemental concentrations and gradients were controlled by the combination of a synchronized shutter mechanism and a triangular mask. The triangular mask was aligned in front of the substrate with the shutter fully closed at the start of sputtering. As deposition continued, the shutter was opened at constant speed so that material from the target was deposited starting at one corner of the triangle and eventually covering the entire sample area. With the shutter moving at a constant speed during deposition process, a film with a linear thickness gradient is formed.[79] Once the shutter reached the fully open position, the sputtering was stopped and the next target material aligned for deposition. Additionally, the substrate was rotated 120^o behind the triangular mask and the shutter was returned to the fully closed position.

The process was then repeated from the first step for the other two materials so that each material was at maximum thickness at a different corner of the triangular thin film and tapered down to minimum thickness at the opposite edge.

The process was performed a total of six times, depositing two layers of each material. Each layer was approximately 20 nm thick. This allowed a relatively short annealing period to achieve interdiffusion between the layers, therefore limiting the lateral diffusion during this step. Additionally, the thinner layers improve the kinetics of absorption, shortening the length of experiments.

5.2.2 Sample Composition

The material library consists of three basic elements, each starting from one corner of a triangle with a thickness of about 20 nm and decreasing to about 0 nm at the opposite edge. Multiple thin layers were deposited alternatively and annealed to at least 150 ^{o}C to ensure interdiffusion of the elements and alloy formation. All samples were capped with 15 nm of palladium (Pd) to protect them from oxidation as well as to enhance hydrogen uptake due to its catalytic property of dissociating hydrogen molecules into atoms. The hydrogen atoms diffuse rapidly through the host lattice compared to molecular hydrogen, increasing reaction kinetics at lower temperatures.[73,74,80] 15 nm Pd films are thick enough to provide continuous coverage without breakup as described in Chapter 2 and Appendix A. Since all measurements were taken through the transparent substrate, the thickness of the Pd films was not as crucial as in the XAS and XES experiments. The limiting factor in this case is to provide a film thin enough not to create a significant barrier to hydrogen atoms as they diffuse through the capping layer to reach the sample surface.

The sample composition was analyzed using Energy-dispersive X-ray spectroscopy (EDX). EDX is performed using the electron beam from a Scanning Electron Microscope (SEM). The high energy beam excites core electrons out of the atom, leaving a hole in an inner shell. Electrons from the valence band then refill the lower energy state while also emitting characteristic electrons. The emitted electrons are then detected by an energy-dispersive spectrometer. Since a core state is involved, the method is elementally sensitive, although there is some overlap between some materials, so it can still be necessary to have an initial guess as to the materials in the sample. Once the peaks are identified, the sample composition can be determined from the intensity of the peaks. Figure 29 shows the results of EDX measurements from an Mg-Ni-Al ternary material library sample with continuous composition variation of three elements. These results confirm the linear gradient of material thickness, leading to a linear gradient in elemental composition after annealing.

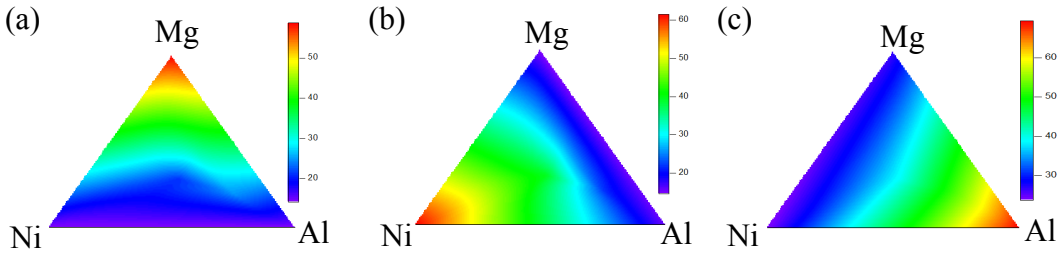

Figure 29. EDX results showing percentage of (a) magnesium (b) nickel and (c) aluminum at each point in the gradient sample.

5.2.3 Experimental Method

After fabrication and annealing, the sample was transferred to a stainless steel chamber with a quartz window. Optical reflectance measurements were taken through the window using a 1064 nm Nd:YAG laser. The reflectance was measured through the transparent substrate to eliminate influence from the palladium capping layer. At this wavelength, the absorption coefficients of Al, Mg, and Ni are in the vicinity of 0.06 nm^{-1}, thus the light is 90% attenuated at a depth of approximately 40 nm in the metallic phase. The combined layers of the gradient film are at least 40 nm thick at any given point in the film, and closer to 60 nm in most regions of interest. Light reflected off of the Pd capping layer would travel through 80-120 nm of the sample before reaching the detector, and is not expected to contribute to our results.

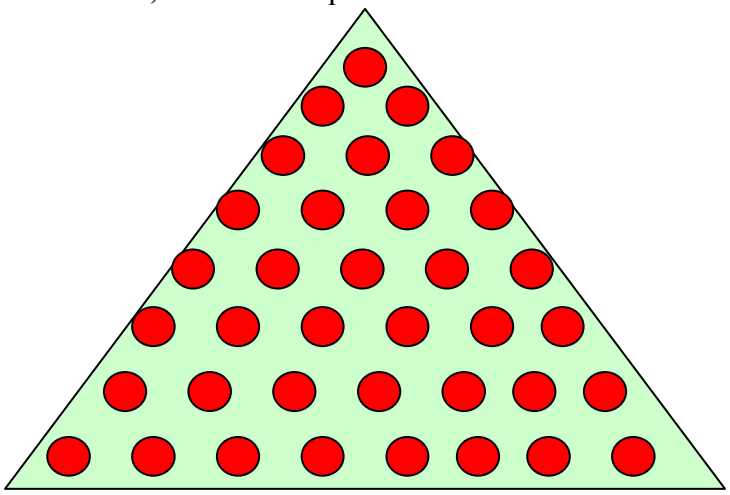

Figure 30. Map of the measurement points used to characterize combinatorial samples during initial testing.

Initial experiments were performed on an X-Y stage and measurements were taken on a point by point basis, as shown in Figure 30. This was a simple setup, but created a time lag between measurements and introduced errors as the stage position was only accurate to about 0.01". In addition, it was necessary to identify points of interest before the results could be analyzed.

In later experiments, a beam expander was inserted in the beam path. The expander and beam path length were adjusted so that the laser beam covered the entire sample surface. A lens

was then used to focus the image down to a small spot so that the image could be recorded using a CCD camera. This added significant complexity to the optical setup, but enabled simultaneous data collection across all points on the sample. Additionally, the error in the sample position was effectively removed and it became possible to examine specific areas of interest selected after the completion of the experiment.

A beam splitter was inserted in the beam path upstream of the beam expander. The intensity of the split beam was measured by a photodiode and used to normalize all results to reduce error due to fluctuations in the laser beam intensity. The final experimental setup is shown in Figure 31.

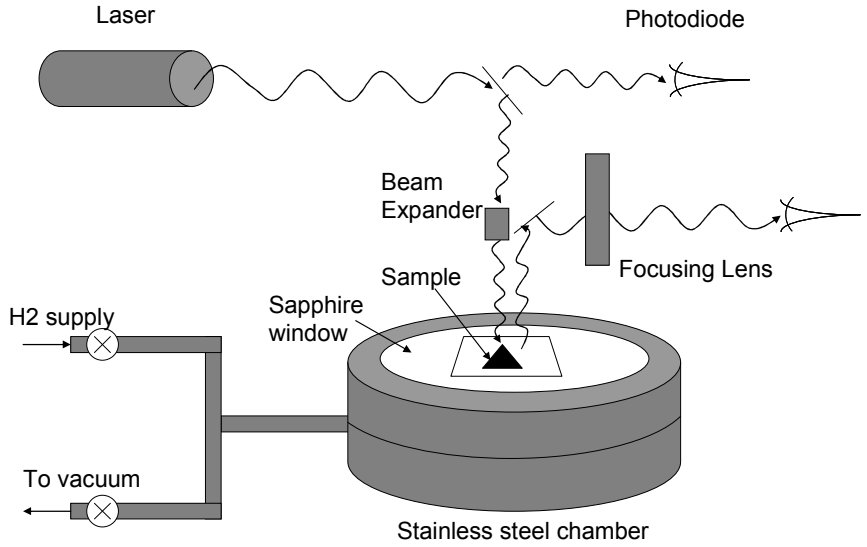

Figure 31. Experiment set up for reflectance measurements during hydrogenation of ternary samples.

The data was collected using a CCD camera and converted into intensity measurements at various points in the sample using ImageJ software. The reflectance at each spot was averaged over an area of approximately 1 mm^2 to reduce error due to minor shifts in the chamber and camera during the experiment. The results were then analyzed and plotted using IGOR Pro. The initial analysis consisted of normalizing the data with reference to the measured intensity upstream of the beam expander and compiling the data back into a plot representing the change in intensity across the sample. Areas of interest were then identified and kinetics data was compiled and plotted for specific points in these regions.

5.3 Results and Discussion

The following sections present the results of experiments conducted on various combinations of promising hydride materials with potential catalysts and destabilizing elements. Experimental details unique to the specific materials are also discussed as appropriate.

The Mg-Ni-Al system was chosen for the initial experiments because the Mg-Ni and Mg-Al systems have been well studied. It therefore served to prove the effectiveness of this testing method by reproducing some of the characteristic traits of the materials. From there, less studied materials with high theoretical storage capacity but poor thermodynamic and kinetic

performance were examined in combination with catalytic elements that worked well in other material systems. For example, Ca and B can form $Ca(BH_4)_2$ with a theoretical capacity of 11.6%, but only releases 9.2% at temperatures up to 800 K.[81] We combined these elements with Ti, a catalyst that has worked well in $NaAlH_4$ and other hydride systems to attempt to reduce this high desorption temperature.[7,63,64]

5.3.1 Mg-Ni-Al System

Samples consisting of Mg, Ni and Al were prepared as described above and annealed at 150 ^oC over night to ensure interdiffusion of the layers. EDX measurements, shown in Figure 29, confirm that there was limited lateral diffusion during the annealing process and therefore the horizontal gradients were maintained in the sample.

Figure 32 shows the change in reflectance after one hour at 323 K in 300 psi hydrogen in the Mg-Ni-Al material library sample. The regions of interest are identified by a plot of the total change in reflectance in Figure 32a. For each region of interest, a curve was generated showing the kinetics of hydrogen absorption, presented in Figure 32b.

(a) (b)

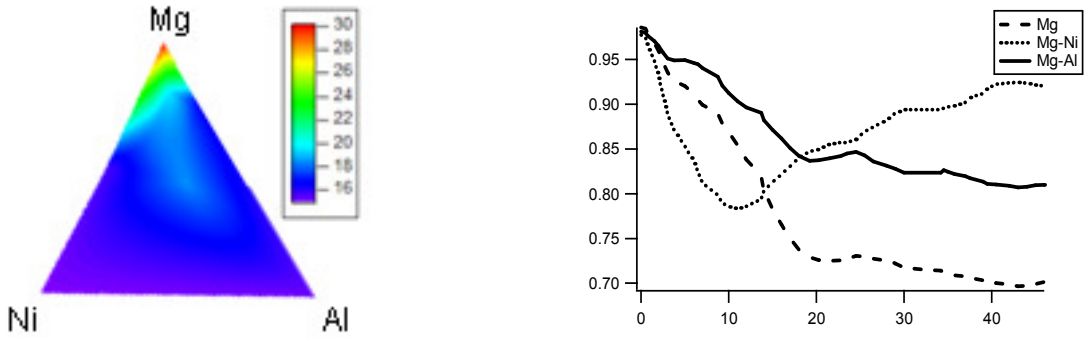

Figure 32 (a) Percent decrease in reflectance after 1 hour in 300 psi H_2 at 323 K. (b) Time resolved reflectance measurements at 323 K in 300 psi H_2. The Mg-Ni and Mg-Al curves are taken from a region at roughly 2 Mg for each Ni or Al atom, respectively.

The time-resolved data show that there is a steady drop in reflectance at the Mg corner. A similar drop is observed along the Mg-Al edge, though the change is smaller. In this sample we do not see the enhanced kinetics of absorption usually associated with Mg-Al alloys at higher temperatures of 623-673 K.[82] The Pd capping layer also acts as a catalyst, providing optimal conditions for hydrogen absorption. The Mg-Al reaction with hydrogen can therefore be considered to depend on temperature, most likely due to changes in crystal structure above some critical temperature, rather than the state of the hydrogen atoms. Therefore under reaction conditions suitable for hydrogen storage applications, it is reasonable to assume that Al will act only as a diluent rather than enhancing hydrogen absorption.

The drop in reflectance followed by a partial recovery shown in Figure 32 is an indication that we have successfully formed the ternary hydride Mg_2NiH_4 in this sample, as discussed in Section 5.1.3. The black state is also a simple way to track the progress of the reaction visually, as the effect also occurs in the optical wavelength range. Figure 33 shows a picture of a sample

before and after hydrogenation at 150 ^{o}C in 300 psi H_2. The black phase is clearly present in the Mg-Ni region of the sample during hydrogenation. The brown regions indicate areas of more complete β-phase Mg_2NiH_4 formation.[44] The picture shown here was taken through the substrate side of the sample, where the formation of the black state occurs.

a) b)

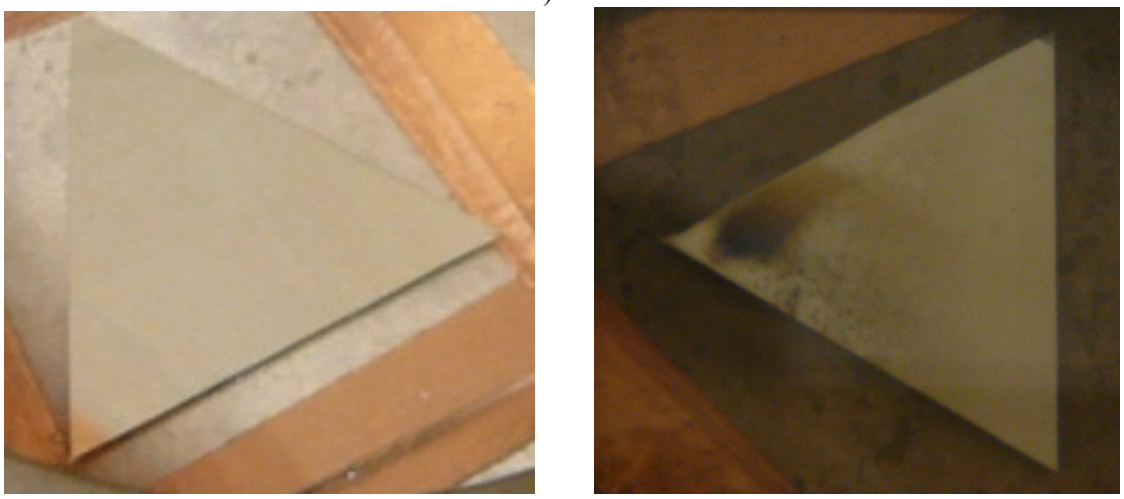

Figure 33. Image of an Mg-Ni-Al sample a) before hydrogenation and b) after hydrogenation showing the presence of a black phase in the Mg-Ni region of the sample.

5.3.2 Mg-Ni-B System

Samples composed of Mg, Ni and B were created by the procedure outlined in Section 5.2.1. This material system was chosen since magnesium borohydride, $Mg(BH_4)_2$, has a high theoretical storage capacity of 14.8%, but is stable up to 320 ^{o}C and does not readily rehydrogenate upon exposure to gaseous H_2.[83] High desorption temperatures and complicated regeneration reactions are typical of borohydride materials,[84] but their high theoretical storage capacities make them worthy of further study.

Recent studies have shown that mechanically milling MgH_2 or MgB_2 with $LiBH_4$ can destabilize the material and enable reversible hydrogen storage.[85] This effect was subsequently shown to enhance hydrogen uptake and release across a variety of borohydride materials.[81] Mg and B are therefore a reasonable starting point for the exploration of borohydride systems. Ni was included in the sample since it is well documented as a catalyst for hydrogen uptake[80] and as a destabilizing agent[44] in magnesium hydride systems. It is reasonable to assume that if MgH_2 destabilizes borohydride materials, Mg-Ni-H compounds should provide even further destabilization.

Due to a temporary difficulty in achieving a steady supply of hydrogen, the Mg-Ni-B samples were measured in vacuum, removed and heated to 150 ^{o}C under 300 psi hydrogen, and were returned to the laser setup while still under hydrogen pressure and heating. The switch was performed in under 5 minutes. Borohydride materials are typically characterized by slow kinetics. Since the Mg-Ni system had reaction kinetics on the order of 20 minutes for the complete reaction, it is likely that any borohydride formation could be observed even with the 5 minute delay in data acquisition.

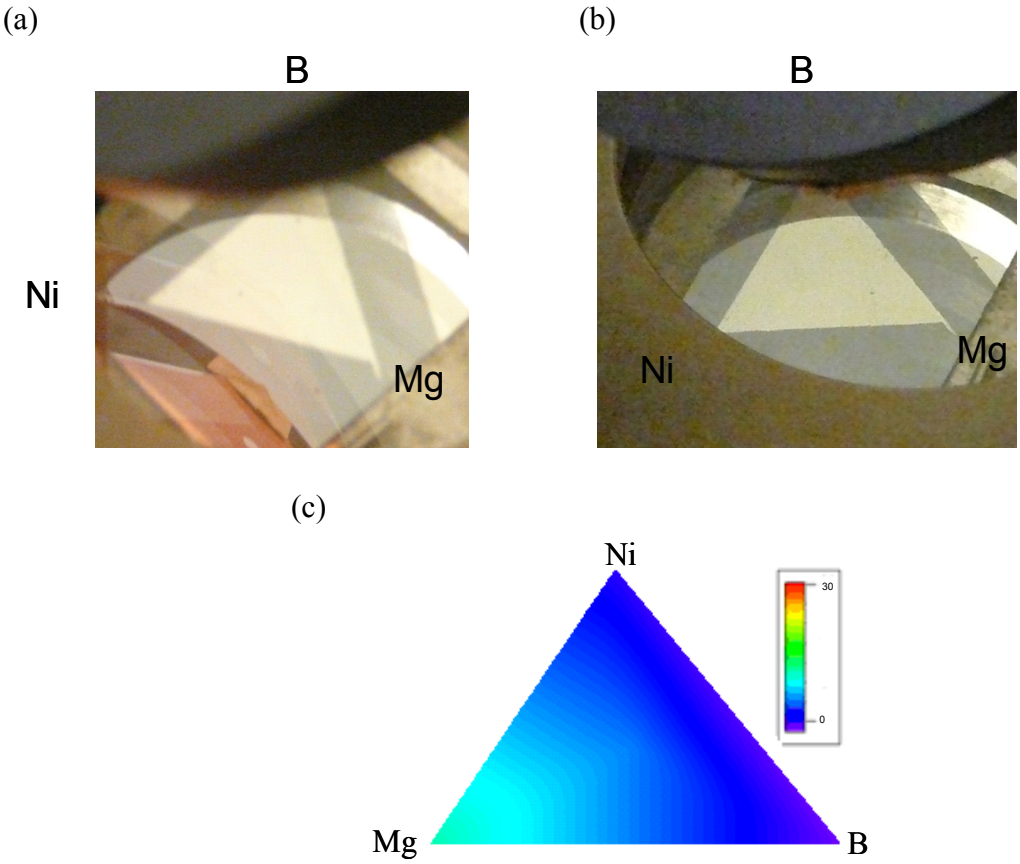

Figure 34. Data from Mg-Ni-B sample showing (a) a picture of the unreacted sample, (b) a picture of the sample after 90 minutes at 150 oC and 300 psi H2 and (c) the percent change in reflectance during hydrogenation.

Figure 34c shows that there is only a minor change in reflectance of about 6%, focused mainly in the Mg region of the sample. This is confirmed but Figure 34a and b which show before and after pictures of the sample. No color change is observed, which is consistent with the constant reflectance. The small change near the Mg corner is most likely due to some MgH_2 formation. The presence of B throughout the sample appears to inhibit other hydrogenation reactions. This could be either by blocking diffusion or binding to potential hydride forming sites. Since this material system did not appear promising, further testing was abandoned and other systems and catalysts were studied.

5.3.3 Ca-B-Ti System

The final sample composition tested was a mixture of Ca, B and Ti. Calcium borohydride, $Ca(BH_4)_2$, is another material with a high theoretical hydrogen storage capacity of 11.6%. It has been demonstrated that 9.2 wt% H_2 can be released simply upon heating to 800 K.[86] As with $Mg(BH_4)_2$, the formation reaction is significantly more difficult. Again, some form of destabilization or catalysis is necessary for hydrogen storage in $Ca(BH_4)_2$ to become

practical. In this case Ti was chosen as a catalyst since it has shown to significantly reduce the reaction temperature of other complex hydrides such as $NaAlH_4$.[7] Ti also has been shown to further reduce the enthalpy of formation of the Mg-Ni system,[10] so it has promise for both thermodynamic and kinetic improvements. It should be noted that materials doped with pure Ti, rather than Ti contained in a compound such as $TiCl_3$ or TiO_2, tend to exhibit little improvement of the dehydrogenation reaction.[62] The hydrogenation kinetics are still improved, so pure Ti was used in these experiments for simplicity, but more complicated compounds may be required to expand the results to a full cycle of dehydrogenation and rehydrogenation. Finally, since this material library was not limited by the low melting and evaporation temperatures of Mg, the Ca-B-Ti samples were annealed at 400 ^{o}C for 12 hours.

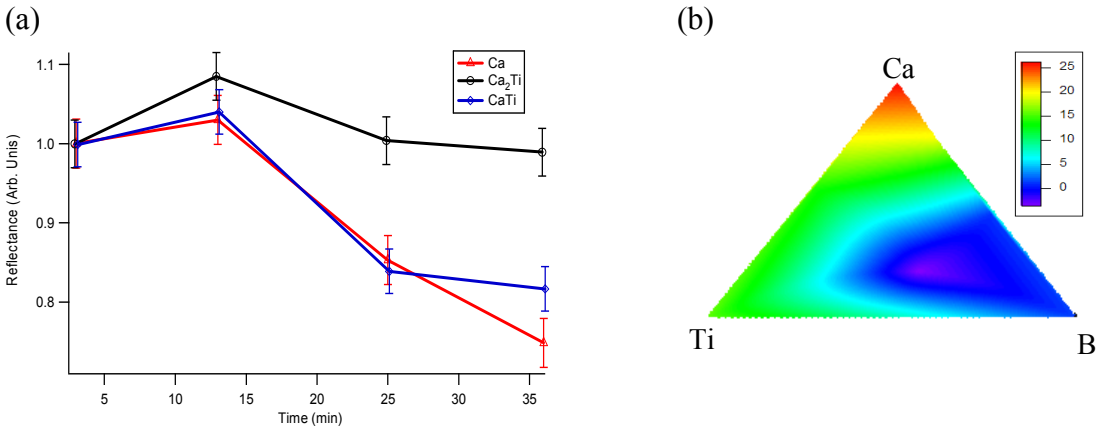

Figure 35. (a) Results from the Ca-Ti region of the Ca-B-Ti sample in 300 psi H_2 at 473 K. (b) Percent change in reflectance after 1 hour at 473 K in 300 psi H_2.

The results in Figure 35 show a large change in reflectance near the Ca corner, a smaller change along the Ca-Ti edge, and a decreasing change with increasing B content. This indicates that again the B is not participating in the hydrogenation reaction. Instead, the likely result is the formation of some CaH_2, potentially catalyzed by Ti but also with the potential for TiH_2 formation. The kinetics plot in Figure 35a shows that the reaction occurs on a time scale of 20 minutes, which is similar to the Mg-Ni system.

5.4 Conclusions

The method presented is this chapter has proven to be an effective tool for scanning many possible combinations of elements for their potential as hydrogen storage materials. A relatively simple experimental setup can be used to rapidly test a variety of potential base materials and catalysts. The simplicity of tracking optical changes also proves to be widely applicable.

We have identified the regions of largest change in samples with a variety of compositions. The identification of a black phase in the Mg-Ni-Al sample indicates significant hydrogen uptake in the region around a composition of Mg_2Ni. Al was determined not to provide significant destabilization or improvement of kinetics at these low temperatures, even with a catalytic Pd layer providing strongly favorable conditions. Al is therefore not recommended for further study in developing practical Mg-based hydrogen storage materials.

Multiple material systems were deposited in an attempt to form borohydride materials from the constituent elements and gas phase hydrogen. Even in a strongly favorable environment with a Pd catalyst layer and incorporation of Ni or Ti to enhance the reaction, no evidence of borohydride formation was observed. Hydride formation in other regions of the sample indicates that the deposition process was clean and successful. Further study is therefore needed to find simple reversible reactions for borohydrides if they are to become viable hydrogen storage materials. It is possible that more complicated catalysts are required, such as TiO_2 or $TiCl_3$. Incorporating targets and deposition techniques which would maintain a constant material composition consisting of multiple elements for a single side of the triangular sample is a conceivable next step for combinatorial materials system.

Chapter 6: Conclusions and Future Work

6.1 Best Practices in Hydrogen Storage Research

The definition of good experimental methods for studying hydrogen storage materials is an ongoing project. Significant progress has been made in creating standard measurement techniques and clarifying conflicting definitions, but so far much of this work has been focused on kinetics and capacity. Many of these details are included in Chapter 2 of this thesis, as well as some work to extend similar standardization to the measurement of thermodynamic properties. Significant work is still required to organize the discussion of thermodynamic properties into the master document discussing kinetics and capacity measurements which is available on the DOE website. Once this is completed, the next step is to expand the document even further to cover a complete discussion of cycle life measurement techniques and avoidable errors. At the end of this project, one master document will be available both as an introduction to the study of hydrogen storage materials for new researchers as well as a valuable reference tool for researchers at all levels.

6.2 Synchrotron Radiation Studies of Hydrogen Storage Materials

There are many challenges in performing successful XAS and XES measurements of metal hydride materials. The most important is the high reactivity of Mg, one of the more promising elements due to its high theoretical storage capacity. Another consideration is the achievement of low vacuum while measuring samples that are unstable in a vacuum environment. Chapter 3 discussed the development of a novel system for performing XAS and XES measurements on materials under gas pressure up to 2 atm.

Much work went into developing oxide free samples. All aspects of the experiment were considered, from the starting materials to sample transportation after deposition was completed. Despite these efforts, oxide formation was a significant impediment to interpretation of the results. Still, some basic aspects of the reaction were observed, indicating that future work to improve the sample preparation and transportation techniques is merited.

A novel reaction chamber which allowed XAS and XES measurements of sample under gas pressure was developed to measure the changes in electronic structure of Mg-Ni mixtures upon exposure to hydrogen and clarify the role of Ni in destabilizing Mg hydride. The system is now used for a variety of materials and studies, such as the investigation of the electronic structure of carbon nanotubes during physisorption of hydrogen. Future applications will include the use of other gases, such as CO_2 or N_2 to test new materials for use in gas sensors.

6.3 Thermogravimetric Analysis of Sodium Borohydride

Borohydride materials have great promise as hydrogen storage materials due to their high theoretical storage capacity, but are severely limited by slow kinetics and poor thermodynamics.

Some of the techniques described in Chapter 2 to study and improve performance were applied to $NaBH_4$ in an attempt to achieve absorption and desorption of hydrogen in a method compatible with onboard regeneration. Specifically, ball milling to reduce particle size and effectively introduce TiO_2 catalyst was performed.

Significant desorption of hydrogen was achieved in two stages with no wet chemical method required. The two stages correspond to two dissociation reactions. The first reaction can release up to 8 wt% H2 with residual NaH and B. The second reaction is the decomposition of NaH. In addition to releasing hydrogen, the second reaction occurs as such high temperature that Na melts and may experience some evaporation, leading to irreversible sample degradation. For this reason, only the first reaction is appropriate for regenerative hydrogen storage applications.

Addition of the catalyst and reduced particle size reduce the time required for desorption by 50%. The desired first desorption reaction also occurred 50 ^oC lower in the catalyzed sample. At least an additional 1.5 wt% H_2 was reabsorbed by the catalyzed sample. The desorption time of almost 2000 minutes, desorption temperature of 290 ^oC, and maximum storage capacity of 5% show significant progress towards meeting the standards required of a viable hydrogen storage system, but further improvements are still necessary.

Future work on $NaBH_4$ should focus on continuing the trend observed in the catalyzed samples or improved kinetics without significant reduction in storage capacity. It would be interesting to separate the effects of particle size and TiO_2 catalyst so that they can be separately optimized. A study on the thermodynamic properties of the system is also of interest, but further improvement in the kinetics is required to achieve equilibrium in a reasonable time period.

The results reported here can also be expanded to research on other borohydride materials. TiO_2 or other Ti compounds can be expected to have a similar catalytic effect on other materials such as $LiBH_4$, just as Ti compounds have a similar catalytic effect in most alanates. While $LiBH_4$ is more difficult to work with due to its higher reactivity, its high theoretical capacity of 18.3 wt% H_2 makes it a promising candidate for future research.

6.4 High Throughput Study of Hydrogen Storage Material Systems

A combinatorial preparation technique was developed to speed the study of mixtures of promising hydrogen storage materials. The measurable change in optical properties of metal hydride materials during hydrogen uptake allowed for rapid data collection across all material combinations present in the combinatorial samples.

This high throughput technique can easily be expanded to other applications where complex metal alloys are required whose properties can be tracked with optical measurements. For example, new high temperature alloys are required for a variety of industries, such as jet engines and solar thermal power plants. Infrared detectors could be used to track the temperature of a gradient film deposited using the technique described above. As heat is applied, any point where the temperature of the film remains constant indicates local melting, and a map of the melting points of the various alloys could be determined. A narrower subset of materials meeting the melting point criteria could then be tested for other important properties such as structural integrity over thermal cycling.

For the hydrogen storage research presented here, the high throughput technique was used to analyze three different materials systems. First, Mg-Ni-Al samples were studied due to the high theoretical capacity of Mg based hydrides and the destabilizing and catalytic potential of

Ni and Al. This system also served to prove the concept of the technique as the optical properties of Mg_2NiH_4 are well known and confirmed that significant hydrogen uptake was achieved. Al was not shown to have the desired effect at low temperature, but a combination of Mg and Ni which maximized the kinetics of the reaction was determined. Next, borohydride two borohydride systems were studied, since borohydrides have even higher theoretical capacities than magnesium hydride systems, but suffer from even worse kinetics and thermodynamics. Ni was added to a magnesium borohydride system, since Ni destabilizes simple magnesium hydride well. Next, Ti was used as a catalyst in the calcium borohydride system. Borohydride formation could not be confirmed in either system at low temperature. Indications of calcium and magnesium hydride were observed, validating the results.

No material has yet been identified that meets all of the requirements outlined in Chapter 1. High throughput combinatorial analyses such as those presented in Chapter 4 present a promising technique to speed the discovery of new materials which may exceed the performance of existing combinations under study. As most of the simpler systems are studied and discarded, the search will move to materials of ever increasing complexity, making the need for efficient testing systems even more important. Future work in this field may require expanding the concept to fourth order systems or even higher to find a material with appropriate kinetics, thermodynamics and storage capacity.

Appendix A: Predicting vacuum levels in tubing

The pumping speed of a pump is only one of the many factors involved in the lowest achievable vacuum of a given system. For example, the outgassing rate of the tube or chamber walls, known as the gas load, can limit the working vacuum achieved from a pumping system. It is difficult to predict the outgassing rate of a system, since it is dependent on a variety of factors such as the amount of water vapor admitted in the last exposure to air, the temperature and length of the most recent or most extreme bakeout, and the life of the chamber.

The size and shape of the tubes or chamber being evacuated can be of even greater importance. When parameters of a vacuum system such as tube inner diameter and pump orifice are reduced below a certain size, these geometric factors can lead to a significant flow resistance. Analogous to heat transfer, where a thermal resistance leads to a temperature difference across a distance, a flow resistance will lead to pressure differences in the system. The resistance, Z, between two points at pressures P_1 and P_2 with a quantitative flow rate Q between them can be written as:

Equation 21

$$Z = \frac{P_1 - P_2}{Q}$$

With the units of Q written as Torr-L/s, it is clear that the flow resistance has the inverse of the units of pumping speed. Conductance, the inverse of resistance, is therefore an interesting property and can be written as:

Equation 22

$$C = \frac{Q}{P_1 - P_2}$$

Since most vacuum systems can be represented by a series of conductances, the total conductance is generally calculated from:

Equation 23

$$\frac{1}{C_{tot}} = \sum_i \frac{1}{C_i}$$

It is possible to incorporate the pumping speed as another conductance in Equation A-3 so that the effective pumping speed can be determined from:

Equation 24

$$\frac{1}{S_{eff}} = \frac{1}{S_{Pump}} + \sum_i \frac{1}{C_i}$$

Various correlations have been developed to calculate the conductance of vacuum system components based on their geometry and the flow regime of the system. For the purposes of conductance calculations, three flow regimes have been defined: viscous flow, intermediate flow, and molecular flow. Viscous flow is defined as the regime where molecules are much more likely to contact other molecules than any chamber boundaries. In other words, viscous forces dominate molecular interactions. Molecular flow occurs under high vacuum, when the density of gas is reduced to the point where the mean free path is on the order of or less than the dimensions of the vacuum chamber or tubing. In this case wall interactions dominate viscous forces. Intermediate flow occurs when both types of molecular interactions are comparable.

In general, vacuum systems initially operate in viscous flow, but the final dynamics are most often governed by molecular flow. This can be seen from a commonly used approximation for the mean free path of air:

Equation 25

$$\lambda_{mfp}(cm) = \frac{5 \times 10^{-3}}{P(Torr)}$$

At 1 mTorr, Equation A-5 yields a mean free math of 5 cm, or more than 2 inches. Since flow resistances are added in series, the most restrictive conductance values are important. Vacuum system components with dimensions less than 2 inches are common, especially in hydrogen supply lines which are often on the order of ¼" or ½". Therefore the calculations presented below are based on the simple correlation for conductance in the molecular flow regime given in Equaton A-6, where D is the diameter of the tube and L is the length, both in inches. C is in units of liters/s.

Equation 26

$$C = 78\frac{D^3}{L}$$

Conductance is useful not only in predicting the speed of pumping, but also the final minimum pressure achievable in a given vacuum system. The concept of minimum achievable pressure is necessary because even a perfectly sealed system will have a continuous addition of gas into the system, Q, due to outgassing from the walls, which balances the flow of gas leaving through the pumping system.[87] The minimum achievable pressure is therefore given by Equaton A-7.

Equation 27

$$P = \frac{Q}{S_{eff}}$$

This type of calculation was used to predict the vacuum level in the gas reaction chamber described in Chapter 3. This was necessary because it was impossible to fit a pressure gauge near enough to the chamber to achieve accurate results due to the extremely large flow resistance at the desired pressures. The calculations were confirmed by pumping from only one side of the reaction chamber and measuring the pressure at the end of tubing about 36" away from either side. The minimum pressure for the chamber is therefore the reading measured on the side that is actively pumped, while the maximum pressure is the reading on the opposite side. The true pressure is somewhere in between, but the minimum and maximum define a range which can be used to determine the accuracy of the conductance calculations and refine the prediction for the minimum pressure achievable in the reaction chamber.

Conductance calculations are also useful in designing vacuum systems and their required components. For example, the Figure A.1 presents the results for the maximum achievable vacuum for a 10 in. long tubing system for a typical gas load of 5×10^{-9} Torr-L/s[88] and pumping speeds for a standard roughing pump and turbomolecular pump. From the figure, it is clear that for tube diameters less than approximately 0.5 in. there is no significant advantage to using a turbomolecular pump over a roughing pump.

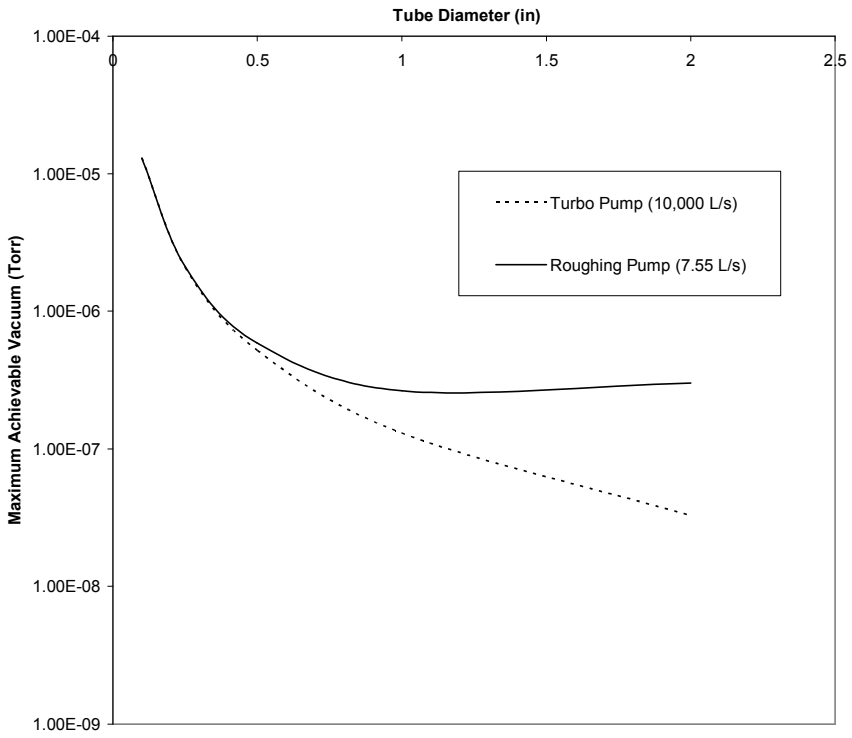

Figure A.1 Achievable vacuum for a roughing pump and turbo pump for various tube diameters.

Appendix B: Analysis of Thin Film Break-up in Pd Capping Layers

Mullins was the first to use the concept of capillary instabilities in thin solid films to explain thermal grooving, where grain boundaries were observed to deepen at elevated temperatures.[89] The three mechanisms that have been proposed to explain the material migration are surface diffusion, bulk diffusion and evaporation/condensation. The melting temperature of Pd is 1808 K, well above the maximum experimental temperature for the films presented here, so the evaporation/condensation effects are likely to be negligible. Wong defined a critical length scale to describe the relative importance of the surface and bulk diffusivity presented in Equation 28:

Equation 28

$$L_c = D_s \Omega^{1/3} / D$$

Where D_s is the surface diffusivity, Ω is the atomic volume, and D is the bulk diffusivity. When the radius of curvature of the film at the contact point is much less than this critical length scale, surface diffusion dominates bulk diffusion.[90] The activation energy of surface diffusivity is less than that of bulk diffusivity.[91,92] If the diffusivities are assumed to obey the Arrhenius law, then as the temperature decreases, L_c increases, and D_s becomes relatively more important. Since the Pd films are always kept well below their melting point, it is reasonable to assume that surface diffusion will dominate.[25,26]

With this assumption, Mullins combined the fact that the chemical potential is dependent on the curvature of a material with the Nernst-Einstein relation to derive Equation 29 for the velocity of a surface normal to itself.

Equation 29

$$V_n = -B\nabla_s^2 \kappa$$

where $B = D_s \gamma \Omega^2 n / kT$, γ is the surface free energy per unit volume equivalent to the surface tension of a liquid, n is the number of atoms per unit area, and $\nabla_s^2 \kappa$ is the surface Laplacian of the curvature.

Many different models have been proposed to solve Equation 29 with a variety of assumptions. Srolovitz and Safran assumed that voids in the film would maintain a circular shape as they grew and used dimensional analysis with a numerical solution to predict the growth rate of the void radius, u, as:[93]

Equation 30

$$u = 0.001 B^{1/4} t^{-3/4} \ln^3 \left[Bt(\beta/a)^4 \right]$$

Where b is the equilibrium contact angle, a is the film thickness and t is the time.

Jiran and Thompson used TEM images to observe a constant void growth rate in contrast to the time dependence predicted by Srolovitz and Safran. They proposed that voids would most likely grow most rapidly towards the thinnest sections of the film, and therefore not be circular. Most importantly, they assumed a constant quarter circle profile for the film, implicitly assuming an equilibrium contact angle of 90^o and a constant radius of curvature. This allows Equation 29

to be discretized, simplifying the analysis greatly and resulting in a constant void growth rate given by:[94,95]

Equation 31

$$V_n = \frac{D_s}{kT}\frac{\Omega^2\gamma}{\pi}\frac{2v}{a^3}$$

Where ν is the surface concentration of atoms. Clearly the void growth rate cannot remain constant for all time, so this model will be most useful to determine the early stages of void growth. Jiran and Thompson avoid the problem by using their theory to calculate the time required for 90% agglomeration of the film.

Wong et al. assumed that films would be deposited with a linear slope similar to that proposed by Srolovitz and Safran, but that the film would spontaneously rearrange to form the equilibrium contact angle in a small region near the surface. They then defined a similarity variable and created a set of charts to be used in combination with the equilibrium and initial contact angles to determine the void growth rate. They found a $t^{-3/4}$ dependence for the void growth rate, as shown in Equation 32:[90]

Equation 32

$$V_n = \frac{1}{4}X(0)B^{1/4}t^{-3/4}$$

Where X(0) is a variable determined from a set of charts based on the equilibrium and initial contact angles. The film thickness does not appear anywhere in Equation 32. This model is therefore fundamentally different from Jiran and Thompson's which assumes that void growth will occur the most rapidly in the thinnest areas of the film, and therefore also occur more rapidly in thinner films than thicker films.

These three methods were compared to experimental data from Pd capping layers on Mg and Mg-Ni thin films to determine which was the most applicable for predicting the breakup of low temperature Pd films. Experience with Pd films has shown that Pd films less than 5 nm thick will agglomerate into islands of material within days of deposition on top of MgNi thin films, while thicker films will tend to remain continuous.[96]

Most of the properties required for Equation 30 through Equation 32 are readily available, and are presented in Table 5.

n (m^{-3})	v (m^{-2})	γ [97] (N/m)	Ω (m^3)
6.8×10^{28}	2.64×10^{19}	6	1.5×10^{-27}

Table 5. Properties of Pd required for void growth rate calculations.

The surface diffusivity of Pd can be estimated using the Arrhenius Law (Equation 33), with the activation energy for surface diffusion Q = 0.91 eV.[91]

Equation 33

$$D_s = D_o e^{-Q/kT}$$

No D_o values were available for Pd, but the surface diffusivity has been described as "high", so it is reasonable to use the value for Au, the highest surface diffusivity listed. This assumption will lead to faster predicted growth rates and yields surface diffusivity values of 2.06×10^{-16} m^2/s at room temperature and $D_s = 2.02 \times 10^{-11}$ m^2/s at 373 K.

The results calculated from each method are presented as the fraction of the film that is agglomerated versus time (see
Figure **36**) and the amount of time required to reach 90% agglomeration (see Table 6). Calculations of agglomeration require an assumption about the initial formation of holes in the film. The number of holes in the film will be related to the magnitude and the frequency of the disturbances in the film that could contact the substrate and cause the nucleation of a hole that would subsequently grow. In a simple model, these would both increase with temperature, so we would expect fewer holes per area in palladium near room temperature. However, since the palladium films are also much thinner, it would take a much smaller disturbance to disrupt the film, so there is still likely to be a large potential for even relatively small disturbances to reach the substrate. Therefore the number of holes per unit area was chosen as 0.5 m^{-2}, which is the lower end of the value from Jiran and Thompson's experiments on gold at temperatures of 700-825 ^oC. This should be a high estimate, and therefore predict faster agglomeration times, especially for the thicker films.

The Wong model predicts extremely slow agglomeration, and therefore cannot explain the rapid breakup of Pd thin films. The Jiran and Thompson model predicts an extremely fast agglomeration for a 5 nm film, and much slower rates for thicker film, which matches well with the observed results. The Srolovitz and Safran model predicts a similar rate of agglomeration for all film thicknesses, and therefore cannot explain the stability of thicker films. It is possible that the discrepancy in the Srolovitz and Safran model could be fixed by a better determination of the initial void formation.

a (nm)	T (K)	Ds	t_W	t_JT (s)	t_SS (s)
5	300	2.02E-16	N/A	14142	N/A
10	300	2.02E-16	N/A	111112	N/A
20	300	2.02E-16	N/A	878788	N/A
50	300	2.02E-16	N/A	14141415	N/A
5	373	2.02E-11	N/A	2	343430
10	373	2.02E-11	N/A	3	555556
20	373	2.02E-11	N/A	12	909091
50	373	2.02E-11	N/A	172.5	1818200

Table 6. Time to reach 90% agglomeration for the Wong (t_W), Jiran and Thompson (t_JT) and Srolovitz and Safran (t_SS) models for various film thicknesses.

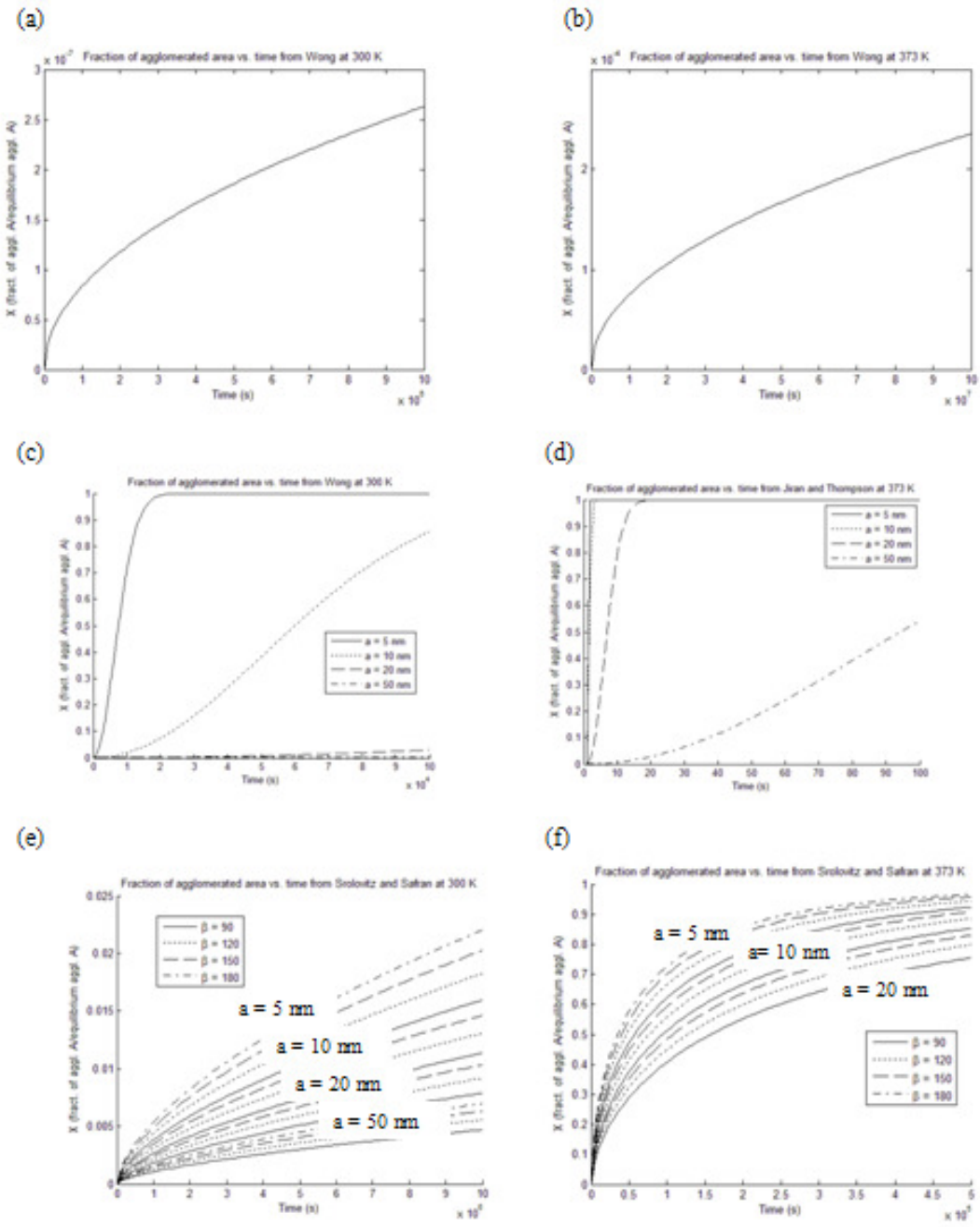

Figure 36. Plots of fraction of area agglomerated vs. T for (a) Wong's model at 300 K (b) Wong's model at 373 K (c) Jiran and Thompson's model at 300 K (d) Jiran and Thompson's model at 373 K (e) Srolovitz and Safran's model at 300 K (f) Srolovitz and Safran's model at 300 K.

Based on these results, the Jiran and Thompson model is the best to apply to low temperature break of thin Pd films. Pd capping layers are crucial to most of the experiments performed in this work. Based on the above indication the Jiran and Thompson model can be used to predict the requirements for thin Pd films under the range of temperatures of the given experiments.

References

1 "Total World Delivered Energy Consumption by End-Use Sector and Fuel." Energy Information Administration [Online]. Available: http://www.eia.doe.gov/oiaf/ieo/ieoenduse.html

2 "U.S. Department of Energy Hydrogen Program." U.S. Department of Energy [Online]. Available: http://www1.eere.energy.gov/hydrogenandfuelcells/

3 J.R. Bolton, "Solar Photoproduction of Hydrogen," The University of Western Ontario, London, Canada, Tech. Rep. IEA/H2/TR-96, 1996

4 A. Zuttel, *Mater. Today* **6** 9 (2003) 24-33

5 A. Zuttel, P. Wenger, S. Rentsch, P. Sudan, Ph. Mauron, Ch. Emmenegger, *J. Power Source* 188 (2003) 1-7

6 B. Sakintuna, F. Lamari-Darkrim, M. Hirscher, *Int. J. Hyd. Energy* **32** (2007) 1121

7 B. Bogdanovic, M. Schwickardi, *J. Alloys Comp.* **253-254** (1997) 1-9

8 A. Zaluska, L. Zaluski, J.O. Strom-Olsen, *J. Alloys Comp.* **298** (2000) 125-134

9 A. Zuttel, A. Borgschulte, L. Schlapbach, Ed., *Hydrogen as a Future Energy Carrier*. Weinheim: Wiley-VCH, 2008.

10 R. Gremaud, C.P. Broedersz, D.M. Borsa, A. Borgschulte, P. Mauron, H. Screuders, J.H. Rector, B. Dam, R. Greissen, *Adv. Mater.* **19** (2007) 2813-2817

11 R.D. McCarty, U.S. Department of Commerce. NBSIR 74-357. Boulder: National Bureau of Standards, Cryogenic Division (1974)

12 A.M. Puziy, A. Herbst, J.G. Poddubnaya, P. Harting, *Langmuir* **19** (2003) 314-320

13 E.W. Lemmon, M.L. Huber, *J. Res. Natl. Inst. Stand. Technol.* **113** (2008) 341-350

14 "Magnetic Suspension Balances" June, 2009. [Online]. Available: http://www.rubotherm.de/PDF/_Rubo_Magn._engl.pdf

15 R.M. Nix, "An Introduction to Surface Chemistry: 5.6 Temperature-Programmed Desorption." School of Biological and Chemical Sciences, Queen Mary, University of London (6/8/2003). [Online]. Available: http://www.chem.qmul.ac.uk/surfaces/scc/scat5_6.htm

16 H.K.D.H. Bhadeshia, "Differential Scanning Calorimetry." Universit of Cambridge, Materials Science and Metallurgy, 2002. [Online]. Available: http://www.msm.cam.ac.uk/phase-trans/2002/Thermal2.pdf

17 Y. Fukai, *The Metal-Hydrogen System, Basic Bulk Properties, 1st ed.,* Berlin: Springer-Verlag (1993)

18 A. Zhukov, R. Karlsson, *J. Mol. Recognit.* **20** (2007) 379-385

19 Measurements performed at Hy-Energy, LLC

20 K.J. Gross, G. Sandrock, G.J. Thomas, *J. Alloys & Compounds* **330** (2002**)** 691-695.

21 A. Chambers, "Modern Vacuum Physics" US: CRC Press, 2005.

22 J.J. Vajo, F. Mertens, C.C. Ahn, R.C. Bowman, Jr., B. Fultz, *J. Phys. Rev. B* **108** 37 (2004) 13977-13983

23 A.R. Ubbelohde, *Proc. R. Soc. London, Ser. A,* **159** (1937) 295

24 T.B. Flanagan, J.D. Clewley, *J. of Less-Common Metals* **83** (1982) 127-141

25 D.G. Westlake, *Trans. Am. Soc. Met.* **62** (1969) 1000

26 N.E. Paton, B.S. Hickman, D.H. Leslie, *Metall. Trans.* **2** (1971) 2791

27 H.K. Birnbaum, M.L. Grossbeck, M. Amano, *J. Less-Common Met.* **49** (1976) 357

28 S. Gahr, H.K. Birnbaum, *Acta Metall.* **26** (1978) 1781

29 T. Schober, *Phys. Status Solidi A* **29** (1975) 395

30 H.C. Jamieson, G.C. Weatherly, F.D. Manchester, *J. Less-Common Met.* **50** (1976) 85

31 K.J. Gross, D. Chartouni, E. Leroy, A. Zuttel, L. Schlapbach, *J. Alloys and Compounds*, **269** (1998) 259-270.

32 R. Gremaud, C.P. Broedersz, A. Borgschulte, M.J. van Setten, W. Lohstroh, H. Schreuders, M. Slaman, B. Dam, R. Griessen *Acta Materialia* **58** 2 (2010) 658-668

33 P.D. Goodell, G.D. Sandrock, E.L Huston *J. Less-Common Metals* **73** (1980) 135-142

34 G.D. Sandrock*, The Metallurgy and Production of Rechargeable Hydrides, Hydrides for Energy Storage.* A.F. Andresen and A.J. Maeland, Eds., Oxford: Pergamon Press (1978), p. 353-393

35 F. Rouqerol, *Adsorption by Powders and Porous Solids*. London: Academic Press, 1999

36 T.J. Richardson, B. Farangis, J.L. Slack, P. Nachimuth, R. Perera, N. Tamura, M. Rubin, J. Alloys Compd. **356-357** (2003) 204-207

37 V. Berube, G. Radtke, M. Dresselhaus, G. Chen, *Int. J. Energy Res.* **31** (2007) 637-663

38 V. Berube, G. Chen, M.S. Dresselhaus, *Int. J. Hydrogen Energy* **33** (2008) 4122-4131

39 J. Israelachvili, *Intermolecular and Surface Forces*. London: Academic Press, 1991.

40 R.W.P. Wagemans, J.H. Van Lenthe, P.E. De Jongh, A.J. Van Dillen, K.P. De Jong, *J. Am. Chem. Soc.* **127** 47 (2005) 16675-16680

41 A.J. Du, S.C. Smith, X.D. Yao, G.Q. Lu, *Surf. Sci.* **600** (2006) 1854-1859

42 J.H. Rose, J.R. Smith, F. Guinea, J. Ferrante, *Phys. Rev. B* **29** 6 (1984) 2963-2969

43 J. Ferrante, J.R. Smith, *Phys. Rev. B* **31** 6 (1985) 3427-3434

44 J.J. Reilly, R.H. Wiswall, *Inorg. Chem.* **7** (1968) 2254-2256

45 S**.** Alapati, J. Johnson, D. Sholl, *J. Phys. Chem. B* **110** (2006) 8769-8776

46 M. Dornheim, S. Doppiu, G. Barkhordarian, U. Boesenberg, T. Klassen, O. Gutfleisch, R. Bormann, *Scripta Mater.* **56** (2007) 841-846

47 A. Krozer, B. Kasemo, *J. Less-Common Met* **160** (1990) 323-342

48 B. Bogdanovic, K. Bohmhammel, B. Christ, A. Reiser, K. Schlichte, R. Vehlen, U. Wolf, *J. Alloys Comp.* **282** (1999) 84-92

49 M. Bououdina, Z.X. Guo, *J. Alloys Comp.* **336** (2002) 222-231

50 J. Guo, *Int. J. of Nanotechnology* **1** (2004) 193

51 M.O. Krause, *J. Phys. Chem. Ref. Data* **8** (1979) 307

52 D. Attwood, *Soft X-Rays and Extreme Ultraviolet Radiation: Principles and Applications*. New York: Cambridge University Press, 1999.

53 M. Rogers, S. Barcelo, X. Chen, T.J. Richardson, V. Berube, G. Chen, M.S. Dresselhaus, C.P. Grigoropoulos, S.S. Mao, *Appl. Phys. A* **96** 2 (2009) 349-352

54 A. Yermakov, N. Mushnikov, M. Uimin, V. Gaviko, A. Tankeev, A. Skripov, A. Soloninin, A. Buzlukov, *J. Alloys Compd.* **425** (2006) 367-372.

55 A. Zaluska, L. Zaluski, J.O. Ström-Olsen, *J. Alloys Compd.* **288** (1999) 217-225

56 R.A. Varin, T. Czujko, C. Chiu, Z. Wronski, *J. Alloys Compd.* **424** (2006) 356-364

57 S.J. van der Molen, J.W.J. Kerssemakers, J.H. Rector, N.J. Koeman, B. Dam, R. Griessen, *J. Appl. Phys.* **86** 11 (1999) 6107

58 T.J. Regan, H. Ohldag, C. Stamm, F. Nolting, J. Luning, J. Stohr, R.L. White, *Phys. Rev. B* **64** (2001) 214422

59 M.B. Smith, G.E. Bass Jr., *J. Chem. Eng. Data* **8** 3 (1963) 342-346

60 Y. Wu, R.M. Mohring, *Am. Chem. Soc.* **48** 2 (2003) 940

61 Y. Kojima, T. Haga, *Int. J. Hydrogen Energy* **28** 9 (2003) 989-993

62 S. Chaudhuri, J.T. Muckerman, *J. Phys. Chem. B* **109** 15 (2005) 6952-6957

63 S.S. Srinivasan, H.W. Brinks, B.C. Hauback, D. Sun, C.M. Jensen, *J. Alloys Compd.* **377** (2004) 283

64 B. Bogdanovic, M. Felderhoff, S. Kaskel, A. Pommerin, K. Schlichte, F. Schuth, A*dv. Mater.* **15** 12 (2003) 1012-1015

65 B. Bogdanovic, R.A. Brand, A. Marjanovic, M. Schwickardi, J. Tolle, *J. Alloys Compd* **302** (2000) 36

66 C.M. Jensen, R. Zidan, N. Mariels, A. Hee, C. Hagen, *Int. J. Hydrogen Energy* **23** (1999) 461

67 R.F. Mohtadi, K. Nakamura, M. Au, R. Zidan, U.S. Patent 20090257938, October 15, 2009.

68 E. Wieberg, R. Bauer, M. Schmidt, R.Z. Uson, *Naturforsch* **6b** (1951) 393

69 B. Bogdanovic, M. Schwickardi, *J. Serb. Chem. Soc.* **128** (2006) 5949

70 J.L. Gole, J.D. Stout, C. Burda, Y. Lou, X. Chen, *J. Phys. Chem. B* **108** (2004) 1230-1240

71 S. Orimo, Y. Nakamori, J.R. Eliseo, A. Zuttel, C.M. Jensen, *Chem. Rev.* **107** (2007) 4111-4132

72 A. Montone, J.G. Novakovic, M.V. Antisari, A. Bassetti, E. Bonetti, A.L. Fiorini, L. Pasquini, L. Mirenghi, P. Rotolo, *Int. J. Hydrogen Energy* **32** (2007) 2926-2934

73 J.N. Huiberts, R. Griessen, J.H. Rector, R.J. Wihngaarden, J.P. Dekker, D.G. de Groot, N.J. Koeman, *Nature* **380** (1996) 231

74 T.J. Richardson, *Appl. Phys. Lett* **78,** 20 (2001) 3047

75 R. Gremaud, A. Borgschulte, C. Chacon, J.L.M. van Mechelen, H. Schreuders, A. Zuttl, B. Hjorvarsson, B. Dam, R. Griessen, *Appl. Phys. A* **84** (2006) 77-85

76 R.J. Westerwaal et al., *J. Appl. Phys.* **100** (2006) 063518

77 Lohstroh et al., *Phys. Rev. B* **70** (2004) 165411

78 G. A. Niklasson, C.G. Granqvist, *J. Appl. Phys.* **55** (1984) 3382

79 X-D Xiang, *Annu. Rev. Mater. Sci.* **29** (1999) 149

80 A. Borgschulte, R. J. Westerwaal, J. H. Rector, H. Schreuders, B. Dam, and R. Griessen, *J. Catal.* **239** (2006) 263-271

81 G. Barkhordarian, T. Klassen, M. Dornheim, R. Bormann, *J. Alloys Compd.* **440** (2007) L18-L21

82 Bouaricha, S., Dodelet, J.P., Guay, D., Huot, J., Boily, S., Schulz, R., *J. Alloys Compd.* **297** (2000) 282-293

83 T. Matsunaga, F. Buchter, K. Miwa, S. Towata, S. Orimo, A. Zuttel, *Renewable Energy* **33** (2008) 193-196

84 T. Ozturk, A. Demirbas, *Energy Sources, Part A* **29** (2007) 1415-1423

85 J.J. Vajo, S.L. Skeith, F. Mertens *J. Phys. Chem. B Letters* **109** (2005) 3719-3722

86 K. Miwa, M. Aoki, T. Noritake, N. Ohba, Y. Nakamori, S. Towata, A. Zuttel, S. Orimo, *Physical Review B* **74** (2006) 155122

87 J. O'Hanlon, *A User's Guide to Vacuum Technology*. Hoboken: John Wiley and Sons, Inc., 2003

88 M. Li, H.F. Dylla, *J. Vac. Sci. Technol. A* **11** (1993) 1702

89 W.W. Mullins, *J. Appl. Phys.* **28** (1957) 333

90 H. Wong, M.J. Miksis, P.W. Voorhees, S.H. Davis, *Acta mater*. **45** (1997) 2477

91 J.M. Blakely, *Introduction to the Properties of Crystal Surfaces*, Pergamon Press, New York, 1973.

92 N.A. Gjostein, in *Metal Surfaces*, p. 99, Am. Soc. Metals, Metals Park, Ohio, 1963.

93 D.J. Srolovitz and S.A. Safran, *J. Appl. Phys.,* **60** (1986) 255

94 E. Jiran, C.V. Thompson, *J. Electronc Materials,* **19** (1990) 1153

95 E. Jiran, C.V. Thompson, *Thin Solid Films,* **208** (1992) 23

96 Conversations with Tom Richardson

97 R. Lamber, S. Wetjen, N. Jaeger, *Phys. Rev. B* **51** (1995) 10968